DATA-DRIVEN BUILDING ENERGY MODELS FOR DESIGN AND CONTROL OF COMMUNITY

ENERGY SYSTEMS

DATA-DRIVEN BUILDING ENERGY MODELS FOR DESIGN AND CONTROL OF COMMUNITY

ENERGY SYSTEMS

By STACEY MARK, B.Eng.

A Thesis Submitted to the School of Graduate Studies in Partial Fulfilment of the Requirements for the Degree Master of Applied Science

Master of Applied Science (2022)   Mechanical Engineering

Mechanical Engineering   Hamilton, Ontario, Canada

TITLE: DATA-DRIVEN BUILDING ENERGY MODELS FOR DESIGN AND

                    CONTROL OF COMMUNITY ENERGY SYSTEMS

AUTHOR: Stacey Mark

                    B.Eng. (Mechanical Engineering)

                    McMaster University, Hamilton, Ontario, Canada

SUPERVISORS: Dr. James Cotton and Dr. Marilyn Lightstone

NUMBER OF PAGES: *xv, 171*

Abstract

Building energy models are used to forecast building energy use to design and control efficient building energy systems. Building energy use can generally be decomposed into heating, ventilation and air conditioning, refrigeration, appliance and lighting loads. These loads will depend on multiple factors such as outdoor weather conditions, occupants, building type, controls and scheduling. Data-driven models have become more popular with the increase in smart meter data available that can be used to train and fit the models. Additionally, buildings with high refrigeration loads have greater heat harvesting potential, however, few data-driven models have been developed for buildings such as supermarkets and ice rinks.

In this work, linear regression models are used to predict the disaggregated space cooling, heating, baseload and refrigeration components of building energy use. In most cases, measured aggregate electricity use is available, however individual appliances or component loads require submetering equipment which can be expensive. Therefore the proposed models use time-based and weather features to separate the thermal and baseload portions of the electrical load. A generalized approach is also used to predict new buildings with data from existing buildings. Furthermore, a simplified model is used to predict hourly space heating from monthly natural gas measurements and hourly weather measurements. The models were evaluated on real data from buildings in Ontario and the disaggregated loads were verified with synthetic data. The results found that aggregate use was predicted reasonably well using linear regression methods, with most building types having a median normalized root mean squared error between 0.2 and 0.3, depending on the forecasting period. The model is flexible as it does not require detailed information related to the building such as lighting or setpoint schedules, however, it can be adapted in the future to include additional information and improve predictive capability.

Acknowledgements

Table of Contents

List of Tables

List of Figures

Notations and Abbreviations

Nomenclature	
EL-CL	Electricity model, cooling season
EL-HT	Electricity model, heating season
GHI	Global horizontal irradiation [Wh/m^2] or irradiance [W/m^2]
GS-DD	Gas degree day model
GS-CP1	Gas change point model 1
GS-CP2	Gas change point model 2
P	Electrical power [kW]
Q	Thermal energy [J or kWh]
SH	Specific humidity [unitless]
T	Temperature [°C]
W	Electrical work [kWh]
β	Linear regression coefficient [units vary]
Subscripts	
in	Indoor setpoint or base setpoint
out	Outdoor value
base	Base portion of the load, not weather dependent
t	Timestamp
Abbreviations	
ALP	Appliance lighting and plug
ANN	Artificial neural network
AR	Autoregressive

ARIMA	Autoregressive Integrated Moving Average
ARX	Autoregressive with external inputs
ASHRAE	American Society of Heating, Refrigerating and Air-Conditioning Engineers
CDD	Cooling degree day
CFD	Computational fluid dynamics
CHP	Combined heating and power
CNN	Convolutional neural network
CO_2eq	Carbon dioxide equivalent
COP	Coefficient of performance
CP	Change-point
DBSCAN	Density-based spatial clustering applications with noise
DD	Degree-day
DHW	Domestic hot water
DOE	Department of Energy (US)
EUI	Energy use intensity
GHG	Greenhouse gas
GIS	Geographic information system
GMM	Gaussian mixture model
HDD	Heating degree day
HVAC	Heating Ventilation and Air Conditioning
ICE-Harvest	Integrated Community Energy and Harvesting
KNN	K-nearest-neighbours
kVA	Kilovolt-amperes
kVAR	Kilovolt-amperes reactive

kW	Kilowatt
kWh	Kilowatt-hour
LASSO	Least absolute shrinkage and selection operator
LDC	Local distribution company
LiDAR	Light detection and ranging
LOESS	Localized regression
LSTM	Long short term memory
LTC	Long-term care home
MA	Moving average
MAE	Mean absolute error
MLR	Multiple linear regression
MPAC	Municipal Property Assessment Corporation
MSE	Mean squared error
MVR	Multivariate regression
NaN	Not a number
NECB	National Energy Code of Canada for Buildings
NILM	Non-intrusive load monitoring
NN	Neural network
NRCAN	Natural Resources Canada
NREL	National Renewable Energy Laboratory (US)
NRMSE	Normalized root mean square error
OLS	Ordinary least squares
OSM	OpenStreetMap
PCA	Principal component analysis
PRISM	PRInceton Scorekeeping Method

RBF	Radial basis function
Relu	Rectified linear unit
RMSE	Root mean square error
RNN	Recurrent neural network
SHW	Service hot water
STL decomposition	Seasonal trend decomposition with LOESS smoothing
SVD	Singular value decomposition
SVM	Support vector machine
SVR	Support vector regression
TMY	Typical meteorological year
TES	Thermal energy storage
VBDD	Variable degree day

Chapter 1

1 Introduction and problem statement

Commercial and residential buildings contribute to a significant portion of Canada's energy consumption and greenhouse gas (GHG) emissions. In 2019, the residential sector produced 63.3 Mt of CO_2eq while the commercial and institutional sectors produced 50.8 Mt of CO_2eq, totalling 22.3% of Canada's 511.1 Mt of CO_2eq of greenhouse gas emissions in the end-use sector [1]. This includes greenhouse gas emissions from energy used for space heating, domestic hot water heating, space cooling, refrigeration and powering appliances and lights. As Canada works to meet its emissions reduction targets, there is potential to help decarbonize the building sector by addressing building energy consumption for thermal and electrical needs together.

Due to Canada's colder climate, space heating makes up the majority of the greenhouse gas emissions in the residential, commercial and institutional sectors. In 2019, 85% and 68% of sector emissions for residential and commercial/institutional buildings, respectively, were from space and water heating [1]. However, individual buildings with high cooling loads such as supermarkets or ice rinks may

reject more heat to the ambient through cooling processes than that required for space heating. These buildings can be classified as "cooling dominant buildings" where the thermal cooling load exceeds the thermal heating load when integrated over the course of a year. Conversely, "heating dominant" buildings will have significantly larger thermal heating loads than cooling. Furthermore, due to more frequent hot weather events and high outdoor temperatures, space cooling loads will likely increase, resulting in more low-quality heat rejected to the environment. There is therefore a significant amount of heat rejected by building space cooling and refrigeration systems to the ambient, that could be utilized by buildings with simultaneous heating demand or coupled with seasonal thermal storage. This reduces the net amount of fuel needed to heat heating dominant buildings. For example, a Chicago supermarket with a medium-temperature refrigeration system is expected to reject 1011 MWh of heat that can be harvested from the condenser each year [2]. Similarly, the prototype ice rinks shown in Figure 1 reject approximately 1800 MWh of heat throughout the year. The condenser heat is also seen to exceed the heating requirements for most of the year. In a case study of two cooling dominant and two heating dominant buildings, Abdalla et al. [3] found that 48% of the buildings' total heating requirements could be met by simultaneous energy sharing.
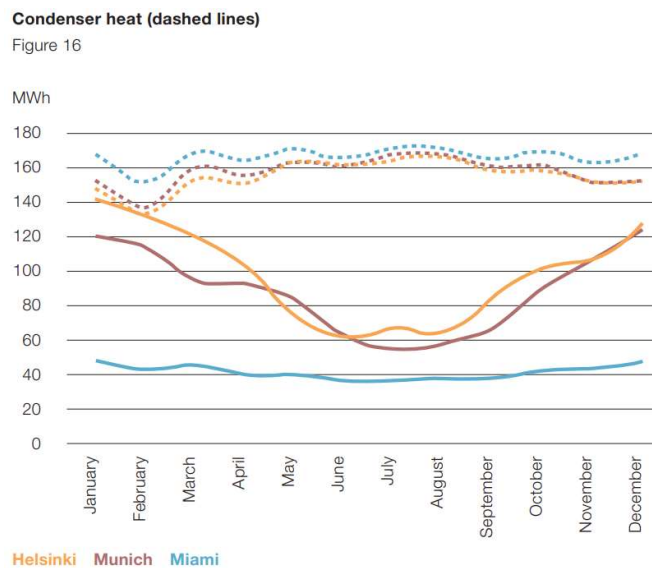
Figure 1: Heating energy need (solid line) and heat from refrigeration condensers (dashed line) for ice rinks [4]

Utilizing this rejected heat can be achieved at a community level by connecting high-energy-density buildings. Smart energy systems that integrate multiple buildings instead of operating each independently can meet both the electrical and thermal needs of buildings while efficiently redistributing heat. The buildings can be connected using a thermal pipe network to facilitate sharing of heat between buildings. An Integrated Community Energy and Harvesting (ICE-Harvest) system [3] has been proposed that uses a micro-thermal network, water source heat pumps, combined heating and power (CHP) and thermal energy storage (TES) to reduce GHG emissions. The ICE-Harvest system uses combined heating and power to offset peaking natural gas power plants for electricity generation while providing heat to the thermal network. The network is short in length, allowing it to respond to the electrical grid at an hourly or sub-hourly timescale depending on whether high-emission power plants are being used for the generation of electricity on the grid.

To evaluate, design and control smart energy systems such as the ICE-Harvest system, detailed information on building energy demand is required. Hourly or sub-hourly profiles are preferred due to the need for fast demand response and integration with intermittent energy sources supplying the grid. Furthermore, knowledge of energy end-use is required to plan for both thermal and electrical needs. Electricity loads may consist of space cooling, refrigeration or appliance, light and plug (ALP) loads [5] and electric heating. Natural gas heating loads can often be divided into space heating, hot water and gas-powered appliances (such as cooking or clothes dryers). Extracting the energy required for heating and cooling from aggregate energy use measurements is valuable for designing thermal networks because most buildings do not have submetered data. Therefore, a building energy model capable of both prediction and disaggregation of electrical and thermal loads is required.

In the design phase of ICE-Harvest systems, predicted electrical and thermal demands for each building will aid in planning the layout, thermal storage sizing and equipment sizing of the system. For system controls, forecasted thermal loads are used to determine the amount of heat leaving or entering the thermal network from each building. This will help dictate whether energy sharing between buildings is

possible, if short or long-term thermal storage should be charged or discharged and if energy should be generated at the energy management centre.

Additionally, to evaluate these systems at a provincial or national scale, a generalized building energy model can be used for pre-feasibility studies. To determine the potential of ICE-Harvest systems on a large scale, predicted building loads are used at potential sites to estimate emissions reductions across the province. However, measured energy data is not available or easily accessible for all buildings to create individual building models. In this case, a generalized model can be used to predict energy use for unknown buildings based on similar buildings.

There are several approaches used to model building energy use. Physics-based building energy models can estimate disaggregated energy consumption by modelling energy flows based on engineering principles. Alternatively, many data-driven and hybrid models have been proposed that utilize measured utility data to model building energy demand. In recent years, the increased installation of smart meters to support grid modernization [6] has led to a large amount of measured data for individual building energy consumption. Figure 2 displays how Ontario's modernized grid helps manage supply and demand. The IESO acts as the system operator, responsible for coordinating the generation and distribution of electricity. This requires balancing supply from nuclear, hydro, natural gas and wind with demand from the consumers. Other technologies such as energy storage and demand response aggregation programs provide flexibility to manage times of peak demand. The smart grid allows communication and data transmission between all of these components to "optimize the usage of the electricity system" [6].
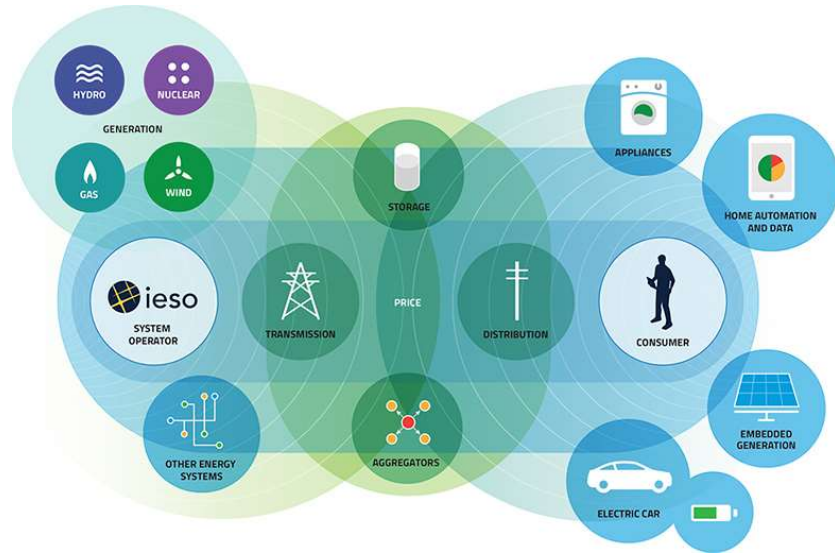
Figure 2: Grid modernization in Ontario [6]

Moreover, data from smart meters measuring consumer electricity consumption from appliances or electric vehicles aid in forecasting demand to determine the optimal supply mix. As part of the Ontario Smart Metering Initiative [7], smart or interval meters are mandatory in almost all Ontario buildings [8] for time-of-use pricing. Most installed smart meters record measurements at relatively low frequencies such as 5 minutes to 1 hour to reduce cost and the amount of storage required. They measure aggregate electricity usage which is the total electricity consumed by the building. Non-intrusive load monitoring [9] has been gaining traction as a method to separate measured aggregate electricity loads into individual appliances. With the increasing amount of energy data available, data-driven methods for forecasting building energy demand are becoming popular and can provide higher accuracy than physics-based models. However, purely data-driven methods may lose insight into building physics, such as distinguishing between contributors to thermal and base electrical loads.

Electricity use is influenced by many factors such as building control systems, occupants and weather. The dependency on weather is mainly due to space cooling needs in the summer if a building has electrified space cooling. More electrical work is required by the compressor and fan of the cooling

system as more heat and humidity enter the building due to outdoor conditions. Occupants are generally more difficult to predict due to their irregular behaviour.

On the heating fuel side, the majority of buildings in Ontario use natural gas [10][11] and measured data is often available in the form of monthly gas bills. Thus a method of temporal disaggregation is necessary to predict gas space heating demand at an hourly rate.

This thesis aims to create simple data-driven building energy models used for designing and controlling community energy systems. The models are trained on aggregate utility data and predict disaggregated thermal and base loads. For use in the application of thermal networks and energy sharing between buildings, specialized cooling models for supermarkets and ice rinks were proposed, since they have unique refrigeration requirements that will reject more heat than conventional buildings. An electricity model is proposed to predict and disaggregate hourly electricity use into space cooling, electrical baseload and refrigeration (if applicable) loads. This model is also evaluated in a generalized form, where similar buildings are used to predict energy consumption for an unknown building. A natural gas model is also proposed that increases the space heating prediction resolution from monthly to hourly. Furthermore, through analysis of the data and model results, factors influencing building performance can be identified.

An overview of the work is as follows. Chapter 2 provides a literature review of different building energy models from physics-based to statistics-based. It also explores common algorithms used in data-driven building energy models and load end-use disaggregation approaches. Chapter 3 gives an overview of the dataset used in this thesis. It also describes the modelling methodology used for the proposed hourly electricity and natural gas models and verifies them with synthetic data. Chapter 4 displays model results for the full building database, predicting total energy use. Chapter 5 provides conclusions and recommendations for future work.

Chapter 2

2 Literature review

2.1 General building energy model types

2.1.1 Energy modelling methods

Building energy models can be classified into three general types: white-box, black-box and grey-box models. Descriptions of each of these model types are provided below.

2.1.1.1 White box

White-box or physical models use physical laws and partial differential equations to simulate building energy flows [12]. They have the advantage of being able to simulate retrofit scenarios by modifying the physical model. They use methods such as computational fluid dynamics (CFD) or a nodal (one-dimensional) approach to model energy use [13].

CFD methods provide a high level of detail by solving the flow field in multiple small control volumes that constitute the entire building. For example, Bellache et al. [14] created a detailed 2D numerical model of heat transfer and airflow in a Montreal ice rink. They predicted daily heat transfer to and from the ice sheet by convection, radiation, condensation as well as ice resurfacing. Partial differential equations were developed for the walls, inside air, external/internal surfaces and the ice sheet, then solved using the SIMPLE algorithm. The model was validated by Ouzzane et al. [15] with temperature measurements at the ice level, brine chiller return and supply and heat measurements for heated and lighted zones. While detailed predictions of all building energy flows are supplied using CFD techniques, it requires significant computational effort.

A simpler nodal approach is also used where each building zone is assumed to have homogeneous characteristics (e.g. EnergyPlus, ESP-r and TRYNSYS programs). Schiefelbein et al. [16] used simulated archetypes, taking advantage of open-source GIS data from OpenStreetMap [17] which was tested on a block of 55 homes in Germany. OpenStreetMap provides data on building geometry, construction year and type, but data quality and availability vary greatly by building or region. A data-enriching method was developed to estimate missing parameters for buildings with insufficient data. They used building type and location to predict parameters based on similar buildings which were then input into the physical building models.

In a similar vein to white-box models, calibrated simulation models use measured data to calibrate a physical simulation model which can be used to predict how energy is distributed by end-use [18]. However, there are often multiple solutions for the simulated model to match measured data, adding uncertainty to the model. Iyer et al. [19] calibrated a physical model in EnergyPlus to disaggregate supermarket loads into weather- and non-weather-dependent components. During the winter, it was assumed no space cooling equipment operated, so all weather-dependent electricity consumption in the winter was attributed to refrigeration. In the summer, the weather-dependent load was assumed to consist of both refrigeration and space cooling loads. Refrigeration loads were 1.2 to 9 times greater than space

cooling loads since they were maintained between 2.2 to -23 °C compared to 24°C for air-conditioning. The authors also noted that cool air escaping from open display refrigeration cases can offset space cooling demand by 58-100%. Occupancy was seen to have little impact on load due to the dominance of the scheduled refrigeration loads. Overall, 45-77% of the store's total electricity use was from weather-independent loads such as lights, cash registers or computers.

2.1.1.2 Black box

While white-box and calibrated simulation models require detailed modelling of the building heat transfer physics and refrigeration requirements, black-box or statistical models use purely data-driven methods to map model inputs to outputs [20]. Despite no knowledge of the physical system, black-box models can be good predictors, making them ideal candidates for problems where the underlying mechanisms are not fully understood or known. In applications where the underlying mechanisms are understood, black-box models have been shown to have comparable accuracy to white-box models [21]. Advanced algorithms can handle complexity well, however sufficient training data is required to produce a robust and accurate predictor. Additionally, black-box models provide less physical understanding when modelling the energy flows of buildings compared to white-box models.

2.1.1.3 Grey box

The third type of model is a grey-box or hybrid model that combines white-box and black-box modelling techniques [22]. There are two types of grey-box models: the first combines a simulated physical model with a data-driven approach (e.g. [19][23][24]) while the second uses knowledge of the governing physical equations to constrain the form of the data-driven model (e.g. [12][25][26][27]). Grey-box models combine the advantages and disadvantages of both white-box and black-box models [22]. Some physical interpretability can be maintained; however it is not as in-depth as a white-box model. Compared to a black-box model, however, grey-box models incorporate assumptions of the underlying physical mechanisms. De Rosa et al. [27] used a thermal resistance and capacitance (RC) model to

account for building thermal mass combined with partial differential equations for the heat transfer mechanisms for the internal air, walls, floor and windows. While the resistance-capacitance model required fewer inputs than a white-box model, knowledge of several physical parameters were still required including internal air volume, wall construction, wall mass, floor construction and window areas. Many studies neglect the effect of thermal mass (e.g. [26][28]) or require knowledge and assumptions regarding building construction (e.g. [27][29]) to account for it properly. John et al. [30] analyzed thermal response patterns in over 10 000 residential buildings using smart thermostats measurements of indoor and outdoor temperatures and HVAC equipment run times. The response of the house was modelled using a simplified first-order resistance-capacitance thermal model with exponential decay. The range of effective time constants was found for each month using histograms and kernel density estimations. Different time constants between the summer and winter were identified which may be due to occupants opening windows in the summer, which was also noted by Neto and Fiorelli [21]. Time constants for the winter season were between 15 to 55 hours, while time constants for summer varied from sub-hourly to 18 hours.

2.1.2 Aggregate models

In addition to individual building models, aggregate-scale models exist for neighbourhoods or countries to evaluate energy conservation measures and plan on large scales. Models at aggregate scales are often modelled using two approaches: top-down and bottom-up.

2.1.2.1 Top-down

Top-down models use aggregate data to account for demographics, hours of occupancy, indoor climate control, shading, wind abatement or the urban heat island effect [31]. They look at the total usage of a large group of buildings. The top-down models are generally not concerned with the end-use of individual buildings, making them suitable for applications concerned only with the aggregate energy use of a group of buildings.

2.1.2.2 Bottom-up

Bottom-up models can be preferable to top-down methods when both the individual building and aggregate use are of interest. Bottom-up models sum the predicted or measured energy consumption from individual buildings to determine cumulative consumption (e.g. [16][25][32][33][34]). Representative buildings or archetypes are commonly used for bottom-up models by using a general model while maintaining the impact of influential parameters during aggregation. Some accuracy is lost through generalization but the need for metered data from every building is not required. For example, George and Swan [5] used a bottom-up approach and identified homes that use electric or non-electric space heating by comparing electricity use during the mild and winter seasons. The model aimed to predict grid demand peaks accurately whereas previous models had the potential for unrealistic peaks and valleys from aggregating a small sample of electricity profiles [23]. It was found that two houses with similar overall electricity use could have different hourly load patterns and technologies. The authors were able to produce 62 unique annual profiles using data from Ottawa and Nova Scotia but noted it is not enough data for the results to be statistically significant since Canada has over 7 million single-detached houses.

2.2   Input features

2.2.1 Dimensionality reduction

Feature selection is an important step in data modelling. Using more input features is not always desirable since it may reduce performance and increase computational costs. Dimensionality reduction chooses which features to use as inputs. It can be performed using expert knowledge by manually selecting features (e.g. [32][35]) or with a data-driven approach (e.g. [36]). For example, Smpokos et al. [37] used a backward search algorithm to select suitable weather features for a multivariable linear regression model of data centre energy consumption. Backward elimination starts with all the regressor features and each iteration removes the feature with the least significance in the model. It is simple but has the limitation that once a feature is removed, it cannot be added back. Alternatively, Dhar et al. [38]

used forward search while Granell et al. [39] used a brute-force method to search all combinations of features. The brute-force method will find the best combination but requires greater computational effort and may only increase performance by a small increment compared to forward or backward search. Due to the large number of feature combinations tested, the authors did not perform sophisticated parameter tuning for some models which could improve performance further.

Principal component analysis (PCA) is another method to select transformed features based on variance. First, the input data is transformed into a new space using eigendecomposition of the covariance matrix, to find the directions of greatest variance. This produces a new set of uncorrelated features that are a combination of the original features [36]. Features with greater variance are selected under the assumption that they are more important for the model. However, the unsupervised nature of PCA can be a disadvantage as the target feature is not considered when selecting features. Reddy and Claridge [40] used a synthetic dataset to test multiple regression with principal component analysis (PCA) to address collinearity between weather regressor variables. They determined that PCA was usually better when regressor correlation was greater than 0.7 between one set of variables, or for a low R^2 model ($R^2 <$ 0.5) if correlation coefficients of about 0.4 or more existed between more than one set of regressors. Their results were inconclusive for high R^2 models and the general guidelines were case-specific since there were several exceptions. Alternatively, Lü et al. [12] used sensitivity analysis and singular value decomposition (SVD) to select significant model parameters.

2.2.2 Weather features

Due to their impact on building thermal loads, weather parameters are commonly used as input features. Temperature is the most common [20] and degree-days are also commonly used (e.g. [23] [24][25][27][28][32][41][42]). Cooling degree-days (CDD) or heating degree-days (HDD) represent the amount of cooling or heating, respectively, required in a specific location based on the outdoor temperature [43]. Timescales other than days can be used such as degree-hours [28]. Degree-days are calculated using the difference between the outdoor temperature and a base temperature. The base

temperature is often set to the indoor setpoint [41] but it can also represent the outdoor temperature at which the heating or cooling system turns on and off.   The equations for cooling and heating degree days are shown below:

$$\text{CDD} = \max\big((\text{T}_{\text{outdoor}} - \text{T}_{\text{base,cool}}), 0\big) = (\text{T}_{\text{outdoor}} - \text{T}_{\text{base,cool}})^{+} \tag{1}$$

$$\text{HDD} = \max\big((\text{T}_{\text{base,heat}} - \text{T}_{\text{outdoor}}), 0\big) = (\text{T}_{\text{base,heat}} - \text{T}_{\text{outdoor}})^{+} \tag{2}$$

The + notation indicates that CDDs and HDDs are positive. When the degree day value is equal to zero, the predicted space cooling and space heating energy use due to temperature will be equal to zero.

To improve upon CDDs and HDDs, variable-degree day (VBDD) models compute regression models with different base temperatures and take the result with the best statistical fit [18].   While the internal setpoint is not known, the base temperature can be thought of as the outdoor temperature at which heating or cooling systems turn on or off. VBDDs were used in Fels' PRInceton Scorekeeping Method (PRISM) [41] which used monthly energy bills and weather data to evaluate retrofit savings in residential buildings. The use of VBDDs allowed for the prediction of the base temperature of the heating degree days along with the heating slope (kWh/°C). The portion of energy use linearly correlated with outdoor temperature was assumed to be for space heating while the base use was assumed to be a constant amount for hot water heating.

The downside to using a degree-day method for heating is the assumption that when the outdoor temperature is above the base temperature, energy use is constant because the space heating system is not operating. However, this is not always true as hot water use may have a relationship with outdoor temperature due to seasonal temperature changes. Residential water heater energy consumption variation has been observed to vary with outdoor temperature in the United States by Masiello and Parker [44] and in Australia by Hart and de Dear [45]. The authors noted that this may be due to changes in occupant behaviour or the mains water temperature. Chmielewska [46] found that the average monthly water main temperature in Poland could vary between 1.7°C in the winter to 22.2°C in the summer. Variation in hot

water heating energy will depend on the location's water source and seasonal variability. Residential water heater energy consumption in Canada was studied by Aguilar et al. [47], but seasonal data in Canada was not available. However, the water main temperature and water heater energy consumed are expected to vary in Ontario because the province experiences a range of temperatures. Additionally, most municipalities studied in this work get water from Lake Ontario or groundwater sources. As shown in Figure 3, the seasonal temperature variation in Lake Ontario can vary between 0 and 20°C from winter to summer. Therefore, degree-day approaches will not always represent hot water heating use accurately.
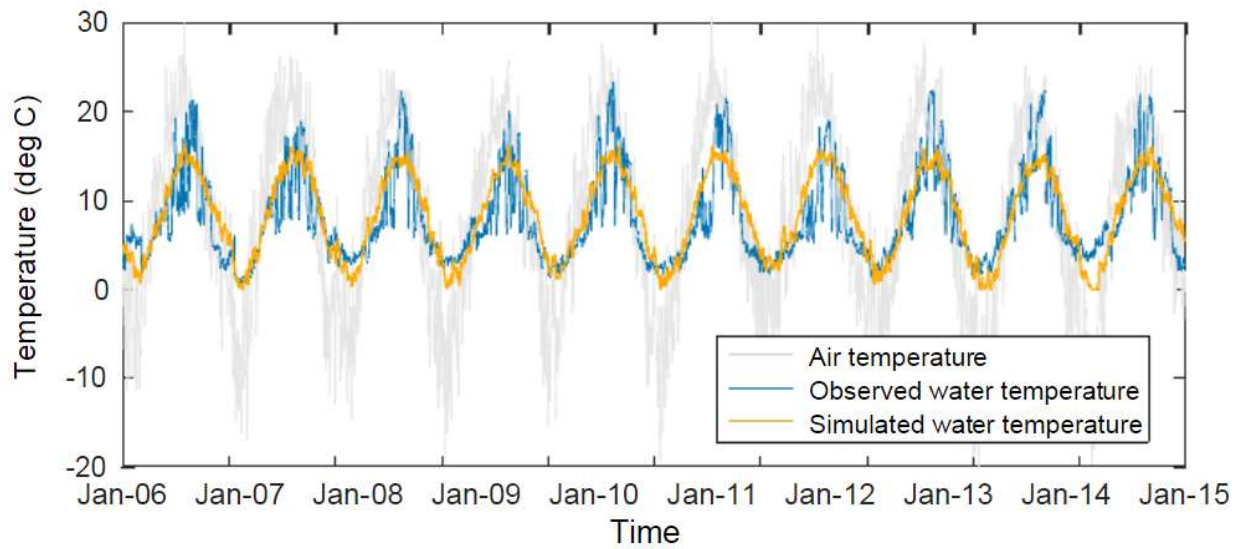
Figure 3: Lake Ontario intake water temperature at Darlington from 2006 to 2015 [48]

Furthermore, instead of using a typical degree-day term, Afshari and Liu [31] defined a composite temperature consisting of smoothed temperature (allowing for thermal mass effects) and sol-air temperature. Sol-air temperature accounts for the envelope heat transfer due to convection and radiation. It can be calculated from the 2017 ASHRAE Handbook: Fundamentals [49]:

$$T_{solair} = T_{outdoor} + \frac{\alpha E_t}{h_o} - \frac{\epsilon \Delta R}{h_o}$$

(3)

Where:

T_{solair} = solair temperature (℃)

$T_{outdoor}$ = outdoor air temperature (℃)

α = surface absorptance

E_t = total solar radiation incident on the surface $\left(\dfrac{W}{m^2}\right)$

h_o = effective coefficient of heat transfer by longwave radiation and convection on surface $\left(\dfrac{W}{m^2 * K}\right)$

ε = surface emittance

ΔR = difference between long-wave radiation incident on the surface from surroundings/sky and radiation emitted by a blackbody at outdoor temperature (W/m²); 20 for horizontal surfaces; 0 for vertical surfaces

2.3   Statistical methods for black and grey box models

Along with feature selection, the choice of a suitable algorithm for black-box and grey-box building energy models is important. Algorithms used in building energy models are outlined in the following section.

2.3.1 Regression

Regression is used for predicting continuous variables, as opposed to classification which classifies samples into groups.

2.3.1.1 Linear Regression

Ordinary least squares (OLS) linear regression fits a line to data by minimizing squared error. Multiple linear regression (MLR) uses multiple features to fit a hyperplane to data. A fast and simple algorithm, linear regression is generally less accurate than complex machine learning algorithms or white-box models. The output variable is modelled as a linear sum of the input variables multiplied by the regression coefficients as shown in Equation 4, so some physical interpretability can be maintained.

$$f(X) = \beta_0 + \sum_{j=1}^{p} X_j \beta_j \tag{4}$$

Where:

X_j = input vector [1 x p]

β_0 = intercept

β_j = coefficient of feature j

p = number of features

Ghiaus [50] used a linear regression model with temperature to evaluate building performance but used data between the 1st and 3rd interquartile ranges to help with noise. The model created 1-degree-C bins based on temperature and used the mean energy consumption for each bin.

Change-point models

Kissock et al. [18] found that Fels' degree-day method [41] was not suitable for commercial buildings that require simultaneous heating and cooling. They developed a 5-parameter change-point model. Change point models (e.g. [18][25][51][52][53]), do not assume constant heating or cooling when the outdoor temperature is below or above the base temperature, respectively. They model two or more lines that meet at a change-point temperature separating the cooling and heating seasons. Similar to the base temperature in degree-day models, the change-point can be set manually or determined using a grid search. It is also possible to have more than one change point.

Schrock and Claridge [51] also used a change-point model to forecast the hourly and daily electricity demand in a supermarket. The change point allowed the model to account for the different cooling slopes during the summer and winter. The data was subset by cooling and heating as well as nighttime and daytime. During the day, it was observed that the temperature dependence was more evident due to HVAC systems being turned on. Ruch et al [52] built on Schrock and Claridge's [51] model by combining a change-point model, shown in Figure 4, with principal component analysis

regression (CP/PCA) for commercial building energy use. A case study was done on a supermarket using sales data, dry-bulb temperature, solar radiation and humidity as regressors. The data was first split into 2 sets based on a change-point temperature. PCA regression was then performed separately on the two subsets. It was found that PCA helped with correlation and stability while the change point model helped select better predictor variables for each subset of data. For example, solar radiation is significant in the cooling regime but not at the base level.
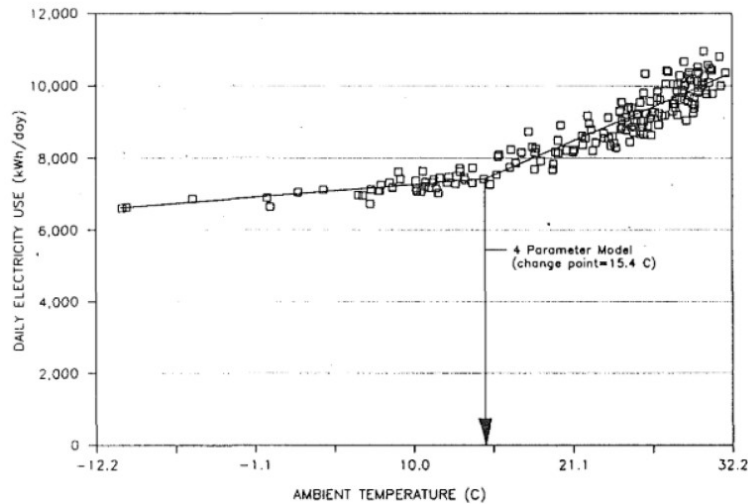
Figure 4: Change-point model for daily electricity consumption versus outdoor temperature [52]

Change-point models were also used by Heidarinejad et al. [24] to create a database of steam, chilled water and electricity use for buildings on two university campuses. Change-point models were created for each of the three energy types with weather data as regressors. Furthermore, buildings were classified as external-load dominant, internal-load dominant or mixed-load dominant based on the R^2 and coefficient of variation determined from linear regression.

Penalized linear regression

Penalized linear regression models can produce more robust models than ordinary least squares (OLS). While OLS linear regression aims to reduce the sum of squared errors, penalized regression models add a penalty based on the magnitude of the regression coefficients [54]. This prevents the

regression coefficients from growing large. In the case of Least Absolute Shrinkage and Selection Operator (LASSO) regression [36], an L1 penalty is used as shown in Table 1. With LASSO, some coefficients are reduced to 0 and can be excluded from the model, giving it natural feature selection abilities. Similarly, ridge regression uses an L2 penalty, shown in Table 1. Both equations for LASSO and ridge regression have a hyperparameter, λ which determines how much the coefficients are penalized and therefore shrunk. The closer λ is to 0, the more the solution will resemble the ordinary least squares solution.

Table 1: Ordinary least squares, LASSO and Ridge linear regression

Linear regression type	Minimized function	
Ordinary Least Squares (OLS)	$\sum_{i=1}^{N} \left(y_i - \beta_0 - \sum_{j=1}^{p} x_{ij}\beta_j \right)^2$	(5)
Least Absolute Shrinkage and Selection Operator (LASSO)	$\frac{1}{2}\sum_{i=1}^{N} \left(y_i - \beta_0 - \sum_{j=1}^{p} x_{ij}\beta_j \right)^2 + \lambda \sum_{j=1}^{p} |\beta_j|$	(6)
Ridge	$\sum_{i=1}^{N} \left(y_i - \beta_0 - \sum_{j=1}^{p} x_{ij}\beta_j \right)^2 + \lambda \sum_{j=1}^{p} \beta_j^2$	(7)

Other non-linear regression models can be used such as quadratic or logistic regression which may be more suitable depending on energy-use trends. Nageler et al. [55] used a bottom-up approach while comparing a white-box GIS-based simulation and a black-box energy signature approach to model heating for 35 buildings. Archetypes were determined based on construction materials and energy use. For the white-box model, not all exact building parameters were known so the model was calibrated by varying the infiltration rate. The data-driven approach used a 4-parameter nonlinear sigmoid function to model heat demand based on weather variables. The sigmoid function is another method to capture the

non-linear relation with temperature. The model was developed for each archetype and used to generate an annual profile of daily demand which was then converted to hourly using a statistical hourly profile. They found that the physical model matched better at an hourly scale than the sigmoid approach because it could factor in estimates of user behaviour. Additionally, the sigmoid approach did not consider thermal inertia sufficiently while the physical approach overestimated thermal mass.

2.3.1.2 Support Vector Machine

Support vector machine (SVM) regression is an algorithm capable of modelling nonlinear relationships used in several building energy models (e.g. [12][39][56]). It builds on the SVM classifier proposed by Cortes and Vapnik [57] which separates data by maximizing the margin width of the separating hyperplane. The hyperplane is defined based only on the samples on the margin which are called the support vectors [36]. A penalty can be applied to misclassified points when determining the hyperplane which will result in a soft or hard margin; a hard margin will classify training data well but can result in overfitting. Support vector machines also use a kernel function to map data to a higher dimension where it is more separable. Support vector machine regression is similar to classification where the support vectors define the hyperplane. It also uses a hyperparameter to define a soft or hard margin and a kernel function to handle nonlinear relationships. A threshold parameter is chosen which determines which samples are the support vectors that define the model.

2.3.1.3 Neural Network

Neural networks (NN) simulate a biological neural network using multiple processing elements arranged in consecutive layers, that produce outputs based on an activation function [23]. The outputs are combined through different weightings within each layer and used as input to the next layer. The weightings are selected through an optimization process. Different neural networks are used such as recurrent neural networks (RNN) and convolutional neural networks (CNN). They can be accurate for modelling occupancy use trends that are not understood using engineering methods [23]. However, as

with most black-box models, the physical meaning of parameters is usually lost and a considerable amount of training data is necessary.

Neto and Fiorelli [21] showed that ANN has comparable accuracy to white-box models for forecasting energy use to evaluate energy conservation measures. A white-box model was created using a design-day simulation in EnergyPlus and calibrated by adjusting the sky clearness value. The authors had difficulty accounting for occupants opening or closing windows, similar to John et al. [30]. They modelled windows as always closed which overestimated cooling energy consumption. It was found that for 80% of the period, the results were within 13% of the measured data. Conversely, the ANN model was a good predictor and required fewer building physical parameters as input, using only weather parameters. The predictions were within a 13.5% error range for 85% of the data. However, the black-box model did not provide enough physical insight to evaluate retrofits like the white-box model.

2.3.2 KNN

K-Nearest Neighbours (KNN) uses distances (e.g. Euclidean distance) calculated based on input features to determine the closest points in the training set to an unknown sample [36]. The neighbours are then used to estimate the unknown sample's value. The number of neighbours used, K, is a parameter that must be chosen during parameter tuning.

Granell et al. [39] tested four methods, including KNN, while predicting electricity daily load profiles for supermarkets. KNN, ordinary least squares step-wise regression, artificial neural network and support vector machine regression were tested, however in-depth parameter tuning for ANN and SVR was not feasible. The average errors ranged from 12-20% depending on if data was partitioned based on season or temperature. KNN performed best when data was partitioned by temperature while OLS worked best with data partitioned by season. Furthermore, the simpler algorithms sometimes outperformed the more complicated ANN and SVR algorithms. The authors noted that the model could be improved by using more supermarket data and features such as the number of customers, HVAC or

refrigeration technology, building age, construction type, materials and insulation. Additionally, while many models predict future usage based on the same building's historical data, this model used known supermarkets to predict an unknown one. Supermarkets can vary by building properties, human factors or weather conditions adding a challenge for predicting an unknown building. A leave-one-out technique was used to select predicting features and model parameters. Similar to [58], the data was subset based on time frames and temperature, but at a coarser scale using season and average temperature.

2.3.3   Time series analysis

In addition to weather, the influence of occupancy and building scheduling is significant when evaluating building performance [59]. Therefore, methods of obtaining detailed predictions and analysis of buildings' operation hours, peak- and base-use and HVAC scheduling are valuable. Techniques reserved for time series data can be useful for gaining insight into building energy use over time.

2.3.3.1 Smoothing

Smoothing algorithms can remove noise from data to reveal the underlying trend. Some popular smoothing methods are moving average, weighted moving average and exponential smoothing [60]. Moving average simply takes the average of a set number of observations within a window which is slid along the time series to get the moving average at each point. A weighted moving average is similar to a moving average but further observations are given smaller weights. Exponential smoothing is a version of the weighted moving average where the weights decay exponentially as they are further from the predicted point.

2.3.3.2 Autoregressive Moving Average (ARMA) models

Autoregressive (AR) models are multiple linear regression models using past values of the target variable as regressors [60]. AR models can be combined with moving average (MA) models, which use past forecast errors as regressors, to create ARMA models. Lü et al [12] used an ARMA and physics-based model to account for heterogeneous buildings, which have usage patterns that vary greatly across

the same building type such as sports halls. First, thermal loads were calculated by simplifying partial differential equations representing the heat flows from the building. In the second phase, an ARMA model was used to profile the thermal models. The convex hull technique was then used to model heterogeneity to account for extreme cases. The model was tested on four sports buildings, including swimming and hockey halls, and compared with SVM and ANN. The model was comparable to SVM and required less training data as SVM would require a minimum of 23 buildings to prevent overfitting. When forecasting a building's use based on its historical use, the model performed well. However, when using one building to predict another, similar to Granell et al. [39], the model was unable to estimate the loads properly.

Yun et al. [58] tested an autoregressive model with external inputs (ARX) to predict 1-hour ahead thermal loads. The addition of external weather variables helped combine the strengths of MLR and AR models to account for both thermal mass and weather effects. A comparison of MLR, AR, ARX, neural network and indexed ARX methods was performed. Based on the standard deviation, coefficient of variation and expected error percentage, the indexed models outperformed the neural network, however they noted the neural network could be improved by modifying it for time indexing as well.

2.3.3.3 Classical time series decomposition

Classical time series decomposition [61] decomposes a time series into three components: seasonality, trend and remainder (error). There are two types of classical time series decomposition: additive (all 3 components sum to the original series) and multiplicative (all three components are multiplied to get the original series). For additive decomposition, moving average smoothing is used to estimate the trend component. The detrended series can then be computed and the seasonal component is estimated by averaging and adjusting the detrended values for each seasonal period. The remainder is the remaining error component not predicted by the trend or seasonal components. Multiplicative decomposition is similar, but instead of subtractions, divisions are performed.

Pickering et al. [61] used differencing and classical time series decomposition to analyze the HVAC schedule and occupancy trends for six commercial buildings. First, the data was subset by weekday type, heating or cooling season and solar load level to consider seasonality and weather. Sub-setting the model by high or low solar load was shown to improve model performance as solar irradiance had a significant impact on some buildings' energy use. The classical time-series decomposition model produced a relative building error of 2.5%. Furthermore, among the six buildings, occupancy and HVAC trends were seen to vary greatly, despite all being commercial office buildings.

2.3.3.4 Fourier series

Similar to time series decomposition, Fourier series are used to consider the seasonality of time series data such as daily, weekly or annual scheduling.

Dhar et al. [38] combined Fourier series representations with weather variables to predict commercial building energy use. First, data was subset by day type for different schedules on weekdays, weekends and holidays. Weather-independent use was considered first, using a Fourier model based on the hour of day and selecting significant Fourier frequencies using forward selection. For weather-dependent use, a regression model using specific humidity, temperature and solar radiation was created. However, to account for the variation of weather-driven use based on the hour of day, the regression coefficients were represented by Fourier series. The methodology had similar performance to 24 individual models for each hour of the day. However, the Fourier terms could represent energy use with fewer coefficients and the important Fourier frequencies provided insight into the load profile shape.

Niu et al. [62] predicted HVAC loads by first extracting HVAC loads from total electricity using a Fourier series decomposition method. A Fourier series-based decoupling was used to account for daily seasonality due to scheduling as well as the impact of temperature on HVAC loads. The decoupled HVAC portion of the load was then predicted using five data-driven algorithms including ARX, discrete

and continuous Bayesian Networks, state-space (SS) and subspace state space (N4S). The authors recommend the use of the two Bayesian Network models which performed best.

Afshari and Friedrich [31] used a model combining Fourier series representations and non-linear regression to account for scheduling and weather. Energy use was divided into weather-dependent and independent to separate the cooling portion with 43% and 62% of the annual electricity consumption and peak demand attributed to cooling, respectively. The model parameters retained some significance and were modified to represent energy conservation measures such as system upgrades and retrofits and evaluated using sensitivity analysis.

2.3.4 Clustering

The majority of algorithms thus far have been supervised techniques where the model is trained using labelled output data. Clustering is an unsupervised technique used to assign objects to groups with similar properties. It is helpful for archetyping applications in bottom-up models as well as for classifying buildings based on performance.

2.3.4.1 K-means

K-means clustering is a commonly used approach that divides samples into k clusters [35]. This is achieved by minimizing the sum of distances, such as Euclidean distance, of each sample to the cluster centre. As stated in the name, the mean of the cluster is used to represent the samples within. Similar to KNN, K is a parameter that is tuned by the modeller. K-means clustering does not perform well for clusters of different sizes, densities or with data containing outliers.

In a study conducted by Luo et al. [59], benchmark profiles were determined through clustering to compare energy use patterns of 2000 buildings in California. They were interested in the shape of daily load profiles for grid peak planning. Due to a lack of area data, use was normalized by peak load, providing an alternative way to analyze scheduling characteristics but less insight into overall efficiency.

Daily load profiles consisting of twenty-four hourly measurements were clustered based on building type, size, age and climate zone using k-means clustering. Additionally, performance indicators were calculated for buildings including hourly mean, peak and base load as well as shape parameters such as peak-base load ratio and workday/non-workday load ratio. The representative profiles were limited to California since weather data was not considered, but the techniques could be extended if all models are split by climate zone. Most models will be limited to the region of their training data due to cultural and scheduling differences across different countries which have a large impact on occupant behaviour.

2.3.4.2 Hierarchical

Another clustering approach is hierarchical clustering which has two types: agglomerative and divisive [35]. The agglomerative method uses a bottom-up approach by starting with individual clusters, then pairing and merging them with the closest ones. Divisive clustering, in contrast, uses a top-down method; it starts with one cluster and splits the clusters at each level. Hierarchical clustering is easy to implement however it can be computationally complex.

2.3.4.3 DBSCAN

Density-based spatial clustering applications with noise (DBSCAN) is an algorithm that divides points into dense regions separated by less dense regions. It is less sensitive to noise and outliers; however it requires complex computations.

Hossain et al. [63] used statistical markers and DBSCAN clustering to classify building operational patterns. First, markers were used to distinguish between day types, HVAC on/off times and base-to-peak load to evaluate energy conservation measures. Daily operational patterns were identified by splitting the data into seven subsets for each day of the week and applying agglomerative hierarchical clustering to find similar clusters. Weekday-weekend patterns of 5-2 were identified in all six buildings. HVAC schedule times were assumed to be at high-density occurrences of first-order differences in

energy. The base-to-peak load ratio compared minimum energy consumption during non-occupied hours to the maximum during occupied hours to analyze building performance.

Ali et al. [35] used clustering techniques to partition buildings into archetypes for a bottom-up model. K-means, hierarchical, density-based and k-medoids clustering were applied to energy performance parameters such as building U-values, building area and fuel source. Feature extraction from energy performance certificates was done based on "expert interpretation" and existing practices. A total of thirty-six building archetypes were identified from the eleven dwelling types to be used. Clustering techniques were evaluated based on cluster compactness, separation and roundness, with the K-means algorithm performing best based on these properties.

2.3.5   Combined and hybrid approaches

Khalilnejad et al. [64] studied methods of extracting HVAC schedules using Haar wavelets, piecewise regression and k-means clustering. Energy time series data was filtered using a Haar wavelet transformation to identify when large-scheduled equipment turned on and off. Additionally, if a high correlation with outdoor temperature was shown, the equipment was assumed to be HVAC-related. Two piecewise regression models using exterior temperature were created for occupied and unoccupied times to estimate the setpoint and cooling slope. K-means clustering was then performed on the heating and cooling slopes to find buildings with similar HVAC operations, with three categories identified: high, low or no HVAC consumption. A median potential savings of 1.6% by reducing baseload use and 2.1% by rescheduling HVAC hours was estimated.

Swan et al. [23] used a hybrid approach combining a neural network and a physical model in a bottom-up model of single-family homes. An artificial neural network was used to model appliance loads and domestic hot water (DHW) to capture occupancy trends while considering socioeconomic and environmental factors. The ANN model produced yearly DHW, appliances and lighting energy sums which were converted to hourly using profiles developed by Armstrong et al. [65] and Jordan and Vajen

[66]. A physical simulation was then created to model heating and cooling by inputting the appliance/lighting and DHW energy use predicted by the neural network. Statistical distributions were randomly assigned to various homes to maintain distribution percentages and scaled up to a national level. The methodology was compared with the top-down Canadian Residential End-Use Model (REUM) [43] estimates which use average year weather data for all house types. The proposed model was able to consider furnace fan and boiler pump as part of appliance/lighting loads which REUM does not include.

A hybrid archetyping approach was used by Pasichnyi et al. [32] to evaluate two scenarios on a city-wide scale for Stockholm, Sweden; conversion to electric heating and building retrofits. Electric heating was modelled using simple linear regression applied to heating degree days. Retrofits were evaluated using a hybrid approach by first segmenting archetypes based on spatial, socio-economic, structural and energy performance factors. The average features of each archetype were then modelled in EnergyPlus to create representative building models. This allowed for simulations of proposed retrofits, but the input parameters of simulated models must be known or assumed which can introduce errors into the model.

Similarly, Sokol [33] used a hybrid approach with simulated building archetype templates. Multivariate regression based on energy use intensity (EUI) was used to create initial simulation templates using weather, energy and building input data. Parameters related to building construction, systems and occupants were gathered from polls and codes, while geometric parameters were gathered from 2D GIS footprints and LiDAR data. Parametric analysis was used to estimate random occupancy-driven parameters which are often difficult to account for with pure white-box models. The methodology was tested on a neighbourhood of 453 buildings in Cambridgeport, MA, showing up to 18% mean goodness of fit and relative error under 6%.

2.4 Time series disaggregation

Ideally, measured hourly (or sub-hourly) data should be used to train an hourly energy consumption model. While most studies involve models with measured output data at the desired time scale, some buildings only have measured energy use available in the form of monthly bills but require hourly outputs. Thus, approximated models that have an input resolution lower than the output have been proposed.

Brideau [29] used a hybrid method to temporally disaggregate simulated monthly data to hourly, for evaluating energy conservation measures in low-rise residential buildings. A lumped capacitance model was created to up-sample the heating, cooling, plug and domestic hot water loads from simulated HOT2000 outputs. Three components output by HOT2000; envelope losses, internal and solar gains, were divided by monthly hours and scaled using hourly weather measurements and schedules from the National Energy Code of Canada for Buildings (NECB) [67] and the National Building Code of Canada (NBCC) [68]. The approach was tested against a complete building simulation in ESP-r of two houses in Edmonton for the first 15 days of February and August. The RMSD for the heating and cooling seasons were approximately 10% and 44% of their average loads respectively and peak cooling loads were found to be under-predicted.

Lamagna et al. [69] took a different approach to disaggregate monthly bills using time-of-use pricing for electricity use. They used breakdowns of the tariff subdivisions and constrained a reference profile to match the overall consumption over each subdivision. Their method was applicable for electricity bills where time-of-use pricing breakdowns were known but the use of a reference profile may introduce errors as each building may have a different hourly schedule.

Alternatively, Pagliarini and Rainieri [42] used annual natural gas use and hourly temperature measurements to predict the hourly heating demand used to model a thermal energy system with combined heating and power generation (TES/CHP) on a university campus. To predict the hourly heat

demand, they used a degree-day method with a dummy variable to account for when the heat was on or off. By assuming the heating demand to be linear with temperature, they solved for the heating slope and produced the hourly profile. Several assumptions were used such as a simple linear relation between energy consumption and temperature only, service hot water usage was grouped with space heating and neglect of thermal mass of the building. However, the authors argue that accurate load demands are not necessary for the goal of their TES/CHP model which was for optimizing controls since it will account for the errors and overall consumption remains the same. The authors improved on their previous model by creating a steady-state inverse model using a non-linear multivariate regression model for extracting hourly heating and cooling demand from monthly energy use [26]. An energy balance was performed on the building accounting for heat transfer occurring from sensible and latent transfer with the outdoors, solar radiation and internal sensible and latent heat gains. An objective function was used to constrain the sum of heat to the building as the heat from the monthly natural gas sum. This objective function was then minimized to solve for the non-linear multivariate regression (MVR) model.

$$q = K(T_i - T_e) + K_l(X_i - X_e) - A_{sol}I_{sol} - q_s - q_l \tag{8}$$

Where T and X were the known air temperatures and specific humidity ratios, respectively. The unknown parameters K, K_l, A_{sol}, q_s, q_l represented the overall sensible heat transfer coefficient, overall latent heat transfer coefficient, effective solar radiation collecting area, internal and latent heat gains. Similar to most grey-box equation models, the unknown parameters are significant within the context of this model but do not have true physical meaning. The model was evaluated using synthetic data modelled in TRYNSYS for multiple buildings with varying levels of outer insulation. The model disaggregated space heating and cooling with a coefficient of determination between 0.74 and 0.96, but as insulation levels increased, R^2 worsened due to neglecting building thermal mass in the short term.

Singh et al. [53] also created a hybrid inverse model, using yearly utility bill data, monitored data of internal loads, energy use and weather over a short period to get operational schedules. First, they created a 4-parameter change-point model using utility bills. The residuals of the initial model were then

regressed against lighting and equipment loads that were measured using short-term monitored data. Their method showed that approximately 2 months of measured high-resolution data was sufficient to combine with utility bills in predicting detailed energy use.

2.5   Non-intrusive load monitoring

Non-intrusive appliance load monitoring (NILM) or energy-use disaggregation, is the problem of disaggregating appliance-level consumption from total measured energy use [9]. As seen in Figure 5, an algorithm is trained and applied to aggregate electricity use data to disaggregate it into several appliances. The field has seen a large amount of growth with the increased installation of smart energy meters [70] as it can help guide energy conservation programs based on occupant behaviour without submetering individual appliances.
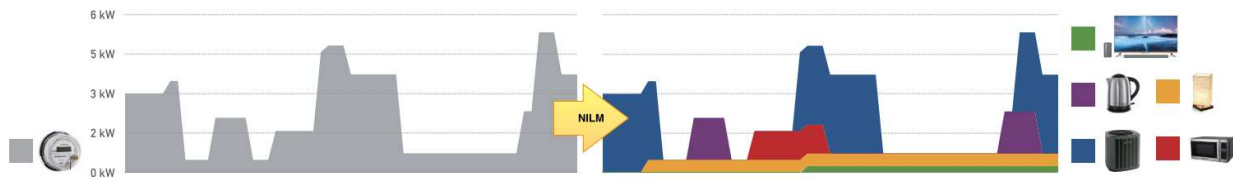
Figure 5: Example of non-intrusive load monitoring for a residential building [71]

NILM learning methods can be categorized into supervised and unsupervised. Supervised approaches use individual-appliance submetered data for training (e.g. [72]), whereas unsupervised methods use only aggregate data (e.g. [71][73][74]). Common algorithms in NILM are Combinatorial Optimization and Factorial Hidden Markov Models. Factorial Hidden Markov Models use hidden Markov models to represent appliance states (e.g. [75]). Combinatorial Optimization aims to solve for the optimal set of appliance states (eg. 0 or 1) that add to the aggregate energy use [9][75]. For example, Rodriguez and Makonin [71] used combinatorial optimization with a probabilistic knapsack approach to determine appliance states.

NILM approaches can also be classified according to timescale; earlier approaches focused on high-rate (greater than 1 Hz [72]) frequency data [76] which can capture distinct energy signatures [9] of appliances turning on and off. However, low-rate NILM is gaining traction as many smart meters only record data at low-rate frequencies from 5 minutes to 1 hour (e.g. [70][77][78][79]). For example, Srivastava et al. [73] combined regression, clustering and a Gaussian Mixture Model (GMM) to perform non-intrusive load monitoring (NILM) of small and medium commercial buildings. The authors used "usage-behaviour" based modelling instead of "appliance-based", to capture when large HVAC equipment or groups of equipment turned on or off. GMM was used to separate HVAC usage-behaviour modes and the working schedule and operational loads were estimated using the signed edges of energy differentials. A regression model with temperature was created for each HVAC mode and buildings were then clustered according to their heating coefficient similar to Khalilnejad et al. [64]. The methodology was evaluated using measured data from 8 buildings in North Carolina with a mean absolute percentage accuracy ranging from 80.8-89.5% for heating and 85.5-92.1% for cooling.

Cetin et al. [28] used a grey-box inverse model to predict disaggregated energy use (HVAC, baseload, variable load) for future months using historical monthly consumption data and high-resolution weather data. A thermodynamics model was created for HVAC energy; however a bin method was used to account for multiple values of indoor setpoints instead of using degree days. The steady-state model assumed that energy use is influenced most by conduction and neglected thermal mass due to the long timescale of monthly data. The model was tested on 3050 buildings, resulting in an 18% error when disaggregating energy consumption and an average of 2.7% error when forecasting.

2.6   Summary

Table 2. Building energy modelling studies sorted by methodology

A summary of algorithms and methods used for building energy models. Examples of input building-dependent features (e.g. construction or operation related) and building-independent features (e.g. weather features) are specified. The type of validation data is also specified; real data is measured data whereas synthetic comes from physical energy models or equations.

Method/ Algorithm/ Approach	Example building-dependent input features	Example building-independent input features	Validation data	References
Linear regression	Store sales data, light and equipment loads, operational and maintenance data, floor area use percentages	Outdoor temperature, global horizontal radiation, relative humidity, dew point temperature, wind chill, rainfall, atmospheric pressure, calendar parameters, sol-air temperature	Real	[32][37][39][41] [50][51][53][64] [73]
			Synthetic	[29][53]
Linear regression with PCA	Store sales data	Outdoor temperature, solar radiation, specific humidity	Real	[18][52]
			Synthetic	[40]
Nonlinear regression	Operational hours, internal setpoints	Outdoor temperature, relative humidity, wind speed, solar irradiation	Real	[31][50][55]
			Synthetic	[26]
SVM	Floor area use %, indoor temperature, ventilation rates, building schedules, construction materials, building geometry	Outdoor temperature, geographical location	Real	[12][39]
			Synthetic	[56]
ANN	*Occupants:* occupancy levels, house employment ratio, store sales data, population density, operational hours *Building construction:* floor area use %, building geometry, dwelling type, heated area %, window materials, wall materials, lighting data *Systems:* ventilation rates, equipment data	Outdoor temperature (dry-bulb and wet-bulb), relative humidity, wind speed, solar irradiation, soil temperature, wind direction	Real	[12][21][23][39]
			Synthetic	[58]
KNN	Supermarket floor area use % (e.g. food, sales, chilled etc.)	Outdoor temperature, geographical location	Real	[39]
Fourier series analysis	Time series parameters	Outdoor temperature, relative humidity, wind speed, solar irradiation	Real	[38][62][80]
Time series decomposition	Building type, building geometry	Climate zone, temperature, solar irradiation	Real	[61][64][81]
Autoregressive model	Occupancy levels, indoor temperature, ventilation rates, building construction materials, geometry, scheduling	Outdoor temperature, solar irradiation, relative humidity, wind speed	Real	[12][62]
			Synthetic	[58]
Statistical correlations	Time of use pricing, calendar parameters, building type, age, retrofits, area, HVAC system type	Outdoor temperature, solar irradiation, relative humidity, wind speed, dew point, sol-air temperature	Real	[5][24][25][30] [63][69]
Convex hull	Indoor temperature, ventilation rates, building construction materials, geometry, scheduling	Outdoor temperature	Real	[12]
Clustering	Building type, geometry, size performance parameters, building age, demographic information	Outdoor temperature, climate zone	Real	[35][59][64][73] [81][82]
Approximated thermal model	*Physical properties*: geometry, materials conductivities, absorbance and transmission coefficients, surface area, building thermal mass *Systems*: scheduling, indoor temperature, ventilation rates, heat transfer coefficient	Outdoor temperature, normal direct radiation, diffuse horizontal radiation, wind intensity, wind direction	Real	[12][28][30]
			Synthetic	[26][27][29]
Building simulation model	Building geometry, layout, operational hours, customer levels, occupancy, age, HVAC system type, construction materials	Outdoor temperature, dew point, relative humidity, pressure, wind speed, wind direction	Real	[19][21][23][24][33] [55]
			Synthetic	[34]
CFD model	Occupancy, lighting, ice resurfacing schedule, refrigeration system specifications, building geometry, building materials, material emissivity, heat transfer coefficients	Outdoor temperature, absolute humidity, sol-air temperature	Real	[14]
NILM	Submetered appliance loads		Real	[9][70][71][72][73] [74][75]

In conclusion, several modelling approaches are used in the literature to model building energy

use. White box models have shown suitable accuracy and provide an interpretable physical model.

However, they are computationally expensive, require extensive knowledge of building properties and do not capture occupancy well. On the other hand, black-box models are good at modelling randomness and do not require detailed knowledge of building geometry and material properties. However, while advanced algorithms generally produce highly accurate outputs, they often require a large amount of training data. ANN models may outperform SVR and linear regression, but modelling and computational effort can be saved if the accuracy requirements of the application can be met with a simpler algorithm. Furthermore, when disaggregated energy use is required, hybrid models can be more desirable. Therefore, grey box models provide a good compromise between white box and black box models.

Many hybrid methods require knowledge of building HVAC equipment, operating hours and construction materials to determine the heat transfer mechanisms and electricity use. If this data is available, the model will be more accurate, however detailed data is not always available to modellers. Therefore, models requiring few physical inputs are desirable, but there is a trade-off between accuracy and input data required. The ideal model will depend on application and data availability.

Many statistical models have been proposed for residential and common commercial buildings, such as offices [61][63], schools [24][42][69] or department stores [73]. Studies on cooling dominant buildings are less common, but knowledge of their cooling loads and therefore rejected heat is useful for designing systems with thermal energy harvesting and sharing. Thus a method for predicting and disaggregating the space cooling and/or refrigeration load from these types of buildings is valuable. While data-driven supermarket and data centre models have been proposed [7][28][36][37] most ice rink models are physics-based [14]. Due to their simultaneous heating and cooling loads, ice rinks can be complex to simulate using white-box models. A simplified data-driven model for this building type could provide an alternative and faster method of predicting ice rink energy use.

Lastly, most models are trained and tested on the same building's dataset to predict its future use. A model capable of predicting a building not used in training can be useful when detailed energy data is not available for all buildings. Archetyping methods are used to predict unknown buildings, but they are

generally used in bottom-up models, making the error due to generalization less significant. Therefore a generalized model that can use easily accessible data to predict a building hourly profile could be used for planning and designing new ICE-Harvest systems. Granell et al. [39] were fairly successful in predicting unknown supermarkets, however, Lu et al. [12] had difficulty modelling unknown sports halls due to a lack of training data.

In this work, k-means clustering is used to subset data by day types. Then penalized linear regression models using a combination of Fourier terms and weather terms are used for hourly electricity modelling, based on the work of Dhar et al. [38]. A natural gas model was also created using a similar linear regression approach to Pagliarini and Rainieri [26], to temporally disaggregate monthly heating values. Finally, a model of 5-minute predictions of ice rink compressor electricity use explored linear regression, support vector regression and a neural network for forecasting.

Chapter 3

3 Modelling methodology and verification

3.1 Modelling overview

There are several frameworks used for data mining with steps that can be generalized as data exploration, problem framing, data preparation, modelling and evaluation [83]. Data exploration involves visualizing the data and gaining an understanding of how it can be used to solve the problem. Data preparation involves cleaning and reformatting the data to a uniform format and ensuring its integrity. Modelling requires choosing a suitable model and training it with training data. The trained model is then evaluated using test data.

3.2 Building energy data description and exploration

The dataset used for this research was provided by utility partners and consists of measured electricity and gas time-series data from anonymized buildings around Ontario. All buildings are located

in southern Ontario, which is a region south of 44°N, and most are near Lake Ontario or Lake Erie. The region experiences four seasons throughout the year. Winter lows can fall below -15 °C while summer highs can be greater than 30°C. The dataset includes data from commercial, institutional and multi-unit residential buildings with high energy use, which are of interest for ICE-Harvest systems. Figure 6 displays the building types for which data is provided, broken down by energy type and timescale. Building types such as restaurants, hotels and grocery stores each have more than 75 buildings with hourly electricity measurements (shown in green). Conversely, other building types have fewer than 5 and their results are less representative of their type.
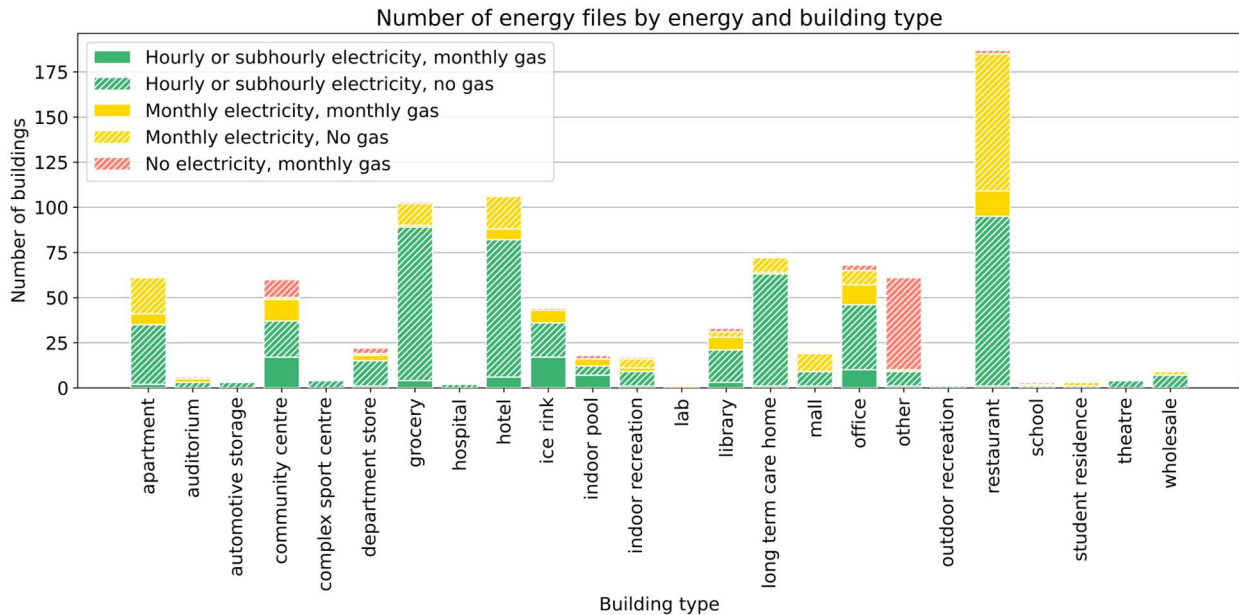
Figure 6: Database description: number of buildings with data by energy and building type

The measurement dates ranged from 2002 to 2020 for different buildings. Generally, the data does not show the early COVID-19 pandemic effects which occurred after March 2020. However, the trained models may not accurately depict building behaviour following the pandemic, since many aspects of energy use have changed. As more data becomes available, the models should be retrained to capture these effects.

Building energy data was received in a variety of file formats, measurement units and timescales from local distributing companies (LDC) and municipality properties owner. As seen in Figure 7; electricity use is measured for each building by the smart meter which is managed by the LDC. Electricity data was provided at 5-minute, 15-minute, hourly or monthly time increments depending on the building and meter type. Electricity measurements were provided in units of power (kW) or energy (kWh). All gas data was provided on a monthly scale. However, the term "monthly" is used generally because the time between gas meter readings can vary from two weeks to two months for the same building. Furthermore, not all buildings with electricity data have gas data provided and vice versa. As seen in Figure 6, only 75 buildings of the approximately 900 in the database have both hourly electricity and monthly gas data.

Figure 7: Smart meter energy data collection responsibilities in Ontario [8]

Figure 8 shows the average hourly electricity use per unit floor area for a variety of buildings. As seen in Figure 8, the average energy use can vary greatly within the same building type. Supermarkets and indoor pools showed some of the highest average energy consumption on a per m^2 basis, due to the equipment required for their operation. Supermarkets require a large amount of electricity to power their refrigeration systems, specifically the compressors. Indoor pools may require significant power for

pumping water through the filtration system as well as ventilation while maintaining a high internal temperature.
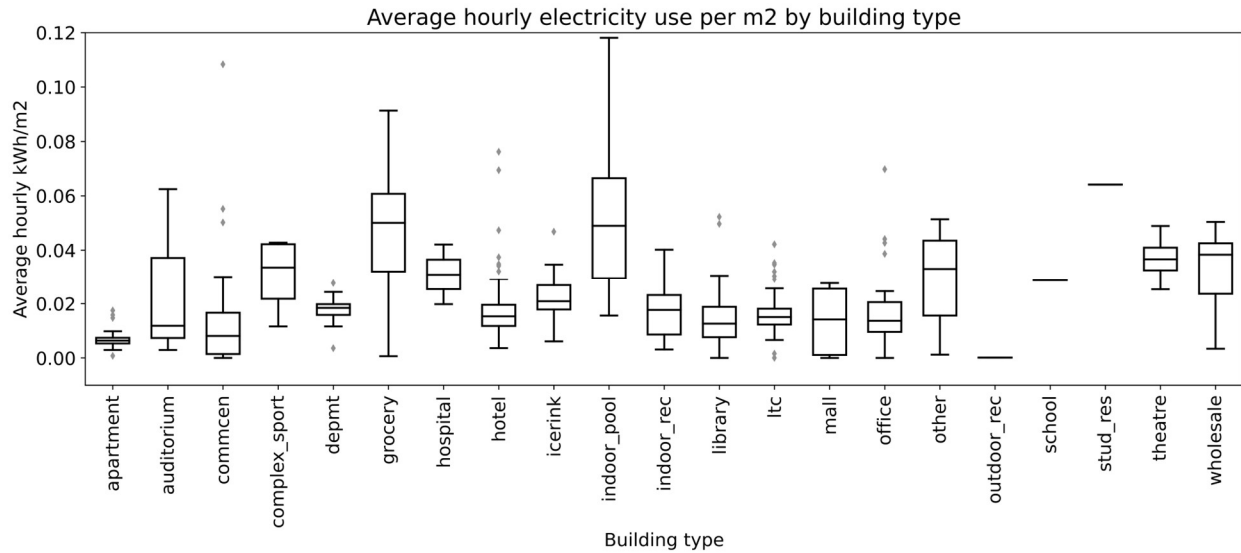
the restaurant and automotive storage building types are excluded from Figure 8 due to low-quality area data

Figure 8: Average hourly electricity use by building type

Figure 9 and Figure 10 display the peak summer and winter electricity demand for different building types. As seen in both figures, there are large ranges in peak hourly electricity demand across the same building types. For example, the peak hourly summer demand's upper quartile for an office building is greater than twice that of the lower quartile. The reasoning for under and over-performing buildings should be explored further, however the depth of this analysis is dependent on the data available. For example, building HVAC equipment, control schedules, temperature setpoints and insulation levels influence average and peak electricity usage. However, in this work, detailed data related to each building's construction and operation was not available. Furthermore, the large range in use presents a challenge for creating a generalized model that can predict unknown buildings.
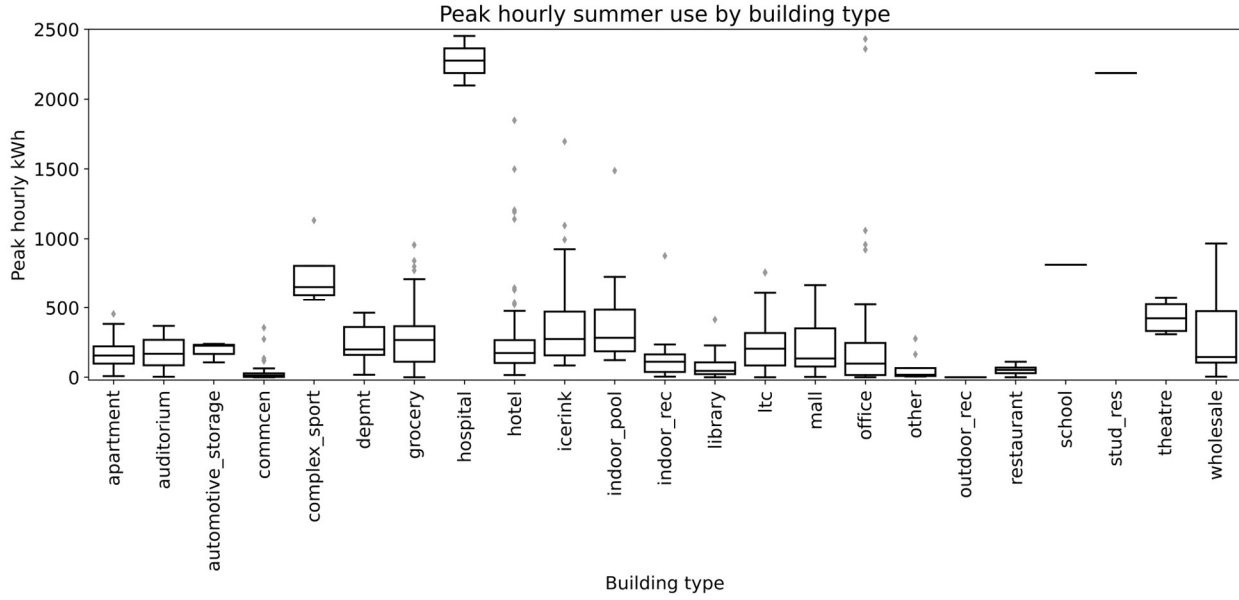
Figure 9: Peak hourly summer electricity use by building type
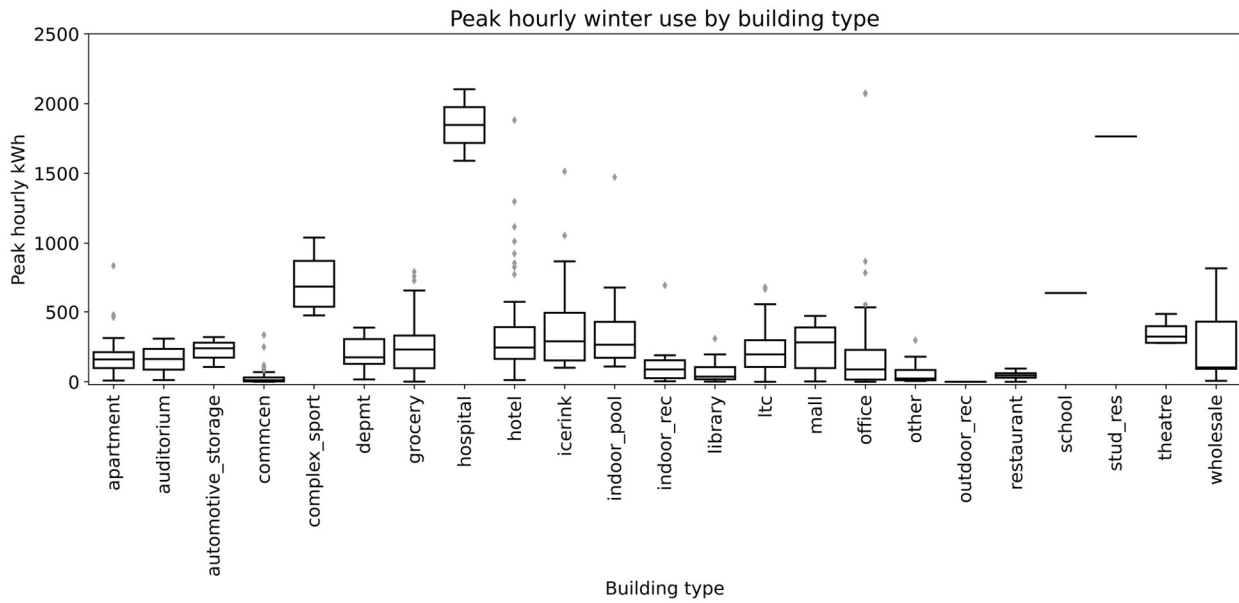
Figure 10: Peak hourly winter electricity use by building type

3.3   Model use cases

There are different cases for the proposed models to be used, depending on data availability and application. An overview of different model use cases is summarized in Table 3, with detailed descriptions in the following sections.

Table 3: Summary of different cases in which models can be used depending on the application

Case	Description	Application
1) In-building sample	Training and test sets are data from the same building.	Design, planning and long and short-term control of community energy systems
2) Out-of-building sample	Training set is from several buildings of the same building type. Test set is one building excluded from training.	Forecasts for buildings with no measured data such as new builds or pre-feasibility studies
3) Calibrated out-of-building sample	Training set is from several buildings of the same building type. Test set is one building excluded from training. Monthly values from the test building are used for the calibration of hourly predictions.	Forecasts for controls, design, and planning with buildings that only have monthly bills available

Figure 11 displays examples of the training and testing datasets for each model use case. For case 1, the model is trained on data from the same building to predict electricity use for a time not seen during training. For cases 2 and 3, the model is trained on a group of buildings to predict electricity use for one building not used in training. The test set for cases 2 and 3 may not necessarily be a period unseen during training, however, it is trained on data from other buildings.

Case 1: In-building-sample prediction

Building A | Training set | Test set
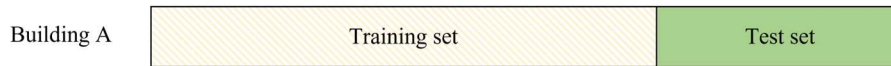
Case 2 & 3: Out-of-building-sample prediction

Building A | Training set

Building B | Training set

Building C | Training set
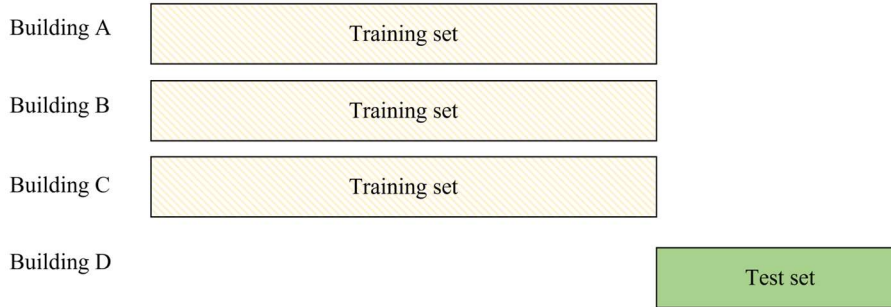
Building D | Test set

Figure 11: Training and testing sets for each model use case

3.3.1 Case 1: In-building-sample - building predicting itself

The first use of the building energy model is as a forecasting tool for controlling the ICE-Harvest system. Forecasted loads are required for year-ahead and day-ahead predictions. In this case, historical data is used from the building for which energy demand is to be predicted, as shown in Figure 11. Additionally, when ICE-Harvest systems are implemented, they may not have submetered data available for each building, so disaggregation into thermal and base loads is required by the model.

Year-ahead predictions are required for long-term controls, for example, to determine when to charge and discharge long-term seasonal thermal storage. This requires predictions for the summer and winter portions of one year. The training lengths for year-ahead predictions are tested on the interval of years (e.g. lengths of 1, 2 or 3 years). Conversely, short-term controls require a day-ahead prediction to determine the energy sources utilized. Both the summer and winter models are evaluated separately for day-ahead forecasts. The training lengths for day-ahead predictions are tested on the interval of days (e.g. lengths of 30 or 60 days). When evaluating the day-ahead predictions, multiple test days are considered and the results are averaged. Finally, a high-resolution, short-term model was desired at an hour or 2-

hour ahead rate for the last layer of controls. Since the majority of data in the database is not at a fine timescale, such as 5 minutes, this was not explored in depth. However, a single high-resolution model for one arena is proposed in Section 3.6.6.

3.3.2 Case 2: Out-of-building-sample: forecasting an unknown building

The second case for the model is when measured data is not available for a building. For example, designs with new builds or pre-feasibility studies to assess the impact of ICE-Harvest systems across large regions can utilize the generalized model. The model will be less accurate since it will not be trained on the specific behaviour of the building of interest. Buildings of the same building type are expected to consume energy similarly although large ranges can be seen.

Out-of-building-sample forecasting was only performed for year-ahead predictions. The low accuracy of the generalized model makes it impractical for short-term predictions. Short-term predictions are needed to control the system, in which case there is likely measured data available for the building and Case 1 applies.

3.3.3 Case 3: Calibrating the generalized model with monthly data

A third case was considered, where monthly bills may be available for a building, but not hourly electricity measurements. In this case, the prediction from the generalized model of Case 2 can be calibrated using monthly data. The hourly electricity predictions over the winter and summer are scaled by the real data sums to provide more accurate predictions.

3.4   Data preparation

The steps for preparing the database are summarized in Figure 12. First, the raw data files are matched to their corresponding addresses which are assigned anonymous ID numbers. For privacy reasons, the anonymous ID is then used to identify the corresponding energy file. The files are cleaned with different Python scripts depending on the incoming format. This may involve combining multiple

years of data, reformatting all data to a standard format and checking for missing values. After cleaning, the data must pass an integrity check. The integrity check ensures that there are no discontinuities in the time series data and flags missing values. After passing the integrity check, the data table is joined with weather data and archetypal building schedules from the National Energy Code of Canada for Buildings [67]. The building code schedules are not used in this work, but the database may be used for other purposes that utilize these schedules. Appendix B goes into more detail in outlining the database preparation procedure.
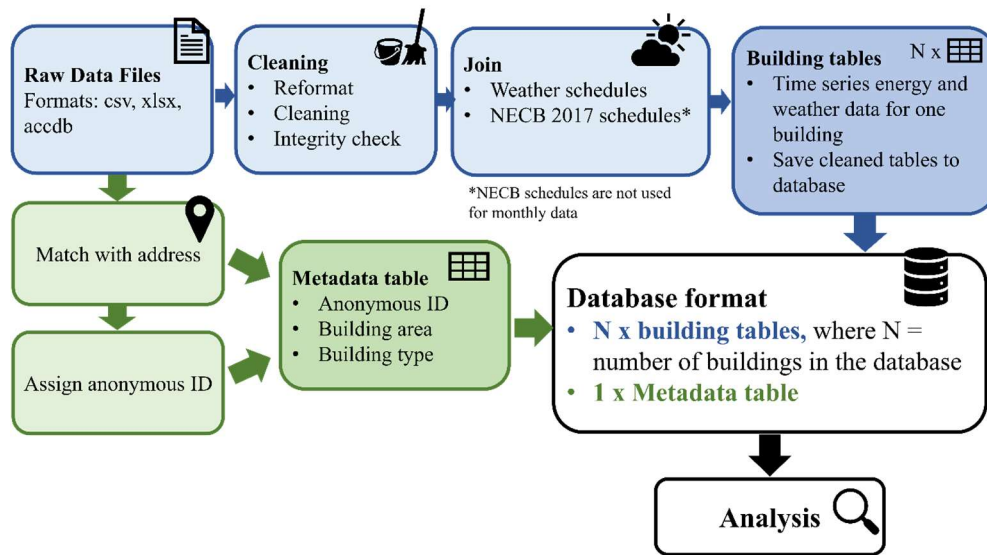
Figure 12: Database preparation flowchart

3.5 Evaluation metrics

The following section outlines some metrics that can be used to evaluate model performance. The main metric used in this work to evaluate the final model performance is normalized root mean squared error (NRMSE). However, some initial model assessments are based on metrics such as the coefficient of determination and silhouette score which are outlined in Table 4.

Table 4: Evaluation metrics used for model evaluation and assessments in this work

Metric	Equation	Description
Mean squared error (MSE)	$$MSE = \frac{\sum_{i=1}^{n}(Y_i - \widehat{Y}_i)^2}{n} \quad (9)$$ Y_i = true value $\widehat{Y}_i$ = predicted value n = number of samples	• Average of the squared error for each sample
Root mean squared error (RMSE)	$$RMSE = \sqrt{MSE} = \sqrt{\frac{\sum_{i=1}^{n}(Y_i - \widehat{Y}_i)^2}{n}} \quad (10)$$ Y_i = true value $\widehat{Y}_i$ = predicted value n = number of samples	• The square root of MSE • error is of the same order as the original data
Normalized root mean squared error (NRMSE)	$$NRMSE = \frac{RMSE}{\overline{Y}} \quad (11)$$ $\overline{Y}$ = sample mean	• Normalises RMSE by some value, in this work, the mean kWh value over the period being evaluated was used • Helps with comparing errors across different buildings and building types, which may have energy use at different scales
Coefficient of determination (R^2)	$$R^2 = 1 - \frac{\sum_i(Y_i - \widehat{Y}_i)^2}{\sum_i(Y_i - \overline{Y})^2} \quad (12)$$ $\overline{Y}$ = sample mean	• Measures the proportion of variance in the target value (energy use in this case) that is predicted by the model • A value closer to 1 is desired
Silhouette score	$$silhouette\ score = \frac{(b - a)}{max(a, b)} \quad (13)$$ a = mean intra-cluster distance (distance between the sample and all points in the same class) b = mean nearest-cluster distance (distance from the sample to all points in the nearest cluster that it was not assigned to)	• Used for clustering algorithms to measure how well samples fit in their assigned cluster • Value can range from -1 to 1, with 1 meaning the clusters are well defined

3.6 Electricity model

This section outlines the proposed electricity models. Hourly electricity models were created for three building types:

- Conventional – typical buildings with electrified space cooling
- Supermarket – space cooling and refrigeration loads
- Ice rink – space cooling and refrigeration loads

The modelling methodology can be broken down into two steps: sub-setting time series data based on season and type of day and training the model as summarized in Figure 13.
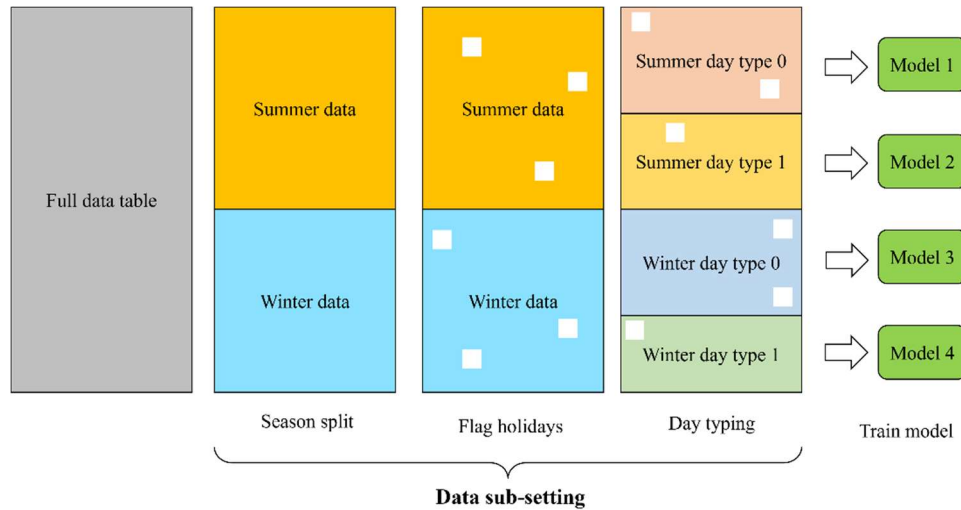
Figure 13: Data sub-setting and training order, the white squares represent holidays that are excluded from the training set

3.6.1 Data sub-setting

The proposed model for hourly electricity is based on a linear regression model which is generally not able to account for all cyclical time trends within the data. Thus, the data is first partitioned based on season, day of week and time of day (Figure 13) to allow for different model parameters based on operating conditions. Data sub-setting was also used by Dhar et al. [38]

3.6.1.1 Season

First, data is subset manually by weather season into two seasons: the cooling (summer) and heating (winter) season. A two-season split between the cooling and heating seasons was found to work best compared to four (winter, spring, summer, fall) or three (winter, summer, shoulder) seasons because

having many subsets of data reduces the amount of training data available for each sub-model. A two-season split produces two different models, which is suitable since electricity use is expected to differ significantly based on whether electrified cooling systems are operating or not. A two-step process is used. First, the data is divided into winter, summer and shoulder seasons. Spring starts April 1st, summer starts June 1st, fall starts September 1st and winter starts November 1st. All data in the winter and summer stay assigned to that season. For the initially assigned spring and fall dates, if the daily average temperature is below or equal to a threshold of 15°C, it will be considered a winter day. If it is above, it is considered a summer day. Future work could include using a smoothed daily temperature instead as it may impact whether the heating or cooling system is turned on. Additionally, the threshold was manually set, but the value could be tuned to improve the model.

3.6.1.2 Holidays

Holidays were also flagged using a calendar for Ontario's nine public holidays [84] as well as the Civic holiday. Two versions of the Ontario holiday calendar were created; shifted and unshifted. The shifted calendar will ensure holidays land on a workday. For example, an office building would shift a weekend holiday to the closest Monday or Friday. The unshifted calendar uses the actual holiday date as the holiday. For example, supermarkets are often open 7 days a week so they will use the true holiday date. Generally, there are not enough days of data to properly train a holiday model and each holiday may exhibit different behaviour. Moreover, different buildings will have different usage patterns on holidays; buildings providing lodging (e.g. hotels and apartments) may have higher use whereas commercial buildings will be closed or have reduced hours. As such, a model specifically for holidays was not created and the holiday data was excluded from the training set.

3.6.1.3 Day typing

As reviewed in Chapter 2, the process of "day-typing" or accounting for different daily characteristics is commonly used (e.g. [63][79][85]). Dhar et al. [38] manually separated weekdays, weekends and holidays while Hossain et al. [63] used unsupervised clustering of daily building markers

to sort day types. Figure 14 shows the weekly profiles for a sample office building during the summer. There is a difference in electricity load profiles for weekdays (hour of the week from 0 to 120) compared to the weekend (hour of the week from 121 to 175). The day typing algorithm aims to identify these operational characteristics.
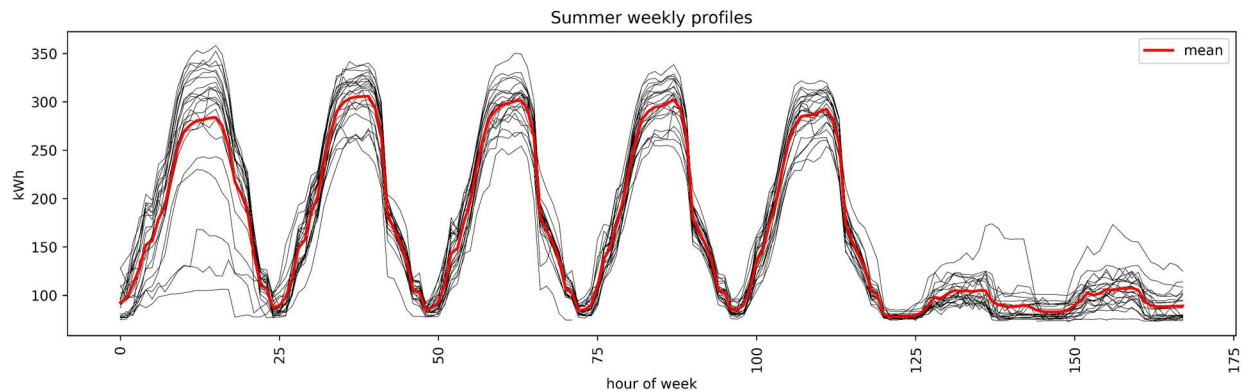
Figure 14: Weekly summer electricity profiles for an office building showing reduced weekend energy use

In this work, time series clustering was performed on each day's hourly profile using the tslearn Python package [86]. The tslearn package contains functions to create clusters based on the energy use for each hour of the day, then each daily profile is assigned to a cluster which has a similar shape and magnitude. Before clustering, the data is centred by subtracting the mean, but not scaled. Centring will negate the impact of an offset, allowing the clustering algorithm to capture similar shapes. Since it is not scaled, it still considers the magnitude of the shape because larger ranges of use should be accounted for. Euclidean k-means clustering was used, as explained in Section 2.3.4. In this case, more advanced time series methods such as dynamic time warping were not used because the scheduled events are assumed to occur at similar hours each day.

Because there are only seven days of the week, it is expected that there are one to three clusters needed to subset the data by day type. Too many clusters will result in multiple models with less training data which is not ideal. The best number of clusters for each building was determined by comparing the silhouette score (shown in Table 4) after testing two and three clusters. Figure 15 and Figure 16 show the

results for two and three clusters respectively for a sample building. Two clusters capture the weekend and weekday differences; however, three clusters can distinguish between two types of weekday profiles.
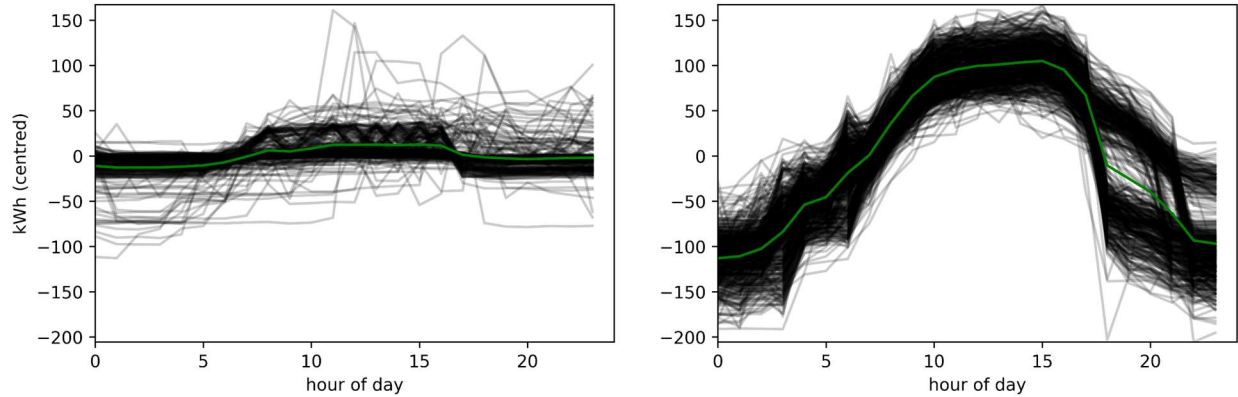
Figure 15: Two summer daily profile clusters for a sample office building (left is representative of a weekend day and right of a weekday)
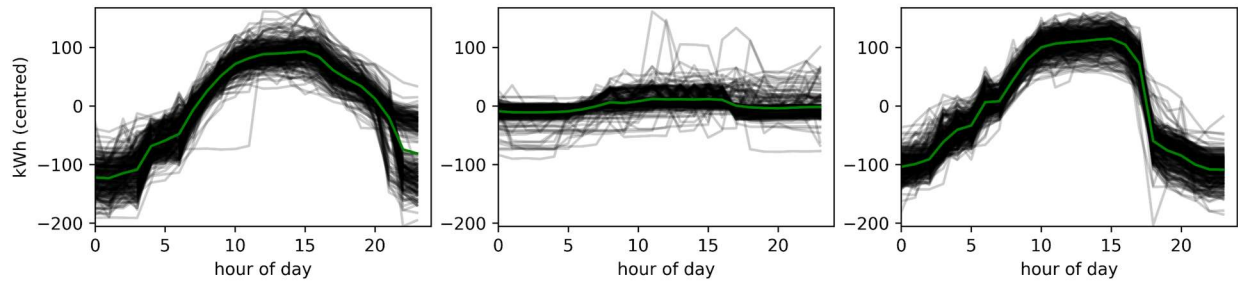
Figure 16: Three summer daily profile clusters for a sample office building (left is representative of a weekday where the building closes around 8 pm, the centre is representative of a weekend day, right is representative of a weekday where the building closes around 5 pm)

3.6.1.4   Operation typing

After sub-setting data by day type, the data can be operation-typed if desired, to set the on and off operational hours. For example, an office building will have different energy use trends during working hours from 9 am to 5 pm compared to the nighttime. Therefore these two time groups can be separated to train different models. Operation typing was only used for in-building-sample testing as it did not work

well in the generalized model. The on and off-hours were detected using the largest jumps or falls in use during the day. If the expected on and off-hours fall out of a reasonable range depending on building type, they are set to default values for each type. In preliminary results, operation typing did not work well for out-of-sample testing because the operation hours are different for each building.

3.6.2 Classification of heating or cooling type

It is also necessary to distinguish building space heating and cooling energy sources, specifically for out-of-building sample forecasts. Natural Resource Canada's 2014 Survey of Commercial and Institutional Energy Use [10] found that 92.6% of space-cooled commercial and institutional buildings in Canada use electricity for cooling. For space heating, 34.4% use electricity while 57.7% use natural gas.

In this work, detailed information related to each building's heating and cooling systems is not available. However, the heating and cooling energy source can be predicted by comparing electricity use in the winter and summer as well as correlation with temperature. As mentioned above, the most common combination for buildings in Canada is an electric cooling system with natural gas heating. In Ontario, there is a greater percentage of buildings using natural gas heating than the Canadian average of 57.7%. In 2011, 76% of Ontario households used natural gas as their main heating fuel which is the third highest percentage after Alberta and Saskatchewan [87]. Data is not available for Ontario commercial and institutional buildings; however, they are expected to have a similar percentage of natural gas-heated buildings. The presence of an electric cooling system can be observed by a positive correlation between electricity and temperature during the summer. Figure 17 displays the hourly electricity demand over one year for two different apartments: one with expected electrified heating and cooling and one with only expected electrified cooling. The profile for a building with expected electric cooling is shown by the blue line in Figure 17. Alternatively, some buildings may have electric heating, displayed by high levels of electricity use in the winter, shown by the red line.
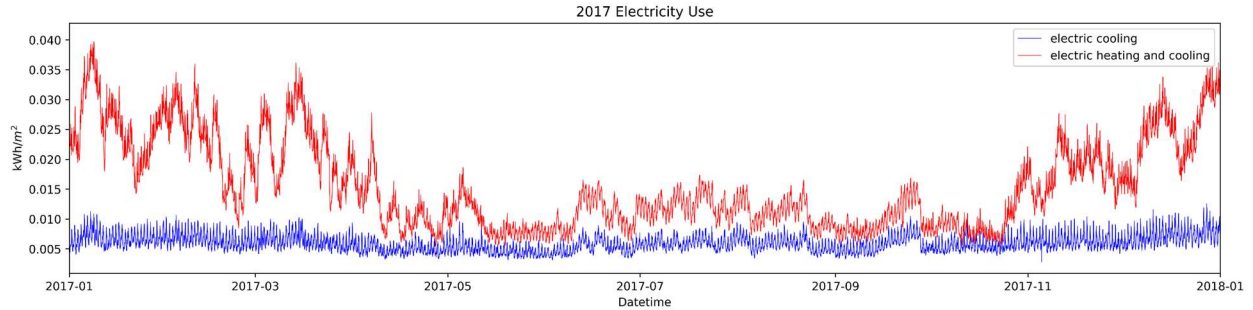
Figure 17: Electricity use over one year for two apartments, one with expected electric cooling only and one with electric cooling and heating

Buildings with all heating needs met with natural gas are still expected to have higher base electricity loads during the winter compared to the summer. This is due to reduced sunlight hours meaning occupants spend more time indoors and increased lighting use. Additionally, due to colder temperatures occupants may use appliances like kettles or ovens more often and furnace fans are operating more frequently.

Cooling type is detected by computing the slope of daily mean electricity use with daily mean temperature during the summer. If the slope is positive the building is assumed to have electric cooling. A positive slope is used as the sole criterion because it is assumed that most buildings analyzed have electric cooling. More advanced detection could use the coefficient of determination; however, it was found that R^2 values were quite low for most buildings, even those with expected electrified cooling. Heating type is specified based on the ratio of the maximum daily energy consumption in the summer compared to the winter. If the ratio is greater than 0.85, the building is assumed to have some form of electric heating. This value was selected manually based on data visualization. A further distinction is made between buildings with ratios between 0.85-1 and greater than 1. Ratios of 0.85-1 may be due to the supplementation of gas heating with electric resistance heaters or the use of more efficient heating systems (e.g. heat pumps). If the cooling type was not assigned as electric, the default heating type is assumed to be non-electric. These specifications are important for the generalized model. However

expected heating or cooling types do not change the model form, only the assignment of loads which is discussed further in the next sections.

3.6.3 Hourly electricity model for conventional buildings

The initial electricity model was developed for buildings with electrified space cooling or heating but no significant refrigeration load. The cooling season model is referred to as the EL-CL (electricity-cooling) model, while the EL-HT (electricity-heating) model is used for the heating season. Conventional buildings do not have high refrigeration loads and include building types like apartments, long-term care homes, department stores, office buildings, and community centres. The EL-CL model is expanded for buildings with high refrigeration loads (for example grocery stores and arenas) in Sections 3.6.4 and 3.6.5.

In the summer, electricity use can be broken down into the base electrical load (ALP loads) and space cooling. In the winter, electricity use can be broken down into the base electrical load and electric heating (if applicable).

3.6.3.1 Assumptions and limitations

Several assumptions are used in the model. First, building energy use is assumed to be driven by outdoor weather conditions and scheduled loads which are presumed to be consistent throughout the season. The base electrical load (consisting of appliance, lighting and plug loads), is modelled as a scheduled load. In reality, the profile will vary day to day depending on occupant behaviour. However, occupant behaviour is difficult to predict, so it is assumed that on average they will behave similarly from day to day. The space cooling load is assumed to be purely weather-driven, by temperature, solar gains and humidity. The space heating load is assumed to be driven by temperature and solar gains. Second, cooling or heating system efficiency (or COP) changes as a result of external temperature are neglected but may be slightly accounted for by the temperature term.

Third, internal sensible and latent gains from appliances and occupants are neglected as contributions to the thermal loads. These sources are assumed to be scheduled, so they will be detected as part of the electrical baseload due to their correlation with the time of day. This will lead to underestimating the cooling load. It will be an issue for buildings with high internal electrical loads due to the significant amount of heat from the appliances that is neglected. Fourth, buildings are assumed to use a heating and cooling control system where the setpoints are set based on current occupancy comfort. The model does not account for buildings with smart or model predictive control to precool and preheat buildings. In the future, these types of buildings control systems may become more common which may require an advanced model that considers ordered time series data. Finally, the model uses a quasi-steady-state assumption, where over each hour the heat entering and leaving the building is equal. However, a simple moving average temperature term is added to account for thermal mass due to the delayed impact of earlier temperatures as heat travels through the building envelope.

3.6.3.2   *Model form and feature selection*

Input features for the model were selected using a mixture of manual and data-driven feature selection. A purely statistical approach was not used since the model form was set as a linear equation to disaggregate loads into HVAC and baseload components. With linear regression models, more features can improve accuracy for predicting total electricity, but produce unphysical or unrealistic results for disaggregated loads.

Heat sources

Cooling season

The space cooling thermal load is assumed to be the sum of the following heat sources; solar gains, ventilation and envelope conduction/convection. The initial model is based on that of Dhar et al. [38] and uses similar weather features: temperature, humidity and solar radiation.

Instead of dry-bulb temperature, a degree day term was used, which is explained in Section 2.2.2, to represent heat transfer through the building envelope and ventilation loads. Similar to [38], a specific humidity term is used to account for the latent load. A base value is used, similar to the degree day base temperature, to account for when humidity is removed (e.g. when moisture will condense on a cooling coil if removed via condensation), as shown below.

$$\text{SH term} = (\text{SH} - \text{SH}_{\text{base}})^+ \tag{14}$$

The specific humidity term was compared to other moisture parameters such as dew point, relative humidity and mixing ratio and evaluated on synthetic and real data. It yielded the lowest MSE for the predicted synthetic cooling load as well as the lowest MSE for total use for a test group of real buildings. Details of the comparison can be found in Appendix C: Moisture terms. Specific humidity is the ratio of the water vapour mass to the total air mass, including both moist and dry air as shown in Equation 15 [88]. The energy required to remove moisture from the air will be mostly proportional to the difference in specific humidity.

$$\text{specific humidity} = \frac{m_{\text{water}}}{m_{\text{dry}} + m_{\text{water}}} \tag{15}$$

Global Horizontal Irradiance (GHI) was included to account for solar gains and can capture the slight baseload variation throughout the year because higher GHI values may reduce the need for lighting. The GHI impact on energy use is relatively low for most buildings, compared to temperature. Lastly, a simple moving average degree-day term is included to account for delayed temperature impacts from thermal mass or occupant comfort. Depending on the window size used, the averaged degree-day term may have a high correlation with the instantaneous degree-day term. To address this, larger window sizes were considered and the current degree-day value was excluded from the average.

The predicted building thermal load for space cooling (EL-CL model) is shown in Equation 16. The first term captures the GHI impact. The second term is the cooling degree day term, which accounts

for the current outdoor temperature. Similarly, the third term considers the current outdoor specific humidity. Lastly, the fourth term is the moving average CDD term, which is calculated by taking the average CDD value between the last hour and the last N^{th} hour.

$$Q_{cooling,t} = \beta_1 * (GHI_t) + \beta_2 * (T_{out,t} - T_{in})^+ + \beta_3 (SH_{out,t} - SH_{in})^+ + \beta_4 * \overline{(T_{out} - T_{in})^+}_{t-N,t-1} \qquad (16)$$

Where:

    Q = thermal load (kWh)

    t = time of observation

    N = window size of the simple moving average (hr)

    GHI = global horizontal irradiance (W/m^2)

    T = temperature (°C)

    SH = specific humidity (-)

The learnt coefficients (β's) do not have exact physical values but represent each component's contribution to the cooling load. For example, β_1 is representative of the surface area of the building, shading factor, external wall orientation, and the number of windows. β_2 is representative of the ventilation rate, envelope insulation level and exterior and interior heat transfer coefficients. β_3 is also representative of the ventilation rate.

Heating season

Similarly, for the winter electricity model (EL-HT), heat transfer from solar radiation, ventilation and conduction are considered. Instead of a cooling degree day term, a heating degree day term is used. However, external humidity is low in the winter and therefore neglected. The building thermal load for space heating is modelled in Equation 17.

$$Q_{heating} = \beta_1 * (GHI_t) + \beta_2 * (T_{in} - T_{out,t})^+ + \beta_3 * \overline{(T_{in} - T_{out})^+}_{t-N,t-1} \qquad (17)$$

Electricity use

The total amount of electricity consumed in the building is the sum of the thermal and base electrical loads. The electrical baseload (ALP loads) is assumed to be scheduling driven so Fourier decomposition is used. It is represented using Fourier terms based on the hour of the day as proposed in [38] and [62]. Since there are 24 hours in the day, only 23 Fourier terms are required to model all the hours of the day. Using 24 terms will over constrain the problem and higher frequencies can often be neglected so only the first 11 frequencies are considered. The electrical baseload is represented by:

$$W_{baseload} = \beta_o + \sum_{n=1}^{11} \left(a_n \cos\left(\frac{2\pi nh}{24}\right) + b_n \sin\left(\frac{2\pi nh}{24}\right) \right) \tag{18}$$

Where:

W = electrical load (kWh)

h = hour of the day (hr)

The coefficients c_o, a_n's and b_n's are learned from the data.

Cooling season

For summer electricity use, the COP of the cooling system is assumed to be constant. Therefore, the electricity used for space cooling is proportional to the cooling thermal load. The constant COP can be absorbed into the unknown coefficients so that each β value accounts for the efficiency of the cooling system:

$$W_{space\ cooling} = \frac{Q_{cooling}}{COP} \tag{19}$$

$$W_{space\ cooling} = \beta_1 * (GHI) + \beta_2 * (T_{out} - T_{in})^+ + \beta_3 (SH_{out} - SH_{in})^+ \\ + \beta_4 * \overline{(T_{out} - T_{in})^+}_{t-N,t-1} \tag{20}$$

This yields the following equation for total electricity use in the summer:

$$W_{total} = \beta_o + \sum_{n=1}^{11} \left(a_n \cos\left(\frac{2\pi nh}{24}\right) + b_n \sin\left(\frac{2\pi nh}{24}\right) \right) + \beta_1 * (GHI) + \beta_2 * (T_{out} - T_{in})^+$$
$$+ \beta_3 (SH_{out} - SH_{in})^+ + \beta_4 * \overline{(T_{out} - T_{in})^+}_{t-N,t-1} \tag{21}$$

If β_1 is negative, the GHI component is attributed to the baseload instead of the space cooling load due to its offsetting lighting needs.

Heating season

The heating season is treated similarly with the heating system efficiency assumed to be constant, yielding the following equation for total electricity use in the winter:

$$W_{total} = \beta_o + \sum_{n=1}^{11} \left(a_n \cos\left(\frac{2\pi nh}{24}\right) + b_n \sin\left(\frac{2\pi nh}{24}\right) \right) + \beta_1 * (GHI) + \beta_2 * (T_{in} - T_{out})^+$$
$$+ \beta_3 * \overline{(T_{in} - T_{out})^+}_{t-N,t-1} \tag{22}$$

As mentioned previously, for a building without electrified heating, electricity use is still expected to increase with colder temperatures and less sunlight. Therefore, the same equation is used to represent non-electric heated buildings as well. However, the total amount of electricity is assumed to be part of the ALP load, instead of splitting it into heating and baseload components.

3.6.3.3 Algorithm

Using the equations outlined in the previous section, an individual model is trained for each building with measured utility data. This involves solving for the unknown coefficients, internal setpoints (or base values) and the window size for the simple moving average temperature value. The temperature and humidity setpoint values make the equations nonlinear. Two approaches were tested: a non-linear least squares solver and multiple linear regression with a grid search. The multiple linear regression approach was chosen, but additional details on the non-linear least squares approach [89] can be found in Appendix D.

The problem was formulated as a multiple linear regression problem with a grid search to determine the ideal internal setpoints for temperature and specific humidity. There is a trade-off between accuracy and time, depending on the grid resolution. To reduce computation time, the following values were tested using:

- Temperature range [°C]: 10, 15, 18, 20, 25

- Specific humidity range [-]: 0, 0.002, 0.004, 0.006, 0.008. 0.015

- Window range [hr]: 5, 10, 20, 60

While a coarser grid provides less accuracy, a significant amount of time is saved. Furthermore, the linear regression model was more stable and accuracy was generally better than the curve fitting algorithm, despite the coarse grid.

$$W_{total} = \boldsymbol{\beta_0} + \sum_{n=1}^{11} \left(\mathbf{a_n} \cos\left(\frac{2\pi nh}{24}\right) + \mathbf{b_n} \sin\left(\frac{2\pi nh}{24}\right) \right) + \boldsymbol{\beta_1} * (GHI) + \boldsymbol{\beta_2} * (T_{out} - T_{in})^+$$
$$+ \boldsymbol{\beta_3}(SH_{out} - SH_{in})^+ + \boldsymbol{\beta_4} * \overline{(T_{out} - T_{in})^+}_{t-N,t-1} \tag{23}$$

Equation 23 shows the cooling linear regression model with the unknown coefficients bolded and the grid searched values highlighted in blue. The linear regression model was solved using the ridge regression algorithm in the Python Scikit learn library [90].

Ridge regression was selected as the algorithm based on the verification results and testing on a small sample of buildings. Scaling and centring were performed with Scikit Learn's Robust Scaler using the interquartile range and median. The penalty parameter λ was selected from a small set of values using two-fold cross-validation, repeated twice to reduce total computational time. However, when training one model for an individual building, in-depth parameter tuning should be performed with a finer set of λ values and a greater number of folds and repetitions. Verification of the model for the in-sample prediction is provided in the next section for a synthetic apartment building.

3.6.3.4   Verification for a synthetic apartment

The synthetic apartment data is from the United States Department of Energy (DOE) Commercial Reference Building dataset [91]. An apartment building in Chicago was chosen for this test because it has a similar climate to that of southern Ontario. The building was modelled by the DOE with EnergyPlus software, using a Chicago typical meteorological year (TMY). The use of a typical meteorological year means that extreme weather events are not represented well compared to real data. Furthermore, because the apartment building was modelled in EnergyPlus, the randomness of occupant behaviour does not appear in the data. The model, therefore, captures the baseload well, however, it should be noted that with real data, the base electrical load will not be as uniform and model performance is expected to be worse. Synthetic data is used in this case because real submetered cooling loads were not available to validate the cooling disaggregation.

Day-ahead

Winter and summer day-ahead predictions were tested with 30 days of training data. Figure 18 and Figure 19 display the day-ahead prediction for a synthetic apartment in the winter. As seen in Figure 19, the predicted and measured total loads for the winter day-ahead prediction match well with an NRMSE of 0.01. The baseload shows a spike in the morning when occupants wake up and a spike in the evening when they return home, which is captured by the model. The portion of the load expected to vary slightly with weather is shown in peach in Figure 18. This is to capture the influence of temperature and solar gains on the base electricity consumption (e.g. furnace fan, lighting) as mentioned previously.
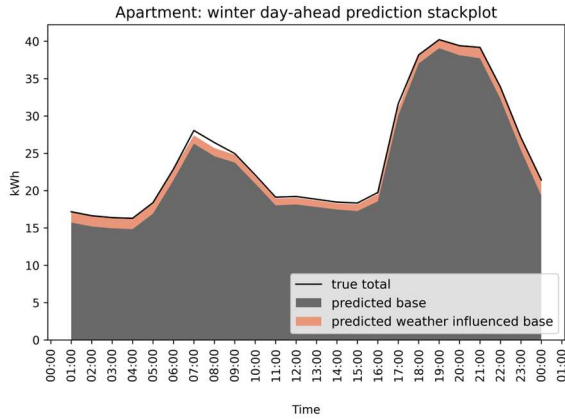
Figure 18: Synthetic apartment winter day-ahead prediction stackplot for December 14th
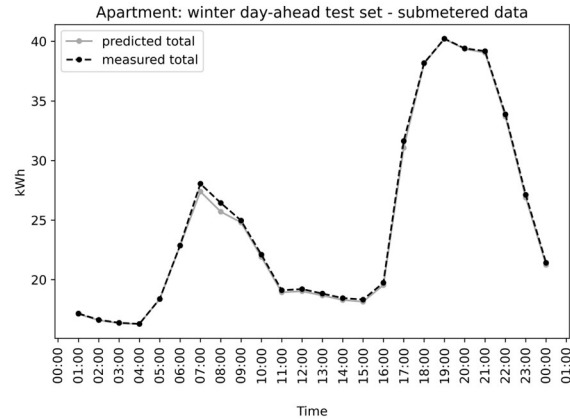
Figure 19: Synthetic apartment winter day-ahead prediction for December 14th

Figure 20 and Figure 21 display the summer day-ahead prediction for a synthetic apartment. The summer day-ahead prediction disaggregates the total electrical load into baseload and space cooling components. Figure 20 shows a sample summer day prediction where the predicted space cooling load makes up a significant portion of the total electrical load. The predicted cooling load is higher at midday when temperature and solar radiation levels are higher. In Figure 21, the predicted total electricity use shown in grey matches the measured data (shown in black) well, with an NRMSE of 0.02. The predicted space cooling, shown in blue, has an NRMSE of 0.23 at the hourly rate. The prediction is shifted earlier than the true cooling load, despite the use of the simple moving averaged cooling degree day term to account for thermal mass. However, on a daily scale, the cooling load is predicted well with an NRMSE of 0.02.
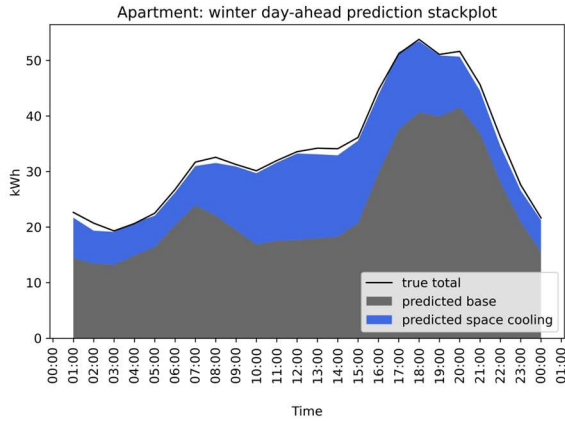
Figure 20: Synthetic apartment summer day-ahead prediction stackplot for July 13th
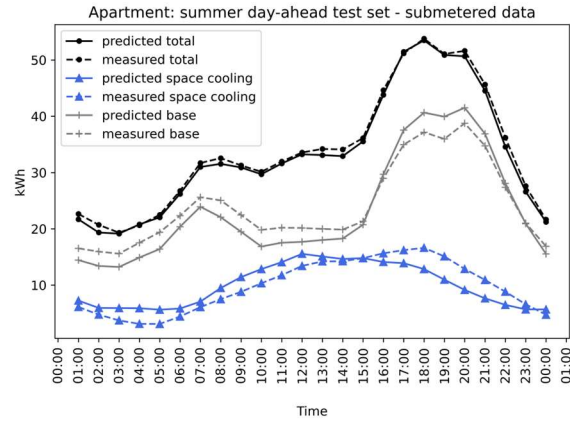
Figure 21: Synthetic apartment summer day-ahead prediction submetered loads for July 13th

Long term prediction

A full year-ahead prediction is not possible for the test case since there is not enough synthetic training data. Alternatively, a long-term prediction with a 60-day test set, using 60 days of training data was evaluated to display long-term prediction performance. Figure 22 and Figure 23 show the long-term winter prediction for the synthetic apartment, while Figure 24 and Figure 25 show a sample day from the full test set. As shown in Figure 22 and Figure 23, the winter long-term predictions match the measured data well with an NRMSE of 0.12 for total electricity use (Table 5). However, due to the season-splitting method used there are some days in October and November when the building has a space cooling load that is not captured by the model. This results in large NRMSE values for the cooling load that are greater than 1 (Table 5). However, the winter cooling loads are relatively low compared to the summer cooling loads. Furthermore, with real buildings, the occupants may turn off their heating and cooling systems based on time of year instead of only temperature. Figure 26 and Figure 27 display the long-term summer prediction for the synthetic apartment, while Figure 40 and Figure 41 display a sample day from the test set. As shown in Figure 26, the long-term disaggregated prediction for the summer shows good agreement with the measured total and has an NRMSE of 0.05. As seen in Figure 27, the predicted

cooling load is overestimated by the model at night but follows a similar trend to the true cooling load with an NRMSE of 0.34.
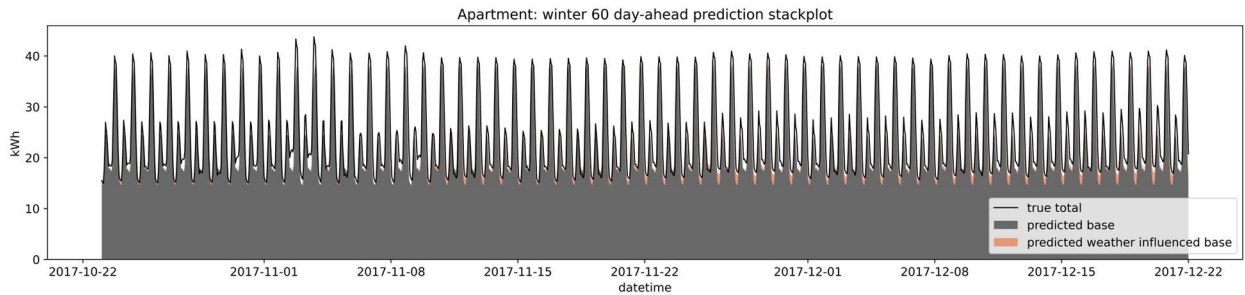
Figure 22: Synthetic apartment winter long-term prediction stackplot from October to December
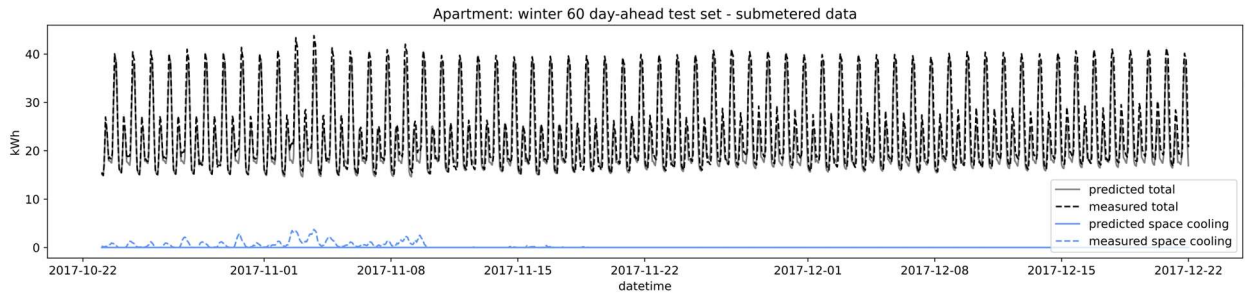
Figure 23: Synthetic apartment winter long-term prediction submetered loads from October to December
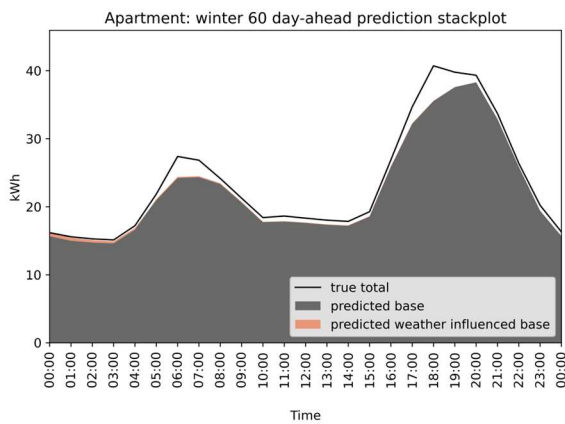
Figure 24: Synthetic apartment winter long-term prediction sample day (November 1st) stackplot
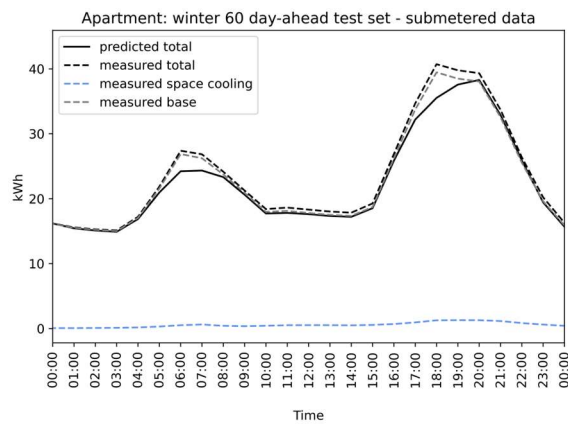
Figure 25: Synthetic apartment winter long-term prediction sample day (November 1st) submetered loads
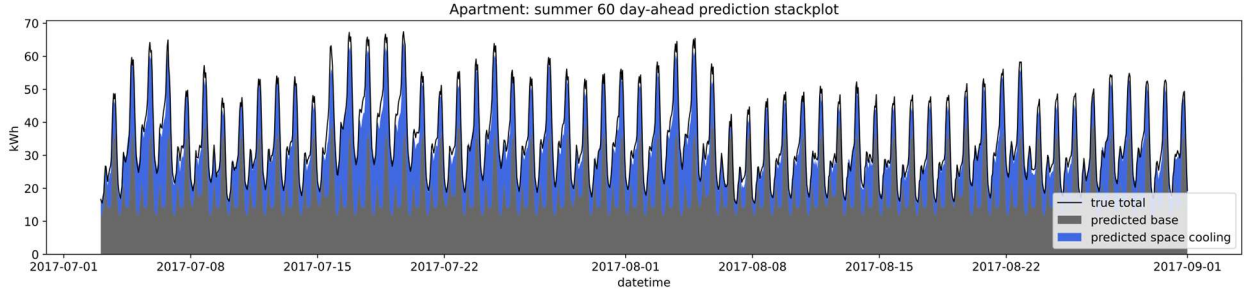
Figure 26: Synthetic apartment summer long-term prediction stackplot from July to September
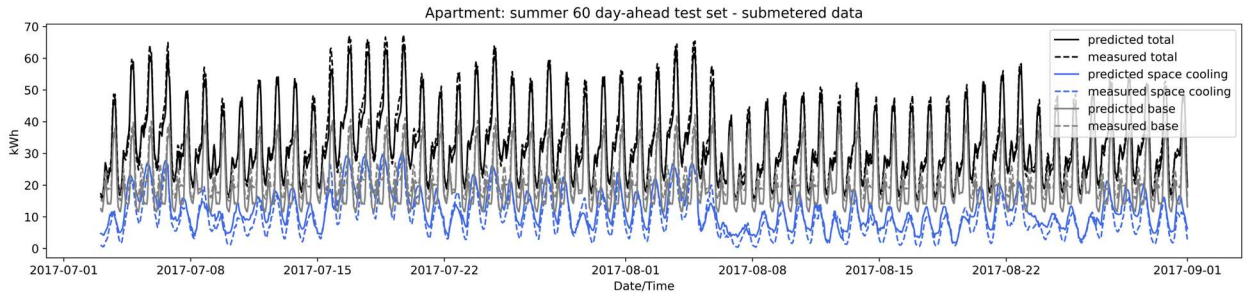
Figure 27: Synthetic apartment summer long-term prediction submetered loads from July to September
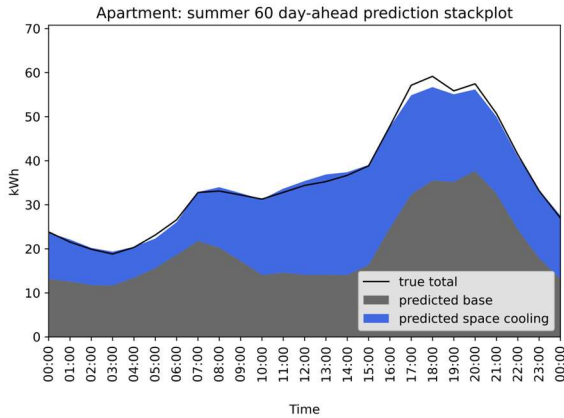
Figure 28: Synthetic apartment summer long-term prediction sample day (July 23rd) stackplot
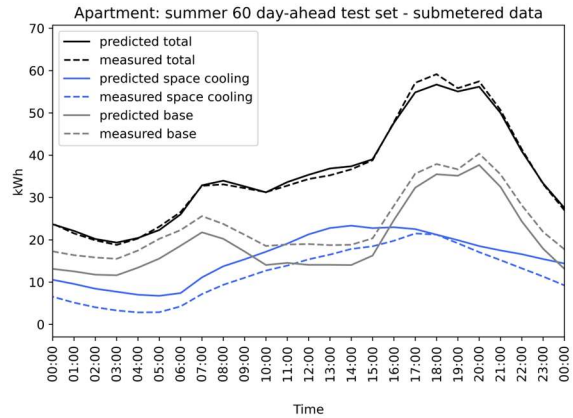
Figure 29: Synthetic apartment summer long-term prediction sample day (July 23rd) submetered loads

The normalized root means squared error for each case is outlined in Table 5. The total hourly error for all four cases is below 0.12 and the daily error is less than or equal to 0.05. In terms of the

disaggregated space cooling load, the day-ahead prediction is significantly better than the long-term prediction with an hourly NRMSE of 0.23 compared to 0.34.

Table 5: Synthetic apartment test case normalized root mean squared error

Case	Season	Train set length	Test set length	Normalized root mean squared error			
				Total [hr]	Total [day]	Space cooling [hr]	Space cooling [day]
A	Winter	30 days	1 day	0.01	0.01	-	-
B	Summer	30 days	1 day	0.02	0.03	0.23	0.02
C	Winter	60 days	60 days	0.12	0.05	2.53	2.14
D	Summer	60 days	60 days	0.05	0.04	0.34	0.29

3.6.4 Hourly supermarket model

Following the formulation of the model for conventional buildings, a model was created for supermarkets. Electricity use for supermarkets can be broken down into the electrical base, refrigeration and dehumidification components in the winter, with space cooling added during the summer. There are several heat transfer considerations in supermarkets, however, due to their complexity, not all are considered in detail in this work.

3.6.4.1   Energy use considerations for supermarkets

The majority of electricity consumption in supermarkets is due to the refrigeration load which can consist of refrigeration cases, freezers and stock rooms for keeping produce fresh. An individual supermarket's refrigeration energy consumption will depend on the temperature and humidity setpoints, type, door type and volume of each refrigerated space. For example, open cases will likely have more heat entering the case than closed cases, depending on the frequency of door openings. Additionally, the refrigerant, refrigeration system setup (e.g. centralized vs decentralized), fan controls, condenser location, defrost controls and insulation will impact the refrigeration electrical load [92].

Furthermore, dehumidification is an important aspect of air conditioning in supermarkets to ensure produce freshness, reduce the refrigeration load and prevent glass fogging. Some supermarkets have dehumidification systems to address this. Desiccant dehumidifiers are commonly used that utilize a large, slowly turning wheel filled with desiccant material [93]. As the wheel turns, incoming air passes through the wheel containing dried desiccant that absorbs moisture from the air. A separate pass blows hot air to dry out the moisture-containing desiccant as the wheel rotates. Some desiccant dehumidifiers use gas for this reheating while others use electricity. Anti-sweat heaters may also be used to prevent condensation from forming on glass cases [94] to ensure merchandise is visible and encourage sales.

Some stores may have cooking areas which can increase energy use intensity by 3% [95] due to the additional heat generated and ventilation requirements. Lighting is also an important aspect since it will add heat to the refrigerated spaces and impact sales of produce and merchandise [92].

3.6.4.2 *Assumptions and limitations*

The following assumptions are used in the proposed model. First, the refrigeration load is assumed to be scheduling-driven with a similar pattern to the electrical baseload. When the building has more occupants, the baseload is higher, leading to more heat entering the refrigeration cases due to occupant heat and door openings. Additionally, during open hours, the lighting load is higher, adding heat to the cases. Second, the complexity of defrost cycles and food restocking schedules are neglected. Without any knowledge of the defrost cycle or controls, it is difficult to account for it in the model other than assuming they have a general daily pattern that is based on the hour of day. The same applies to the food restocking schedule.

Third, the supermarkets' dehumidification load is modelled separately from space cooling and refrigeration. In the proposed model, the humidity-related load can be associated with the reactivation electricity for the desiccant dehumidification system, the fan electricity for the dehumidification system, anti-sweat heater operation or the additional latent load on the refrigeration system. This will depend on

the building's system, but if more information on the dehumidification system becomes available, the loads can be assigned more specifically. Fourth, all buildings are assumed to have externally located refrigeration system condensers. Most modern supermarkets have condensers located outdoors, but small stores may reject heat indoors. Finally, the impact of COP changes with outdoor temperature is not modelled as a multiplicative relationship (ie. $COP^{-1} * Q_{rej}$), it is instead considered as an additional load due to higher temperatures. This provides a more stable and accurate model despite being less physically reasonable.

The model has many simplifications and does not consider each heat transfer component in detail. This is due to the nature of the data provided because data related to the operation or lighting schedules, number or area of freezers and fridges and individual case setpoints were unavailable. Therefore this model is an initial starting point for cases where little to no data is available for the building. It provides a simplified way of extracting the disaggregated loads from existing data but can be expanded later to include detailed schedules and provide a more accurate estimate of the disaggregated loads. For example, when designing an ICE-Harvest system with an existing supermarket, detailed information related to the store layout and refrigeration system will likely be available.

3.6.4.3   Model form

Heat sources

The refrigeration thermal load is assumed to be purely scheduling-driven, dependent on lighting, occupants and case door openings. While there is heat exchanged between the refrigerated and non-refrigerated spaces, which would reduce the space cooling load and increase the refrigeration load, it is not considered in detail and is lumped in with constant refrigeration use. Similar to the EL-CL (electricity-cooling) model, the space cooling thermal load is assumed to be the sum of the following: solar radiation on the exterior surfaces, ventilation and conduction based on the temperature difference

between the inside and outside and the latent load due to external humidity. The thermal contributions to the electrical load are formulated as:

$$Q_{refrigeration} = k_1 * \sum_{n=1}^{11} \left(a_n \cos\left(\frac{2\pi nh}{24}\right) + b_n \sin\left(\frac{2\pi nh}{24}\right) \right) + k_2 * \beta_0 \tag{24}$$

$$Q_{dehumidification} = \beta_2 * (SH_{out} - SH_{base})^+ \tag{25}$$

$$Q_{space\ cooling} = \beta_3 * (T_{out} - T_{base})^+ + \beta_4 * GHI + \beta_5 * (SH_{out} - SH_{base})^+ + \beta_6 \tag{26}$$

Electricity use

The total amount of electricity consumed in the building is the sum of the refrigeration, dehumidification, space cooling and base electrical loads. For the baseload, Fourier decomposition is used to model the scheduled loads. This includes all the non-HVAC and non-refrigeration appliances such as lighting, cash registers and computers. The refrigeration electrical load consists of the scheduled refrigeration load and a component to account for COP changes with external temperature. The outdoor temperature impact on COP is represented using the inverse Carnot COP multiplied by an unknown coefficient. This results in the following equations for winter electricity consumption:

$$W_{base} = (1 - k_1) * \sum_{n=1}^{11} \left(a_n \cos\left(\frac{2\pi nh}{24}\right) + b_n \sin\left(\frac{2\pi nh}{24}\right) \right) + (1 - k_2) * \beta_0 \tag{27}$$

$$W_{refrigeration} = k_1 * \sum_{n=1}^{11} \left(a_n \cos\left(\frac{2\pi nh}{24}\right) + b_n \sin\left(\frac{2\pi nh}{24}\right) \right) + k_2 * \beta_0 + \beta_1 * \left[\frac{T_{out} - T_{fridge}}{T_{fridge} + 273.15} \right]^+ \tag{28}$$

$$W_{dehumidific} = \beta_2 * (SH_{out} - SH_{base})^+ \tag{29}$$

$$W_{total,winter} = W_{base} + W_{refrigeration} + W_{dehumidification} \tag{30}$$

Combining equations 27-30 gives the equation for total electricity consumption:

$$W_{total,winter} = \sum_{n=1}^{11} \left(a_n \cos\left(\frac{2\pi nh}{24}\right) + b_n \sin\left(\frac{2\pi nh}{24}\right) \right) + \beta_0 + \beta_1 * \left[\frac{T_{out} - T_{fridge}}{T_{fridge} + 273.15} \right]^+$$
$$+ \beta_2 * (SH_{out} - SH_{base})^+ \tag{31}$$

Where:

h = hour of day

T_{out} = outdoor temperature (°C)

T_{fridge} = average refrigerator temperature (°C)

SH = specific humidity

The coefficients β's, a_n's and b_n's are learned from the data

The constants k_1 and k_2 are values between 0 and 1. The default values are set manually, based on literature, to represent the refrigeration and base loads separately. Refrigeration loads can account for 40-70% percent of electricity consumption in North American supermarkets [96][92][97], therefore k_1 and k_2 were set to 0.4 because there will also be a contribution from the β_1 term. However, k_1 and k_2 could be adjusted in the future based on the percentage of refrigerated space in a building, if the data is available. The symbol T_{fridge} represents the average temperature of the refrigerated spaces since different cases and stockrooms will have different temperatures.

The winter model is trained before the summer model. The learned coefficients are then used to predict the refrigeration and baseload profiles for the full year. This assumes no seasonal variation of the baseload which is likely untrue since lighting use will increase in the winter. However, the addition of terms to account for this (eg. considering heating degree day or GHI terms) was found to reduce model performance. Thus, the baseload is assumed constant throughout the entire year but the baseload may be overestimated in the summer, resulting in a lower predicted space cooling load.

The summer equations are built off of the winter model, using the same coefficients as the winter for the baseload and refrigeration load. Equations 27-29 are used, with the remainder attributed to space cooling using similar terms to the EL-CL model:

$$W_{space\ cooling} = \beta_3 * (T_{out} - T_{base})^+ + \beta_4 * GHI + \beta_5 * (SH_{out} - SH_{base})^+ + \beta_6 \qquad (32)$$

$$W_{total,summer} = W_{base} + W_{refrigeration} + W_{dehumidification} + W_{space\ cooling} \qquad (33)$$

Combining equations 27-29, 32 and 33, yields Equation 34 for summer electricity use. Equation 34 has two sets of seemingly identical coefficients: β_o and β_6 as well as β_2 and β_5. However, β_o and β_2 are learned from the winter season, while β_6 and β_5 are learned from the remainder of the prediction during the summer.

$$
\begin{aligned}
W_{total,summer} = \sum_{n=1}^{11} \left(a_n \cos\left(\frac{2\pi nh}{24}\right) + b_n \sin\left(\frac{2\pi nh}{24}\right) \right) + \beta_0 + \beta_1 * \left[\frac{T_{out} - T_{fridge}}{T_{fridge} + 273.15} \right]^+ \\
+ \beta_2 * (SH_{out} - SH_{base})^+ + \beta_3 * (T_{out} - T_{base})^+ + \\
\beta_4 * GHI + \beta_5 * (SH_{out} - SH_{base})^+ + \beta_6
\end{aligned}
\tag{34}
$$

3.6.4.4   *Verification with synthetic data*

Similar to Section 3.6.3.4, the model is validated with synthetic supermarket data from the DOE Commercial Reference Building dataset [91], using Chicago weather. It has the same limitations outlined in Section 3.6.3.4. Synthetic data is used for verification in this case because real submetered space cooling and refrigeration loads were not available to validate the end-use disaggregation. The synthetic building does not have a desiccant dehumidifier system so moisture is removed by condensation on the evaporator coil. The results in this section display the sum of the predicted refrigeration and dehumidification loads.

Day-ahead

Winter and summer day-ahead predictions were tested with 60 days of training data. Figure 30 shows the day-ahead winter predicted disaggregated load. For this test day, the humidity had no impact, so the load consists of refrigeration and base electrical loads. Figure 31 displays the predicted disaggregated loads compared to real measurements. The total predicted load matches the measured values well with an NRMSE of 0.07, however, some refrigeration spikes are not captured, as seen in Figure 31. The general trend of the refrigeration and baseload are predicted well, however times when the refrigeration energy use increases for a short period, are not captured at the 9th, 12th and 20th hours of the day. Figure 32 and Figure 33 display the day-ahead predictions for the summer. As seen in Figure

33, the refrigeration is predicted with an NRMSE of 0.13. The refrigeration load is underpredicted for most of the day, while the base load is overpredicted, which is similar to the winter prediction. It should be also noted that there is a small amount of dehumidification within the space cooling load that is not shown as part of the dehumidification load but can help capture the higher humidity effects during the summer.
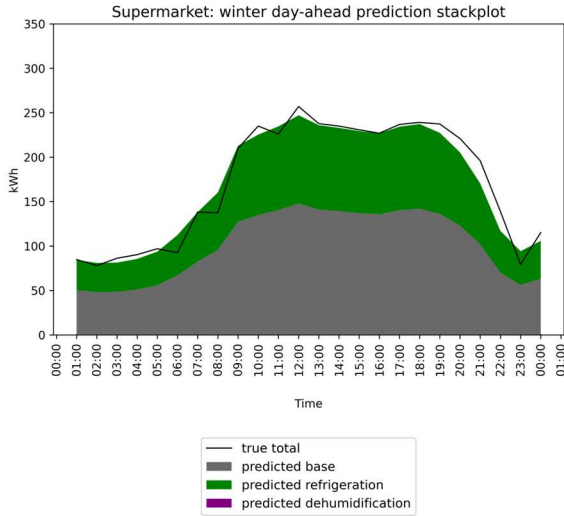
Figure 30: Synthetic supermarket winter day-ahead prediction stackplot for December 14th

Figure 31: Synthetic supermarket winter day-ahead prediction submetered loads for December 14th

Figure 32: Synthetic supermarket summer day-ahead prediction stackplot for July 13th
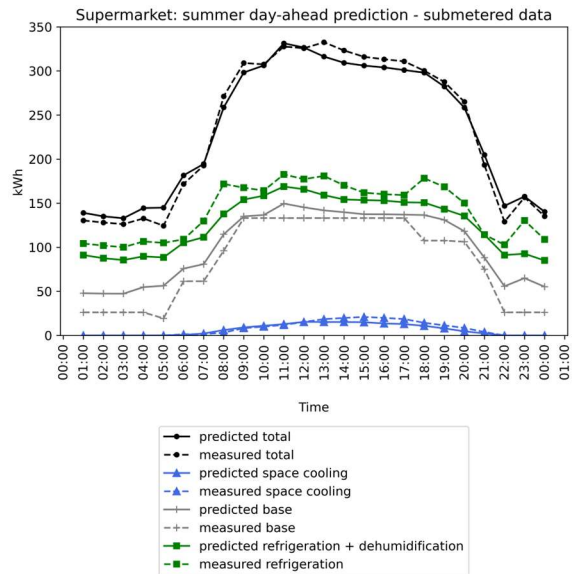
Figure 33: Synthetic supermarket summer day-ahead prediction submetered loads for July 13th

Long term prediction

Similar to Section 3.6.3.4, a full year-ahead prediction is not possible for the test case since there is not enough synthetic training data. A long-term prediction with a 60-day test set, using 60 days of training data was evaluated for the winter and summer. Figure 34 and Figure 35 display the long-term winter predictions while Figure 36 and Figure 37 display one sample day from the long-term prediction. The winter model predicts the hourly total load well, with an NRMSE of 0.14. In Figure 35, the model captures the increase in total load due to temperature (green) and humidity (purple) levels in early November. There are also two days in the test set with poor predictions: November 11th and November 23rd which are American holidays for the reference building dataset. However, the proposed model will be used on buildings following the Ontario holiday schedule, so they can be neglected. Figure 38 and Figure 39 show long-term summer model predictions, with one sample day displayed in Figure 40 and Figure 41. As seen in Figure 38, long-term summer electricity use is predicted with an NRMSE of 0.06. In Figure 39, the space cooling load prediction is poor with the load underpredicted with an NRMSE of 0.79. However, the refrigeration load is larger because it makes up 40-50% of the electrical load and will result in more recoverable heat. Therefore it is more important to accurately capture the refrigeration load, which has an NRMSE of 0.13, than the space cooling load.
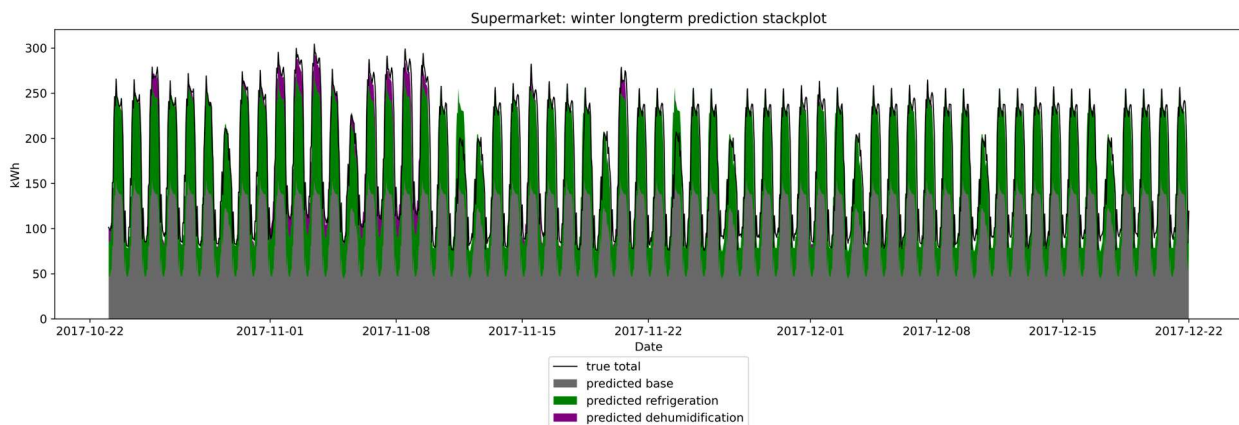
Figure 34: Synthetic supermarket winter long-term prediction stackplot from October to December
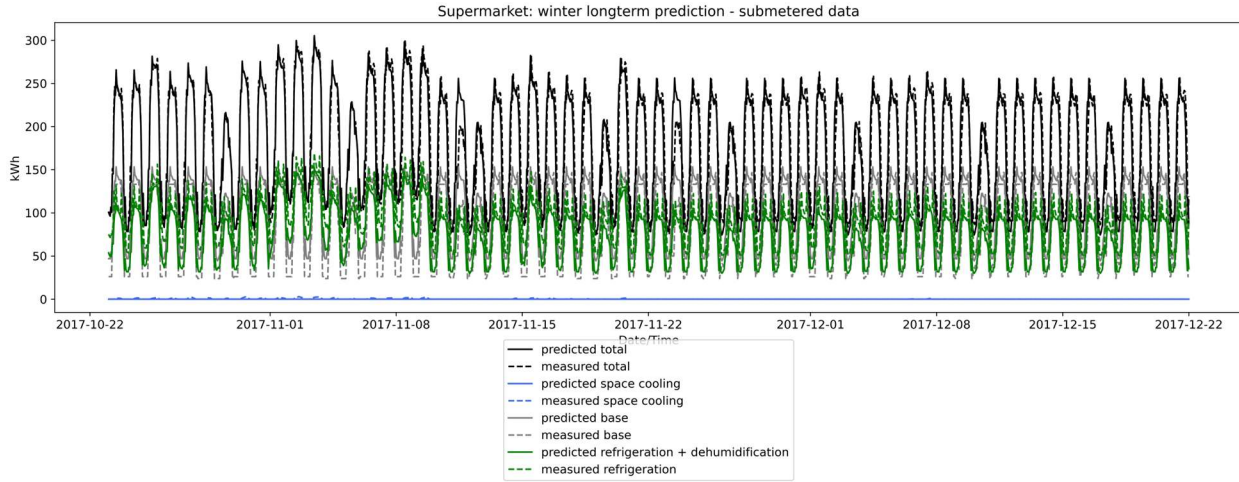
Figure 35: Synthetic supermarket winter long-term prediction submetered loads from October to December
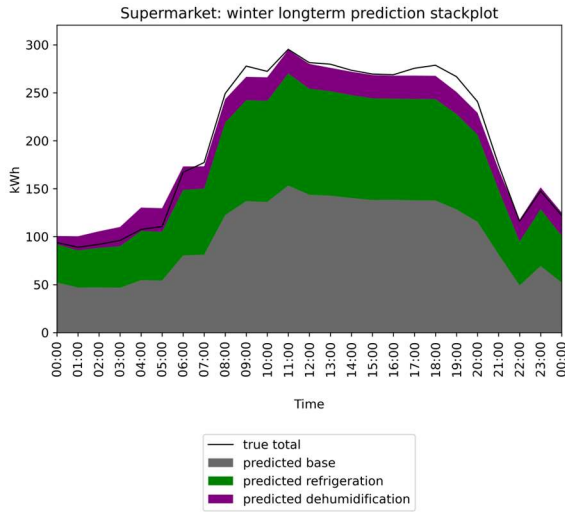
Figure 36: Synthetic supermarket winter long-term prediction sample day (November 1st) stackplot
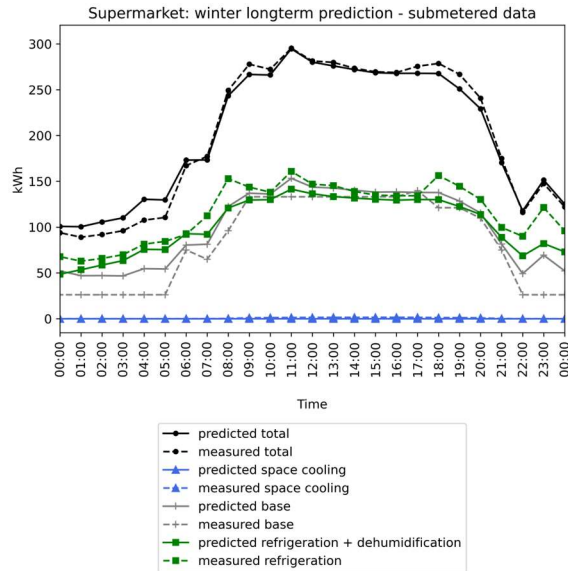
Figure 37: Synthetic supermarket winter long-term prediction sample day (November 1st) submetered loads
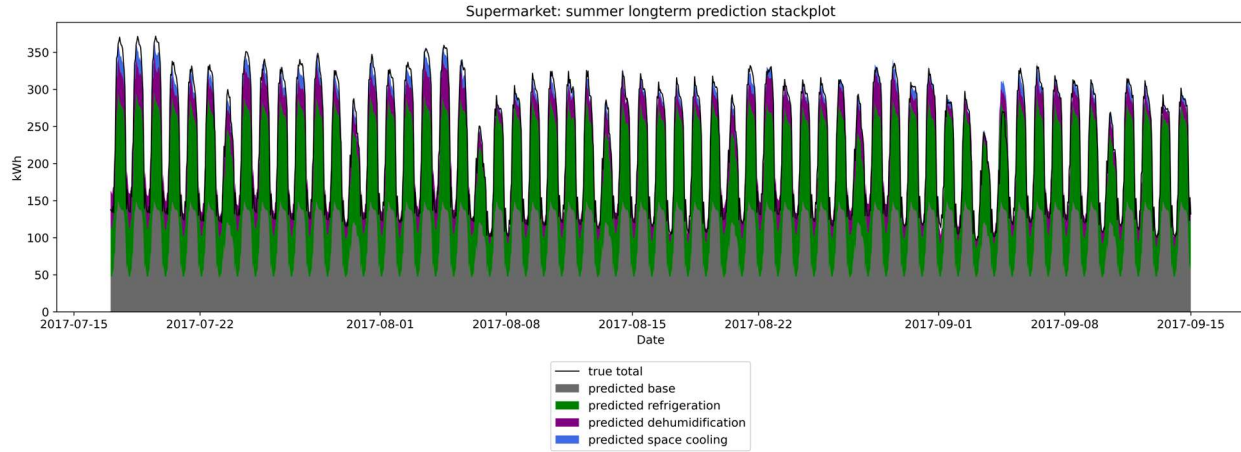
Figure 38: Synthetic supermarket summer long-term prediction stackplot from July to September
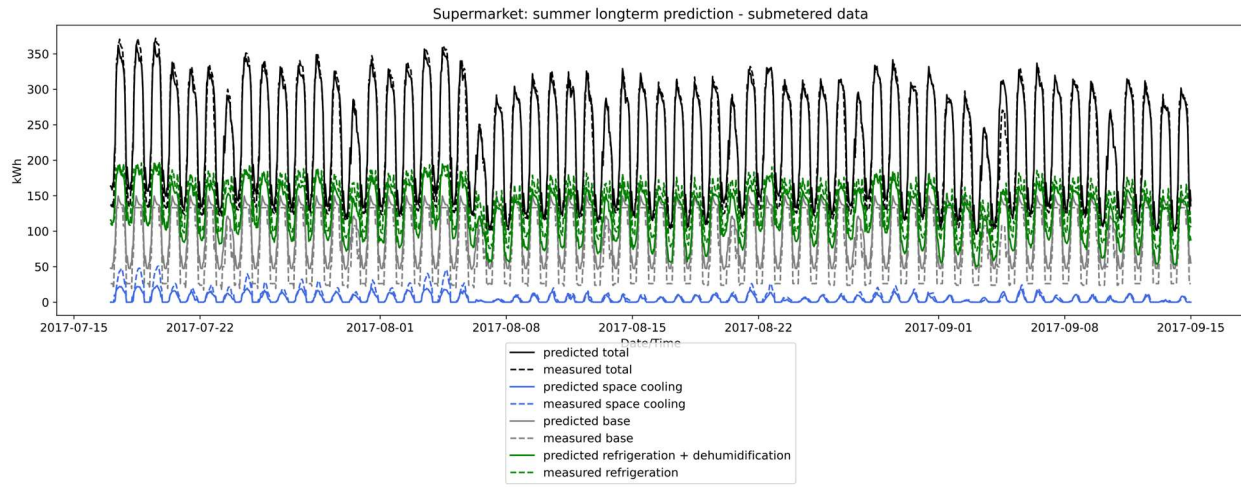
Figure 39: Synthetic supermarket summer long-term prediction submetered loads from July to September
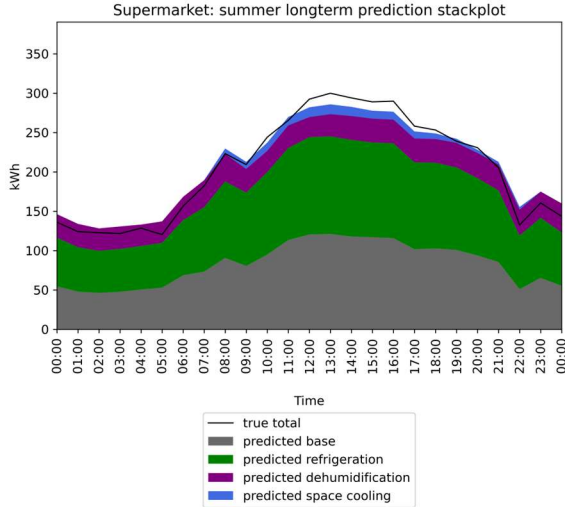
Figure 40: Synthetic supermarket summer long-term prediction sample day (July 23rd) stackplot
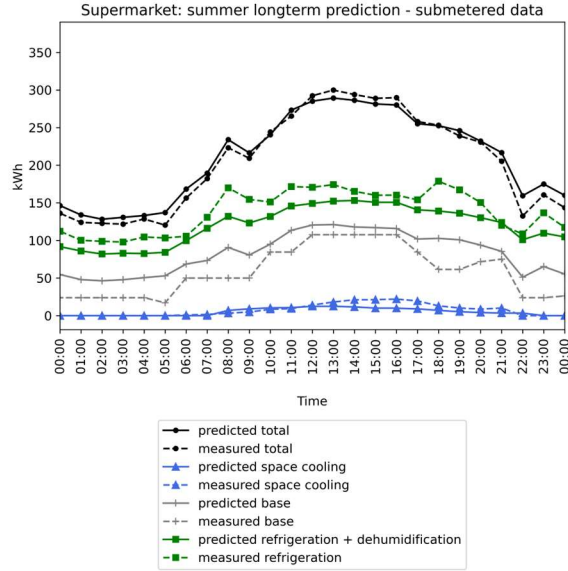
Figure 41: Synthetic supermarket summer long-term prediction sample day (July 23rd) submetered loads

Table 6 summarizes the normalized root means squared error for each supermarket test case. The total hourly error for all four cases is below 0.14 with the daily error below 0.04. Performance on synthetic data is better than expected because there is no sporadic occupant behaviour, as mentioned in Section 3.6.3.4. Notably, the disaggregated refrigeration load prediction is worse in the winter, despite the summer model being trained on winter data as well. The daily average refrigeration loads are predicted better than the hourly scale for long-term predictions, however, the opposite applies for the sample day-ahead predictions.

Table 6: Synthetic supermarket verification normalized root mean squared error

Case	Season	Train set length	Test set length	Normalized root mean squared error			
				Total [hr]	Total [day]	Refrigeration [hr]	Refrigeration [day]
A	Winter	60 days	1 day	0.07	0.02	0.22	0.23
B	Summer	60 days	1 day	0.04	0.002	0.13	0.15
C	Winter	60 days	60 days	0.14	0.04	0.24	0.19
D	Summer	60 days winter /	60 days	0.06	0.03	0.13	0.11

		60 days summer					

3.6.5 Hourly arena model

The following section outlines a model for an ice rink arena which will have a high refrigeration load to maintain ice conditions.

3.6.5.1   Heat transfer considerations

There are many heat transfer considerations for ice arenas, making them difficult to model physically even with detailed computational fluid dynamics models [14]. There are various building zones with different thermal needs such as the ice pad, spectator area, change rooms, referee rooms and lobby. This can result in simultaneous refrigeration and space heating in the same zone and ice resurfacing operations and occupants will add additional complexity.

Several sources will add heat to the ice pad such as lighting, radiation from ceiling and walls, skaters and spectators, resurfacing operations, subfloor heating, condensation, refrigeration equipment, convection and ground conduction. Buildings may also have heat recovery systems, spectator heating, heating in other areas such as the lobby or change rooms and dedicated dehumidification systems [98]. The ice rink heat transfer considerations are discussed in more detail in Appendix E: Ice rink refrigeration system.

3.6.5.2   Assumptions

Due to the desire for a simpler model and the limitations of the data available, not all of the heat transfer components mentioned above can be considered in detail. Several loads are grouped as scheduled components, similar to the supermarket model. Analysis of ice rinks is fairly complicated, even with detailed data, due to simultaneous heating and refrigeration needs.

Regarding resurfacing operations, they are scheduled but can vary slightly day-to-day. When multiple ice pads are in the arena, the resurfacing load may be harder to detect on an hourly scale.

Resurfacing load will also depend on the resurfacing machine type and the operator. Different activities will also impact the refrigeration load since the number of spectators and skaters, the amount of heat emitted by skaters and the ice temperature will vary. Compressor energy use, which is based on the heat transfer to the ice, is more difficult without knowledge of refrigeration plant controls, compressor and pump capacities. Therefore many simplifications were made for this model to have a general idea of the refrigeration, space cooling and plug loads from the total electricity based on trends in the data. The model does not consider transfer between spaces such as the lobby or spectator area and the ice rink area. It is difficult to account for this without knowledge of each building's layout and geometry. For simplification, day-typing is not performed for the ice rink, it is assumed that the weekdays and weekends are two day-types.

3.6.5.3   Types of arenas

Four types of arenas were identified based on operation: year-round ice operation, winter-only ice operation, summer-reduced ice operation and entertainment arenas. Heatmaps for one year of electricity use for the first three rink types are displayed below (Figure 42-44). The heatmaps have the hour of the week on the x-axis and the week of the year on the y-axis. Blue colouring depicts higher electricity use whereas light yellow colouring means electricity use is closer to zero. Travelling along the x-axis, each ice rink shows fairly consistent daily patterns over the week. The differences in seasonal operation can be seen by the differences in energy use along the y-axis.

Year-round ice rinks have operational ice pads throughout the entire year. Their electricity use is fairly constant throughout the entire year, shown in the heatmap of total electricity use displayed in Figure 42. The small period of lower electricity use between the 28th and 34th week was for ice pad maintenance, which does not occur every year. Alternatively, winter-only rinks only operate ice pads during the winter months. Some will not operate at all during the summer while others may be open for other activities that do not require ice. A sample arena shown in Figure 43 displays significantly lower electricity consumption in the summer weeks compared to the winter. The third type, summer-reduced, operates all

of their rinks in the winter months, but only a portion of them during the summer as seen in Figure 44. Entertainment rinks are separated as a fourth type with large spectator seating areas that may also be used for events such as concerts. Only three rinks in the database are this type, but their operation should be differentiated from smaller community rinks. The rink types are summarized in Table 7. Arenas were classified into four types based on data from the arena or municipal websites. If data was not available related to the monthly operation, they were classified by visualizing the data.
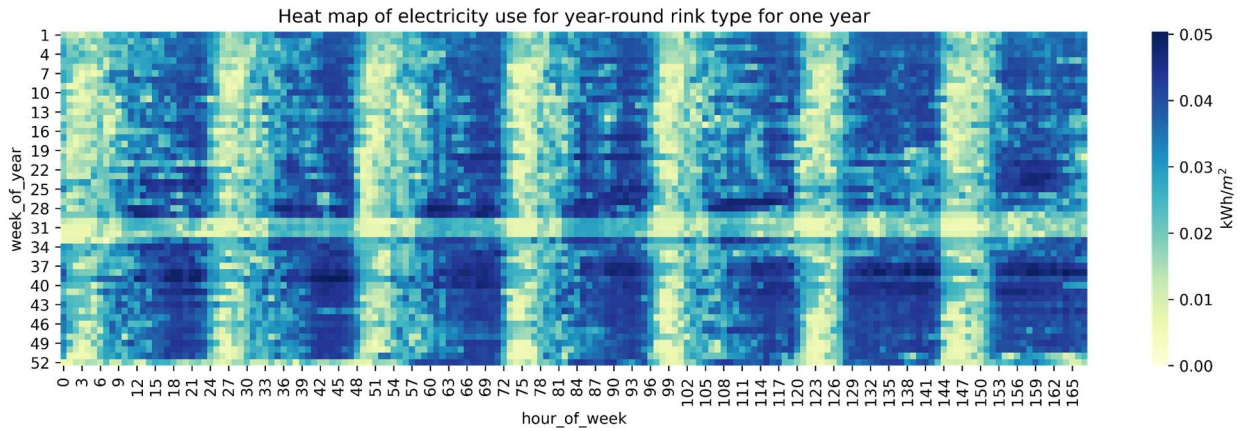
Figure 42: Electricity heatmap for a year-round arena (Arena 1) for one year
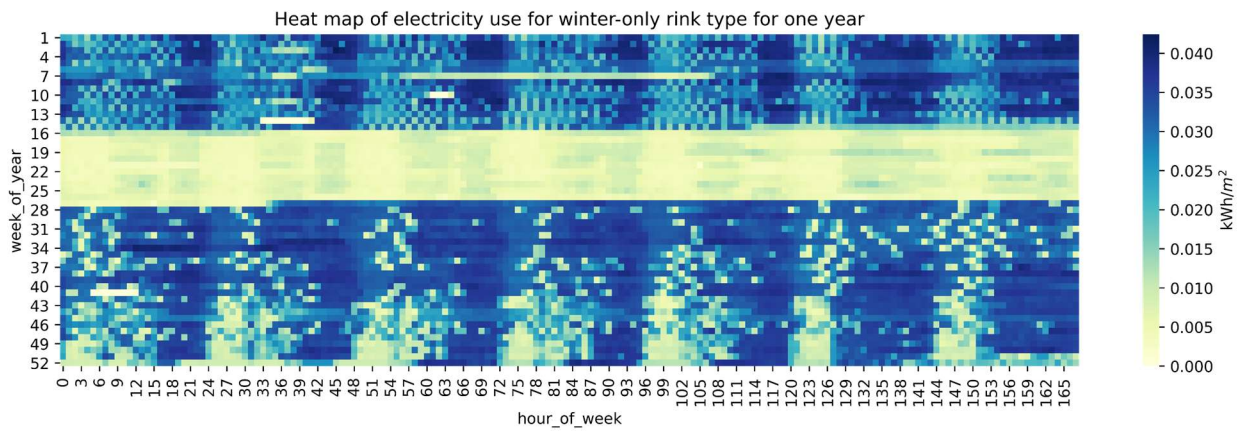
Figure 43: Electricity heatmap for a winter-only arena (Arena 2) for one year
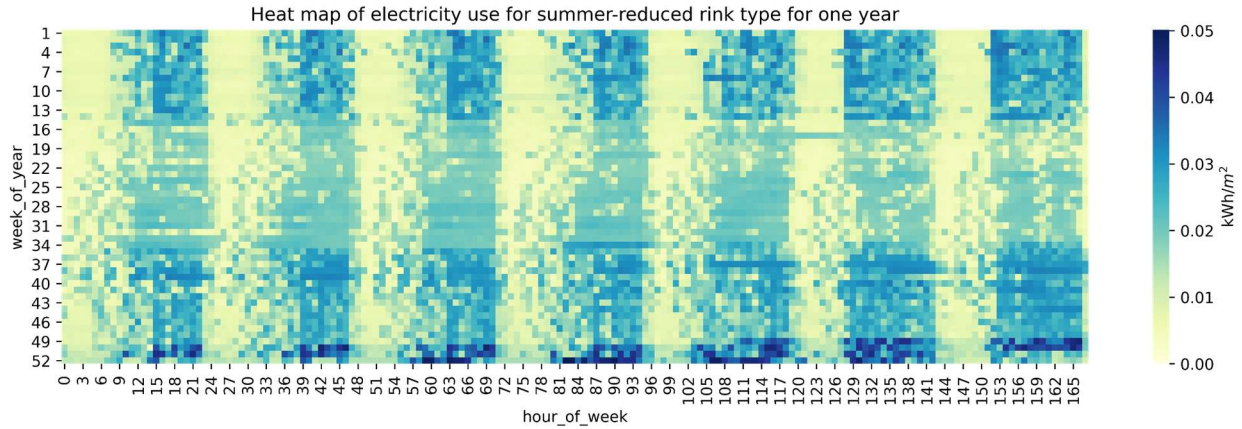
Figure 44: Electricity heatmap for a summer-reduced arena for one year

3.6.5.4   Arena seasons

After specifying the arena operation type, different models are used based on the operation and weather season, as shown in Table 7. The summer, on-season model disaggregates total electricity into the refrigeration, space cooling and base loads. The winter, on-season model disaggregates total electricity into refrigeration and base loads. The summer and winter off-seasons use the EL-CL (electricity-cooling) and EL-HT (electricity-heating) models, respectively, explained in Section 3.6.3. The last season is the transition or ice-making season when new sheets of ice are created [98]. Generally, it only applies to winter-operating and reduced rinks, however, year-round rinks are shut down occasionally for maintenance and the ice is rebuilt. This season could range from a few days to a couple of weeks depending on the rink. The transition season model is not expected to be accurate since there is significantly less training data, but this portion of the year should be excluded from the other sets. Higher and continuous refrigeration loads are expected due to the initial cooling of the slab as well as the freezing of each layer of water added to the ice sheet. The model details are summarized in Table 8. The operation season was assigned manually based on data visualization by specifying the week where operational changes could be detected (e.g. the second week of March). For each building, the season switching dates were set to the same values each year, however, arenas change their opening and closing seasons from year to year. This may be a reason for higher error values in the arena model.

Table 7: Arena electricity models used depending on rink operation type

Rink Type	Weather seasons	Operation seasons	Models
Year-round	Summer, Winter	On*	• Summer-on • Winter-on
Winter-only	Summer, Winter	On, Off, Transition	• Summer-on • Summer-off • Winter-on • Winter-off • Transition (Winter-on)
Reduced	Summer, Winter	Full-on, Reduced-on, Transition	• Full-on (Winter-on) • Reduced-on (Winter-on) • Transition (Winter-on)
Entertainment	Summer, Winter	Case-by-case	Case-by-case

*year-round operation ice rinks will likely have an ice-making period every few years when the ice sheets are removed and rebuilt for maintenance

Table 8: Arena model type descriptions

Model name	Description
Winter-on	• Refrigeration system is on • No space cooling load • Used by all arena types since most will operate through the winter
Summer-on	• Refrigeration and space cooling loads • Train winter-on model before the summer with winter data to predict the refrigeration and baseloads • Train the remainder in the summer to model space cooling
Winter-off	• Baseload only, no refrigeration or space cooling • Uses EL-HT model (the electricity-heating season model) • Time of winter-off period is expected to be short or nonexistent compared to other seasons
Summer-off	• Space cooling and baseload, no refrigeration • Uses EL-CL model (the electricity-cooling season model) • Only used for winter-operation rinks

Transition	- Captures the initial ice-making phase - Compressor use is higher for slab cooling and freezing water - Season is short, ranging from a couple of days to weeks depending on the arena - Uses the winter-on model

3.6.5.5 Model form

Heat sources

The arena refrigeration load is modelled as the sum of scheduled loads and weather-dependent loads. Scheduled loads include heat from lighting, occupants, resurfacing, and pump work which are grouped and modelled with Fourier decomposition.

$$Q_{refrigeration,scheduled} = Q_{lights} + Q_{resurfacing} + Q_{occupants} + Q_{pumps} + Q_{ground\ conduction}$$

$$= k_1 * \sum_{n=1}^{11} \left(a_n \cos\left(\frac{2\pi nh}{24}\right) + b_n \sin\left(\frac{2\pi nh}{24}\right) \right) + k_2 * \beta_o \tag{35}$$

Weather loads include convection from internal air to the ice surface, radiation from internal surfaces to the ice and condensation due to external humidity. Convection from the internal air to the ice surface is based on the temperature difference between the outdoor air and ice temperatures. Radiation is considered by defining the ceiling temperature as a function of internal and sol-air temperatures. The calculation of sol-air temperature is explained in Section 2.2.2. The 2017 ASHRAE Handbook Fundamentals [49] also provides the following values:

$$\frac{\alpha}{h_o} = 0.026\ (\text{light}) - 0.052\ (\text{dark}) \tag{36}$$

$$\frac{\varepsilon \Delta R}{h_o} = 4\ (\text{horizontal}),\ 0\ (\text{vertical}) \tag{37}$$

Using the average values, this yields a general equation for sol-air temperature when building surface areas, properties and orientations are unknown:

$$T_{solair} = T_{outside} + 0.026 * GHI - 2 \tag{38}$$

Due to the combination of radiative and convective heat gains to the ice, it is difficult to solve directly for the ceiling temperature. Therefore, the ceiling temperature is simply assumed to be the average of the sol-air and indoor air ice temperatures. The indoor air temperature, T_{air} is found iteratively and assumed to be a constant value.

$$T_{ceiling} = (1 - f) * T_{air} + f * T_{solair} \tag{39}$$

Where f = 0.5

Heat transfer to the ice in the winter can then be modelled as:

$$Q_{refrigeration} = Q_{scheduled} + Q_{ceiling\,to\,ice} + Q_{convection} + Q_{condensation} \tag{40}$$

Where:

$$Q_{ceiling\,to\,ice} = \beta_1 \left[(T_{ceiling} + 273.15)^4 - (T_{ice} + 273.15)^4 \right]$$

$$Q_{convection} = \beta_2 (T_{solair} - T_{ice})$$

$$Q_{condensation} = \beta_3 (SH_{out} - SH_{in})^+$$

Which yields:

$$Q_{refrigeration} = k_1 * \sum_{n=1}^{11} \left(a_n \cos\left(\frac{2\pi nh}{24}\right) + b_n \sin\left(\frac{2\pi nh}{24}\right) \right) + k_2 * \beta_0 +$$
$$\beta_1 \left[(T_{ceiling} + 273.15)^4 - (T_{ice} + 273.15)^4 \right] + \beta_2 (T_{solair} - T_{ice}) + \beta_3 (SH_{out} - SH_{in})^+ \tag{41}$$

Where:

T = temperature

SH = specific humidity

h = hour of day

In the summer, the space cooling thermal load is the sum of solar radiation, ventilation and the latent load, as outlined in Section 3.6.3. The dehumidification component in Equation 41 is shown as part

of the refrigeration load, however, if the building is known to have a separate dehumidification system, the component can simply be separated and attributed to dehumidification, similar to the supermarket model.

Electricity Use

Electricity use during the on-season is modelled similarly to the supermarket model. The total amount of electricity consumed in the building is the sum of the refrigeration, space cooling and base electrical loads. For the baseload, Fourier decomposition is used. The refrigeration electrical load considers the thermal refrigeration load and adds a component to account for COP changes with external temperature. The efficiency of the refrigeration system is absorbed into the unknown constants, other than the additional inverse Carnot COP component. As noted earlier, while in reality, the inverse COP has a multiplicative effect (i.e. the thermal terms are multiplied by the inverse COP), it is considered an additive component for model stability.

$$W_{base} = (1 - k_1) * \sum_{n=1}^{11} \left(a_n \cos\left(\frac{2\pi nh}{24}\right) + b_n \sin\left(\frac{2\pi nh}{24}\right) \right) + (1 - k_2) * \beta_0 \tag{42}$$

$$W_{refrigeration} = k_1 * \sum_{n=1}^{11} \left(a_n \cos\left(\frac{2\pi nh}{24}\right) + b_n \sin\left(\frac{2\pi nh}{24}\right) \right) + k_2 * \beta_0 +$$
$$\beta_1 * \left[\left(T_{ceiling} + 273.15\right)^4 - \left(T_{ice} + 273.15\right)^4 \right] + \beta_2 * (T_{solair} - T_{ice}) + \beta_3 (SH_{out} - SH_{in})^+ +$$
$$\beta_4 * \left[\frac{T_{out} - T_{ice}}{T_{ice} + 273.15} \right]^+ \tag{43}$$

$$W_{total,winter} = W_{base} + W_{refrigeration}$$

$$W_{total,winter} = \sum_{n=1}^{11} \left(a_n \cos\left(\frac{2\pi nh}{24}\right) + b_n \sin\left(\frac{2\pi nh}{24}\right) \right) + \beta_0 +$$
$$\beta_1 * \left[\left(T_{ceiling} + 273.15\right)^4 - \left(T_{ice} + 273.15\right)^4 \right] +$$
$$\beta_2 * (T_{solair} - T_{ice}) + \beta_3 (SH_{out} - SH_{in})^+ + \beta_4 * \left[\frac{T_{out} - T_{ice}}{T_{ice} + 273.15} \right]^+ \tag{44}$$

Similar to the supermarket model, the default values of constants k_1 and k_2 are set manually, based on literature and submetered data, but can be adjusted based on the ratio of rink area to total building floor area. For this model, we assume that around 50-65% of the electrical load is used for refrigeration, when the ice is in use, based on example ice rinks (e.g. [4][99][100][101][102]) and submetered data.

The ice temperature, T_{ice} is a scheduled setpoint value. For this model, it is assumed based on literature and a survey of one arena [Energy coordinator, personal communication, April 2022]. The daytime setpoint is assumed to be -8 °C while the nighttime setpoint is -7 °C. The daytime and nighttime switching times are detected based on edge detection of total electricity use. For a more accurate model, the actual schedule and setpoints can be used if they are known.

The summer-on model simply builds off of the winter-on model, with the addition of the space cooling load, shown in Equation 45. However, some buildings may not have space cooling loads in the summer if they are not in use during those months. A similar method to the grocery store model is used where the winter model is trained before the summer model. The learned coefficients are used to predict the refrigeration and baseload profiles throughout the full year which assumes no seasonal variation of the baseload.

$$
\begin{aligned}
W_{total,summer} = \sum_{n=1}^{11} & \left(a_n \cos\left(\frac{2\pi nh}{24}\right) + b_n \sin\left(\frac{2\pi nh}{24}\right) \right) + \beta_0 + \\
& \beta_1 * \left[\left(T_{ceiling} + 273.15\right)^4 - \left(T_{ice} + 273.15\right)^4 \right] + \\
& \beta_2 * \left(T_{solair} - T_{ice}\right) + \beta_3 \left(SH_{out} - SH_{in}\right)^+ + \beta_4 * \left[\frac{T_{out} - T_{ice}}{T_{ice} + 273.15} \right] + \\
& \beta_5 * \left(T_{out} - T_{in}\right)^+ + \beta_6 * GHI + \beta_7 * \left(SH_{out} - SH_{in}\right)^+ + \beta_8
\end{aligned} \tag{45}
$$

As mentioned earlier, the off-seasons are modelled with similar terms as the EL-CL and EL-HT models explained in Section 3.6.3.

3.6.5.6   Verification with real data

The model is validated with real, submetered data for two arenas. Arena 1 operates year-round, while Arena 2 operates its ice pads during the winter only. There are some integrity issues with the submetered data because all the submetered loads do not sum exactly to the total measured use. The total refrigeration and heating and cooling values are given, so the baseload is calculated as:

$$\text{baseload} = \text{total} - \text{refrigeration} - \text{heating and cooling}$$

to ensure the three sub-loads add up to the total measured electricity. However, the inferred baseload may contain some HVAC or refrigeration-related loads that are not submetered which can be seen in Figure 45.
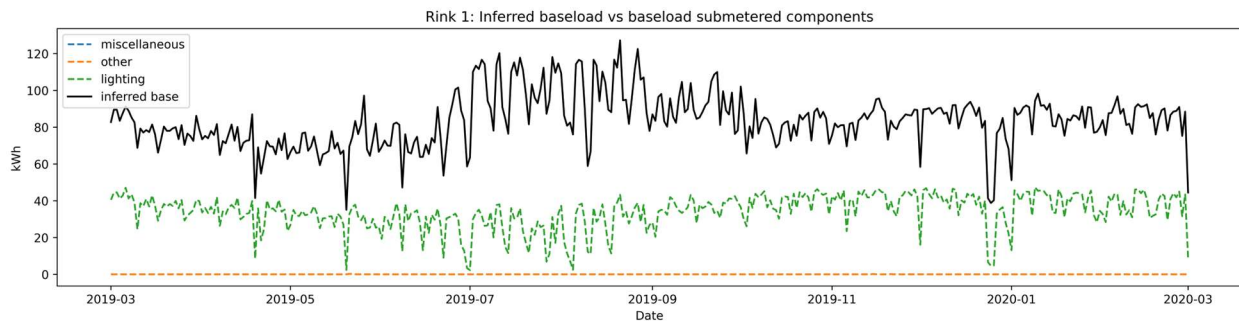
Figure 45: Arena 1 inferred baseload vs submetered base components for one year from March 2019 to March 2020

Arena 1 (Year-round)

Rink 1 had approximately five years of submetered data from 2017-2021. This included submetered loads for condenser fans, pumps, compressors, lighting, heating and cooling fans. However, the years 2020 and 2021 were not considered due to the impact of the COVID-19 pandemic.

Arena 1 has four ice pads with concrete floors and rentable community rooms that operate year-round. Two rinks are shut down for four to eight weeks of maintenance every three years.   After maintenance is performed, it takes approximately seven to ten days to build a fresh pad of ice after maintenance. A heatmap of electricity use for Arena 1 during 2017 is shown in Figure 42, with

maintenance seen to occur around week 31. The daily operation of the arena is from 5 am to 12:45 am. The ice pads are resurfaced two to eight times during the day depending on programming and season, and 8-15 times in the evening hours. The rink area does not have air conditioning, and infrared heaters are located above the spectator area but are not often used. The ice plant uses seven compressors: four 50 HP reciprocating compressors, two 75 HP reciprocating compressors and one 45 HP screw compressor.

Day-ahead

The winter day-ahead prediction was trained on 60 days of training data, while the summer was trained with 60 days of summer data and 100 days of winter data. Figure 46 and Figure 47 display the winter day-ahead prediction for Arena 1. As seen in Figure 47, the model is not able to predict the sharp changes in refrigeration load due to the compressors and pumps cycling on or off. A large fall in electricity consumption is seen around 8 am in Figure 47 which the model did not predict. For most weekdays in the winter, the compressor load increases in the morning when the arena opens due to lights turning on and the ice temperature setpoint being reduced. The compressor load then falls, perhaps once the setpoint has been reached and with reduced activity early in the day. The load then increases in the afternoon and evening, as activity levels increase. However, the time at which the compressors cycle off and on is different each day. Figure 48 and Figure 49 show the summer day-ahead prediction for Arena 1. During the summer, the refrigeration load is under-predicted for most of the day. As a result the peaks in total electricity use are under-predicted around 12 pm and in the evening. Additionally, the model overpredicts space cooling consumption because Arena 1 does not have air conditioning in the rink. However the rooftop units run occasionally during the summer, so it may have air conditioning in other areas of the building, as seen in Figure 49. Overall the daily load is captured reasonably well for both the summer and winter days with NRMSEs of 0.02 and 0.08.
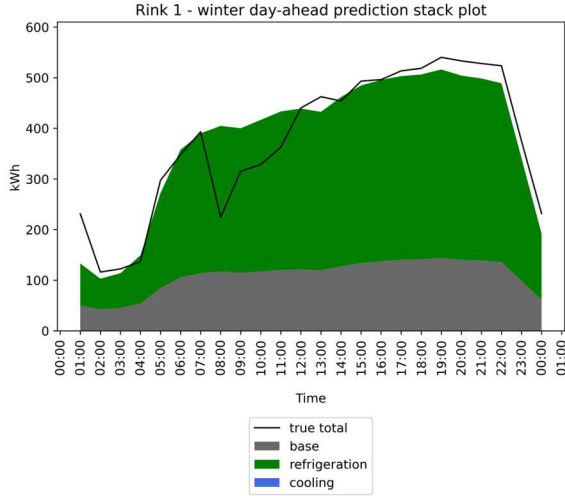
Figure 46: Arena 1 winter day-ahead prediction stack plot for December 13th, 2019
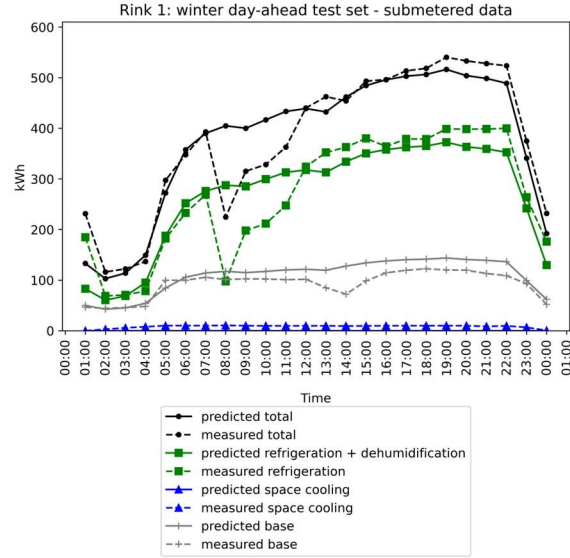
Figure 47: Arena 1 winter day-ahead prediction with submetered loads for December 13th, 2019
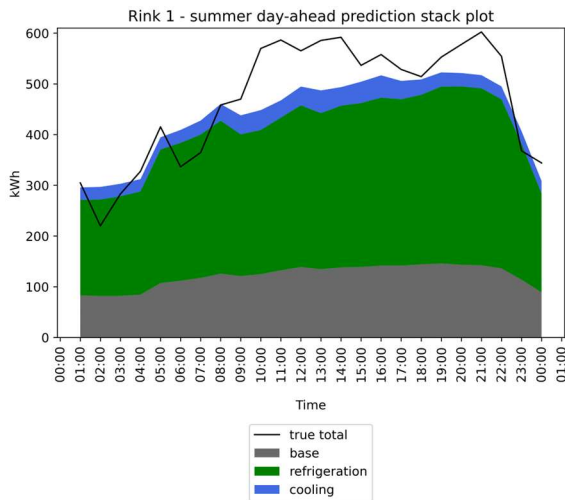
Figure 48: Arena 1 summer day-ahead prediction stack plot for July 2nd, 2019
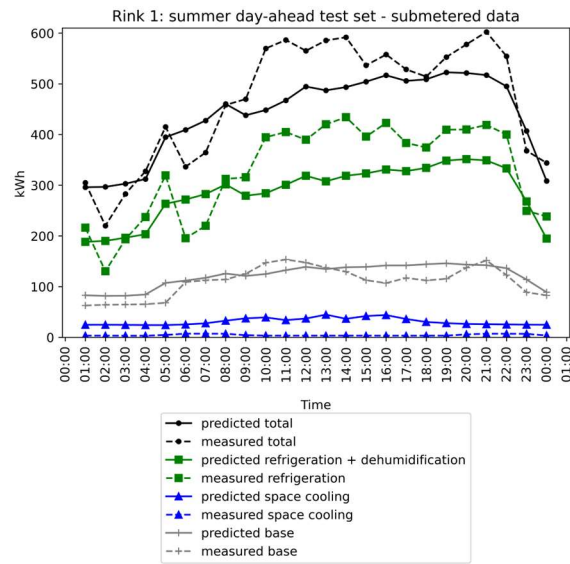
Figure 49: Arena 1 summer day-ahead prediction with submetered loads for July 2nd, 2019

Year-ahead

The year-ahead prediction was performed with one year of training data. Figure 50 displays the year-ahead prediction as hourly average loads for each day to improve data visibility. Figure 51 and Figure 52 display a sample winter day from the year-long prediction. Figure 53 and Figure 54 display a

sample summer day from the year-long prediction. As seen in Figure 50, the daily average total and refrigeration are modelled fairly well at the daily scale with an NRMSE of approximately 0.1 for both loads. However, the highs and lows are not captured as well on an hourly scale; the hourly NRMSE is 0.2 and 0.24 for the total and refrigeration loads respectively. The electrical baseload prediction does not capture any seasonal variation, as it assumes the same hourly baseload profile for each day. In reality, the electrical baseload varies seasonally which is confirmed by the submetered lighting loads in Figure 45. However, the data integrity issues noted earlier should be considered because the lighting loads increase during the winter, not the summer as shown in Figure 45.
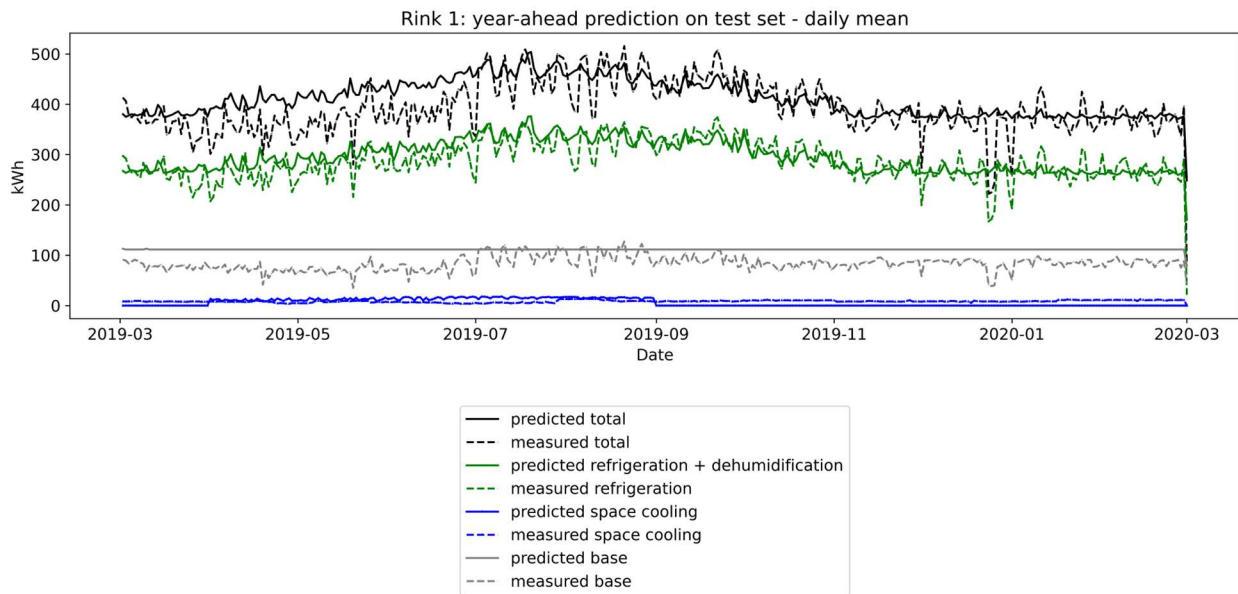
Figure 50: Arena 1 year-ahead prediction with submetered loads on a daily average scale from March 2019 to

March 2020
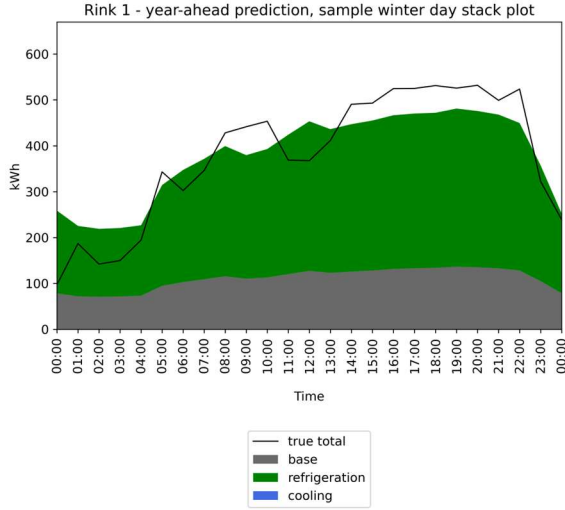
Figure 51: Rink 1 long-term prediction, winter sample day (November 1ˢᵗ) stackplot
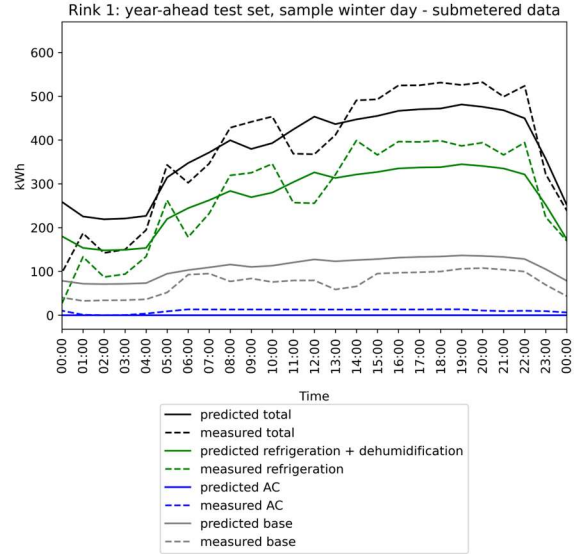
Figure 52: Rink 1 long-term prediction, winter sample day (November 1ˢᵗ) submetered loads
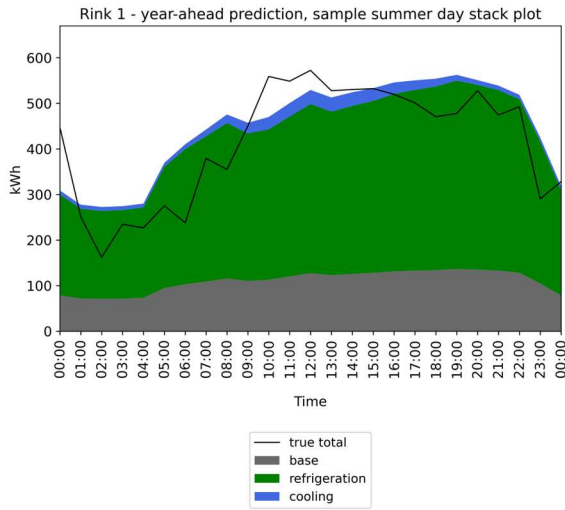
Figure 53: Rink 1 long-term prediction, summer sample day (July 9ᵗʰ) stackplot
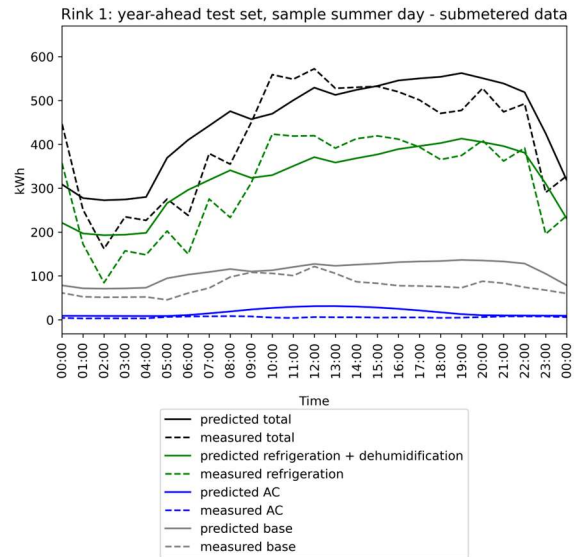
Figure 54: Rink 1 long-term prediction, summer sample day (July 9ᵗʰ) submetered loads

Table 9: Normalized root mean squared error for Arena 1 electricity predictions

Case	Season	Test set length	Normalized root mean squared error			
			Total [hr]	Total [day]	Refrigeration [hr]	Refrigeration [day]
A	Winter	Day	0.15	0.02	0.21	0.02
B	Summer	Day	0.13	0.08	0.21	0.18

| C | N/A | Year | 0.20 | 0.10 | 0.24 | 0.09 |

Arena 2 (Winter-only)

Arena 2 operates its two ice pads during the winter season from July to March, although exact dates may vary year to year. It also has community rooms available and the empty pads are used for other activities during the summer. The electricity use from 2017 is displayed in Figure 43.

Day-ahead

The winter day-ahead prediction was trained on 60 days of training data, while the summer was trained with 30 days of summer data. Figure 55 and Figure 56 show the winter day-ahead prediction for Arena 2. As seen in Figure 56, the hourly model has difficulty capturing the cycling in the refrigeration load. The measured refrigeration load fluctuates between 50 to 150 kWh; however, the predicted loads are smoother. This is because the Fourier terms in the model are not able to capture the different cycling times on different days, so the loads are averaged. Figure 57 and Figure 58 display the summer day-ahead prediction for Arena 2. As seen in Figure 58, the model also does not capture the peaks well for the summer off-season day with an NRMSE of 0.20. Additionally, the space cooling load is overpredicted while the baseload is underpredicted. This may be due to the arena being open sporadically during the summer when the ice pads are not in use, so the model does not produce accurate results. However, the summer off-season loads are approximately one fifth of the on-season loads as seen in Figure 59, so the error is not as significant compared to the refrigeration load during the on-season.
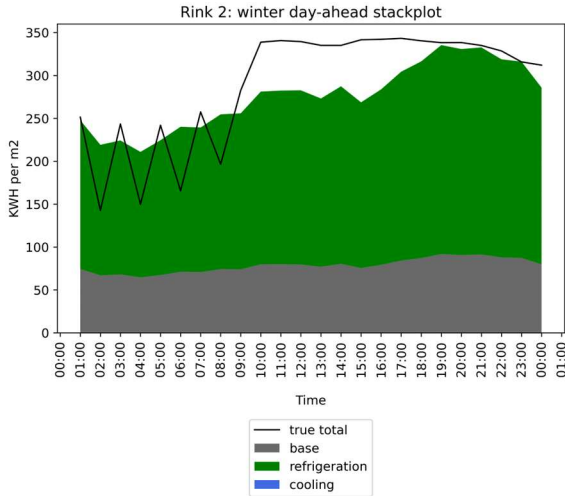
Figure 55: Arena 2 winter day-ahead prediction stack plot for December 8th, 2019
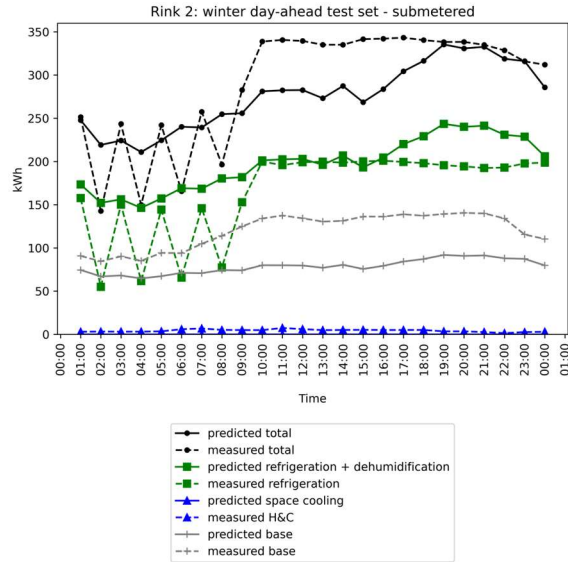
Figure 56: Arena 2 winter day-ahead prediction with submetered loads for December 8th, 2019
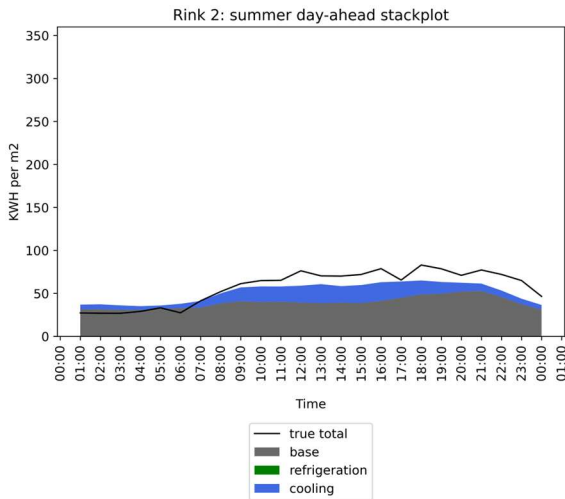
Figure 57: Arena 2 summer day-ahead prediction stack plot for July 2nd, 2019
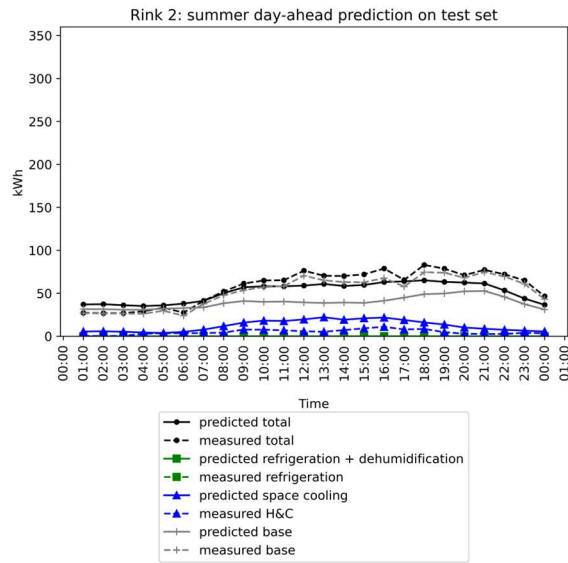
Figure 58: Arena 2 summer day-ahead prediction with submetered loads for July 2nd, 2019

Year-ahead

The year-ahead prediction was performed with one year of training data. The transition season occurs in August; however, it is not as important as the regular season prediction. Figure 59 displays the year-long prediction for Arena 2 on a daily-average scale. As seen in Figure 59, during the on-season, the total is underpredicted resulting in a year-round NRMSE of 0.34, due to the baseload being

underpredicted. The refrigeration load prediction is significantly worse than Arena 1, with a daily

NRMSE of 0.40 and an hourly NRMSE of 0.57. The high hourly error is likely due to the compressors

cycling on and off; Arena 1 has more rinks than Arena 2, making the aggregate compressor electricity use

appear smoother. However, with Arena 2, each compressor will have a larger impact on total energy use

and the complicated cycling is more distinguishable in the total electricity load. During the off-season,

the space cooling load is over-predicted, and the measured baseload is fairly random depending on when

the building is in use. The NRMSE for each test case explored for Arena 2 is summarized in Table 10.
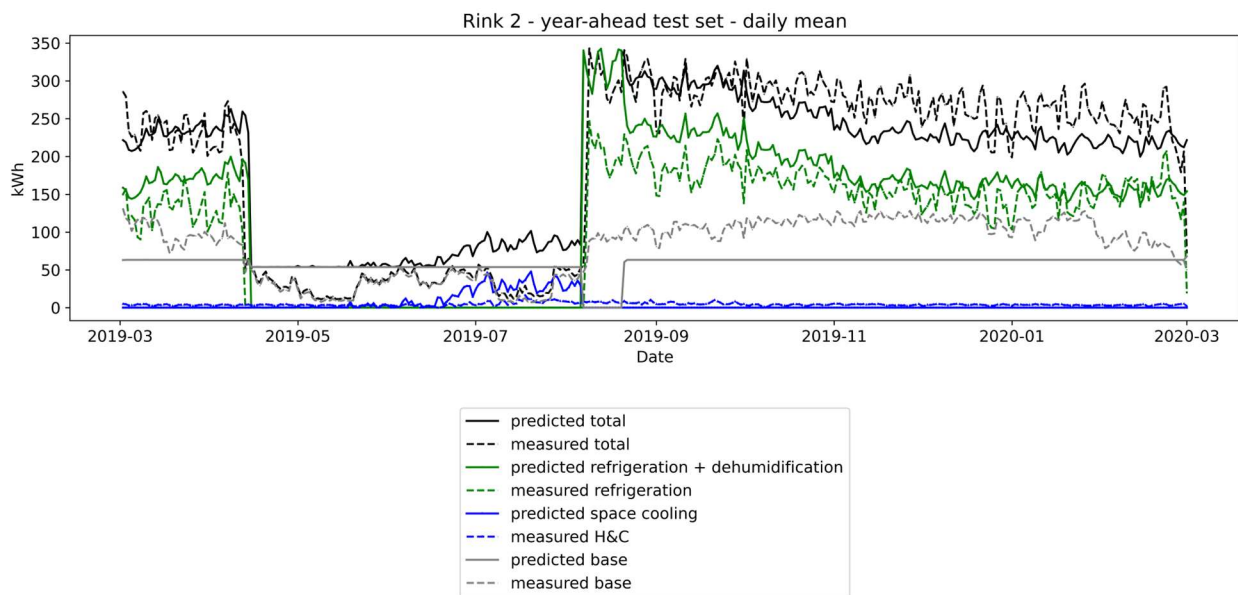
Figure 59: Arena 2 year-ahead prediction with submetered loads at the daily average scale from March 2019 to

March 2020
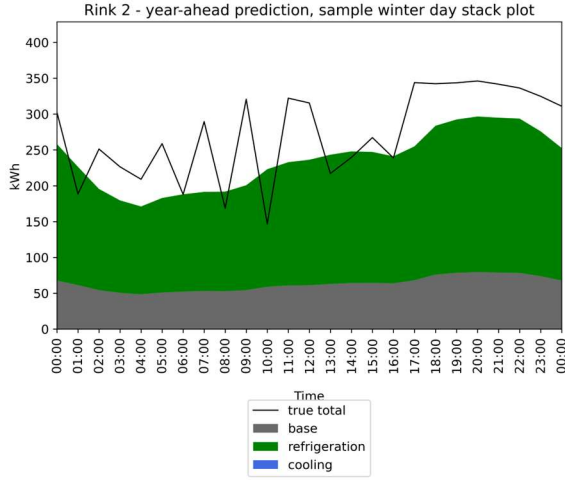
Figure 60: Rink 2 long-term prediction, winter sample day (November 1st) stackplot
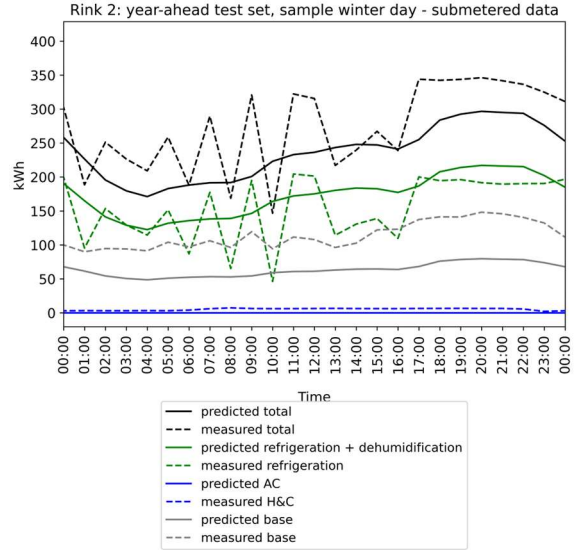
Figure 61: Rink 2 long-term prediction, winter sample day (November 1st) submetered loads

Table 10: Normalized root mean squared error for Arena 2 electricity predictions

| Case | Season | Test set length | Normalized root mean squared error | | | |
			Total [hr]	Total [day]	Refrigeration [hr]	Refrigeration [day]
A	Winter	Day	0.15	0.06	0.28	0.27
B	Summer	Day	0.20	0.14	-	-
C	N/A	Year	0.34	0.22	0.57	0.40

3.6.6 Five-minute arena model

The earlier proposed models offer a simplified method of disaggregating use at an hourly timescale when little information is available for the building. When ICE-Harvest systems are implemented, more information for each building could be available such as equipment specifications, expected day-ahead schedules and floor area breakdowns. Additionally, for short-term controls, a day-ahead model at a sub-hourly timescale is required. Therefore this model focuses on accurate day-ahead predictions.

A higher-resolution model is proposed using a NILM (non-intrusive load monitoring) approach to produce a more detailed and accurate model. It can be used when high-resolution data is available, 5 minutes in this case, in addition to more detailed information related to the building. The model first disaggregates electricity into refrigeration and non-refrigeration loads using a combinatorial optimization approach. Then a predictive machine learning algorithm is applied to the disaggregated loads to forecast refrigeration compressor energy use. Because the model consists of two stages, the accuracy of the initial disaggregation stage will impact the forecasting stage. A single model was created and tested for Arena 1, for which detailed submetered data and knowledge of the building operating and equipment were provided.

3.6.6.1   Disaggregation

A combinatorial optimization approach was taken to disaggregate the refrigeration load from the total load, treating the problem as a knapsack problem [71]. Detailed disaggregation was performed for the compressors over the other loads (e.g. lights, pumps, heating and cooling) to allow for calculation the amount of residual heat available for harvesting. Rodriguez and Makonin's [71] method has a training stage using submetered data, however, in this work, it was desirable to use a semi-unsupervised approach that does not require extensive submetering. The disaggregation approach only takes the expected capacity of each compressor, as well as the average expected capacity of the other total loads (lights, pumps, heating and cooling system). This may require calculations or short measurements of appliance power draws but is less intensive and expensive than submetering each component for an extended period.

Each time sample is treated as a version of the 0-1 knapsack problem where the sum of the capacities of each component is set to ON or OFF depending on the total measured power as described by Hart [9]:

$$P(t) = \sum_{i=1}^{n} a_i(t)P_i + e(t) \tag{46}$$

Where:

i = component

$P(t)$ = measured aggregate building power consumption (kW)

$a_i(t) = \begin{cases} 0, \text{component i is off at time t} \\ 1, \text{component i is on at time t} \end{cases}$

P_i = component power (kW)

$e(t)$ = error

In the classic knapsack problem, each component has a weight and profit. The algorithm aims to maximize total profit while keeping the combined weights below the knapsack capacity. In this case, each component's profit is assumed to be equal and the sum of the collection of components with the lowest error is selected instead of constraining the sum to be less than the knapsack capacity. Therefore, $a(t)$ is found that minimizes the error [9]:

$$\hat{a}(t) = \underset{a}{\text{argmin}} \left| P(t) - \sum_{i=1}^{n} a_i(t)P_i \right| \tag{47}$$

The downside to this approach is that each time step is treated separately, so it does not consider that components are likely to remain on or off in consecutive time steps. This is why Hart [9] chose to use an event detection method instead. In this work, because a non-supervised approach is desired and the resolution is low, component energy signatures are difficult to learn. However, the aim is to disaggregate by component groups instead of individual appliances and the compressor energy use and capacities are large relative to the other loads. As a result, the total compressor load is disaggregated reasonably well by treating the problem as a knapsack problem despite the fallbacks. The model could be improved in the future to account for interactions of components and consider the time series nature of the data.

Before applying the disaggregation algorithm, a bilateral filter is applied to the aggregate power measurements similar to Rodriguez and Makonin [71]. This helps reduce the impact of sudden spikes when components turn on. While these are important features in the data, for the sake of disaggregation based on average expected power draws, they are removed. Additionally, combinatorial problems with large datasets can be solved with optimization approaches such as the evolutionary algorithm, particle swarm optimization or simulated annealing. In this case, total power is disaggregated into components rather than individual appliances. The number of components considered is low and a brute-force approach was able to disaggregate around 26 000 samples in under 5 minutes.

3.6.6.2   Forecasting

Following disaggregation, several algorithms were tested for predicting the total compressor loads: ordinary least squares linear regression, ridge regression, support vector regression and a neural network. The models were tested as single-step predictions using temperature, specific humidity and time-of-day input parameters to predict one time step, 24 hours ahead. The ridge regression model was trained with a regularization parameter of 100. The support vector regression model used a radial basis function kernel with a regularization parameter of 100 and epsilon of 0.1.

A long short-term memory recurrent neural network (LSTM RNN) was also trained using the past 24 hours (288 5-minute measurements) of predicted disaggregated compressor loads and the expected temperature, dew point, relative humidity and pressure. After light parameter tuning, the model was created with two LSTM layers with 4 and 8 units respectively, with dropout of 0.1 and one dense layer with 1 unit. The network was trained for approximately 200 epochs using the Adam algorithm and a learning rate of 0.0001. More in-depth parameter tuning could be performed to improve results.

3.6.6.3   Verification with submetered data

90 days of submetered, 5-minute electricity consumption data from Arena 1 were disaggregated using the approach explained in Section 3.6.6.1. The predicted, disaggregated compressor loads over two

days are displayed in Figure 62. The 5-minute disaggregated predictions have sufficient noise compared to the actual submetered values, with an RMSE of 33 kW. The 5-minute predictions were upsampled to hourly time steps and showed better agreement with the measured compressor loads at 60-minute increments with an RMSE of 20 kW.
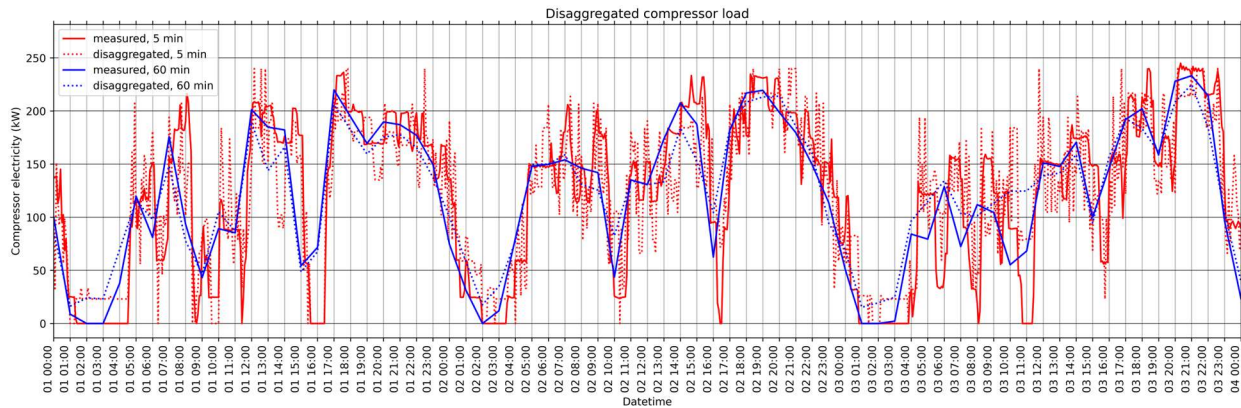
Figure 62: Disaggregated compressor loads using combinatorial optimization for three days

Following disaggregation, the predicted disaggregated load is used to train a forecasting model. The predictions from ordinary least squares (OLS), ridge and support vector (SV) regression and an LSTM RNN are shown in Figure 63, compared to the predicted disaggregated and true compressor loads. None of the algorithms were able to predict the cycling of compressors well, with the RMSE ranging between 47 and 52 kW as summarized in Table 11. This is partially due to the RMSE in the predicted disaggregated load of 33 kW. It is difficult for the algorithms to detect the patterns in compressor use, however, the models, specifically the neural network may be improved with different architecture, different features or more input data.
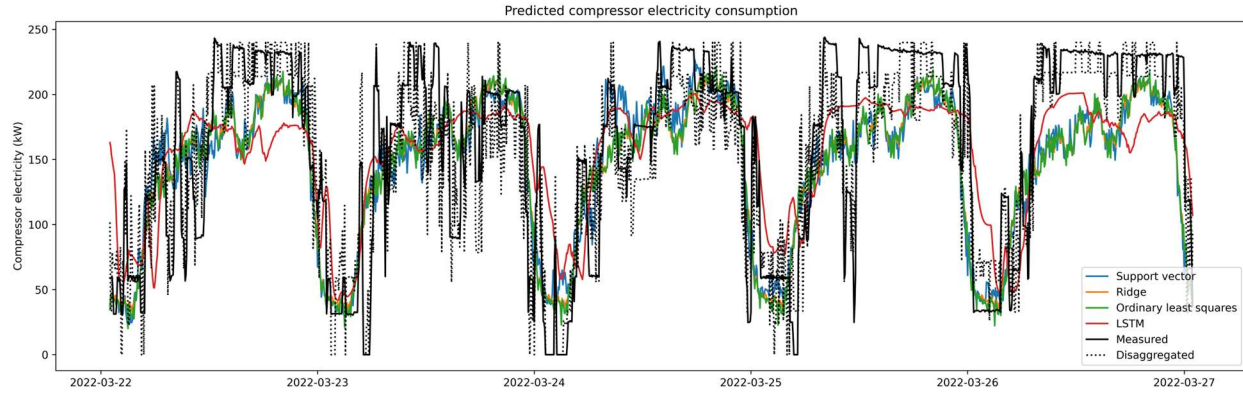
Figure 63: Forecasted compressor loads – single-step prediction on the test set for five days

Table 11: RMSE on the test set for compressor prediction algorithms

Algorithm	Disaggregated	SVR	Ridge	OLS	LSTM RNN
RMSE (kW)	33.0	47.5	47.4	47.5	51.4

3.7   Natural gas model

The majority of heating data provided by utility partners are in the form of monthly gas bills. Periods between bills can range from around 2 weeks to 2 months for the same building. However, for the design of ICE-Harvest systems, an estimate of the hourly heating load is desired. Therefore a methodology is required to perform temporal (time-series) disaggregation of monthly heating data to predict hourly heating demand. This involves increasing the resolution of the data by a factor of approximately 720.

3.7.1 Heat sources

Similar to the electricity model, a steady state approach is used where during each month and hour, the amount of heat entering and leaving the building is assumed to be equal. Only the impact of temperature was considered to account for convection and conduction through the envelope as well as ventilation. A simpler approach is used because of the goal to increase the resolution with fewer data points. For example, if two years of data are available, there are only twenty-four data points, making hyperplane-fitting in multiple dimensions difficult. Similar to the electricity model, gas use is split into a

thermal and base load, with the baseload consisting of hot water heating. For simplicity, the base heating load is only attributed to hot water heating, however appliance gas-use could be considered if the schedule of appliances is available. For example, grocery stores or restaurants may use gas-powered stoves. Ice rinks and grocery stores may use gas-heated desiccant dehumidifiers, however, the impact of humidity was not considered in this analysis

3.7.2 Model form

Variable-degree-day [41] or change-point (piece-wise linear regression) [18] approaches were used, depending on the building gas use trend. Both assume a simple linear relationship between gas use and a temperature term. Some buildings' gas use may display non-linear patterns such as exponential terms or higher-order equations. However, a simple linear model was fairly accurate and interpretable with less data points. Additionally, when fitting higher order functions, the predicted gas use at temperatures outside of the limits can grow to unreasonable values.

The degree day approach assumes constant gas use when the outdoor temperature exceeds the base temperature, which is interpreted as similar to the internal setpoint. This means the service hot water heating energy use does not change with outdoor temperature. The degree day model is referred to as the GS-DD model and is formulated as:
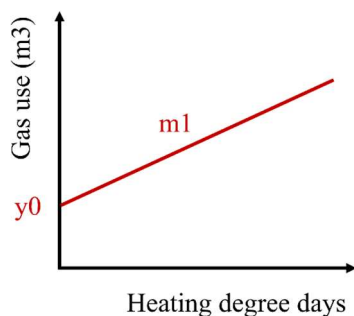
$$Gas = m_1 * (T_{base} - T_{outdoor})^+ + y0 \qquad (48)$$

Figure 64: Gas heating degree day model

Alternatively, the change-point model fits two separate lines that join at a change-point. It can capture the impact of outdoor temperature on service hot water heating because it will fit the energy-use

trend during warmer months and is referred to as the GS-CP1 model. However, if the elbow temperature is below a specified temperature, the change-point may be associated with a large increase in space heating at significantly colder temperatures. The threshold temperature was set to 10°C which is between the temperature at which space heating systems are expected to turn on and the minimum water mains temperature. This is simply due to the building having increased heating needs at extreme temperatures and is referred to as the GS-CP2 model.

$$Gas = \begin{cases} m_1 * T_{outdoor} + b_1, & T_{outdoor} < x_0 \\ m_2 * T_{outdoor} + b_2, & T_{outdoor} \geq x_0 \end{cases} \quad (49)$$

Where:

$$b_1 = y_0 - m_1 * x_0$$
$$b_2 = y_0 - m_2 * x_0$$
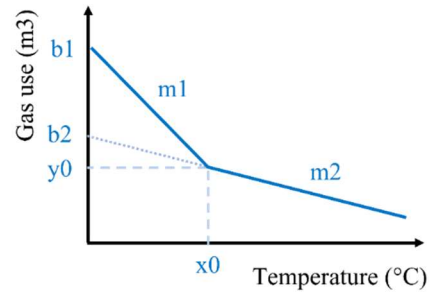
Figure 65: Gas heating change point model

The degree day model may appear to be a special case of the change-point model where the slope of the second line is equal to zero. However, it should be noted that the degree days are calculated at an hourly scale and then resampled to the gas bill dates. This is different from simply calculating a degree day value based on the mean monthly temperature. Some buildings do not show variation in heating use during warmer months which can depend on the water main source as well as the amount of hot water used. Therefore the proposed approach fits both a CP and DD model and takes the model that provides the best fit based on the coefficient of determination.

3.7.3 Algorithms

The degree-day model is a simple linear regression model with a grid search at 5°C increments to find the best base temperature. The linear regression solution is found using scikit learn [90], however since there is only one feature; temperature, it is simply the slope of a line.

The change-point model was modelled with the piecewise-regression library [103] in Python which is based on Muggeo's work [104] to estimate the change points. It starts by predicting lines and adjusting the change points until there are no discontinuities.

3.7.4 Temporal disaggregation

The majority of buildings in this work have monthly gas data but no hourly data is available to infer the building schedule. In this case, the degree day setpoints are assumed to be the same for every hour of the year. This assumption will impact accuracy at the hourly scale since scheduling is expected to impact gas use. However, due to the coarse resolution of the given heating data, it is difficult to account for scheduling without assumed values. Furthermore, buildings with different control systems may have advanced methods of determining setpoints (e.g. pre-cooling). The hourly data is assumed to have a comparable slope to the fitted monthly model, similar to the method proposed by Pagliarini and Rainieri [26], allowing temporal disaggregation of the data by inputting hourly temperature or degree-day values.

For the change-point model, the second line with slope m_2 is used to predict the gas consumption for hot water heating based on the monthly average temperature instead of the hourly temperature. This is because the water main temperature is not expected to change dramatically on an hourly scale, but it is expected to vary over the seasons, as mentioned in Section 2.2.2. An improvement could also be made by using a moving average temperature value.

There are approximately 60 buildings with both monthly heating data and hourly electricity data. For these buildings, the on and off hours were detected from the hourly electricity data. The detected hours are used to compute "scheduled degree-day" values by varying the setpoint between day and night hours. A difference of 3°C was used between day and night, with the night setpoint being lower. The model is then fit using the scheduled degree days and gas use. This helps account for scheduling but has its limitations as mentioned above.

3.7.5 Verification with synthetic data

Two verification cases were tested for the heating model; the DOE synthetic apartment and medium office building [91]. The office building heating is strongly influenced by scheduling, whereas the apartment responds more to weather changes. The model was trained on data from January to November and tested on December.

3.7.5.1 *Apartment*

Figure 66 and Figure 67 display the change point and degree day models, respectively, fit with monthly apartment heating data. The change point model selected a change point temperature of 8°C, while the degree day model had the best fit with a base temperature of 10°C. After comparing the coefficient of determination for both models, the change-point model was selected for this building. The monthly linear regression model was applied to hourly temperature measurements to predict hourly heating consumption, as shown in Figure 68. The general trend of hourly space heating is captured with an NRMSE of 0.2, however, the high spikes in heating are not captured. The service hot water heating daily hourly profile is not captured because it is assumed to be constant over each month. It is difficult to estimate the service hot water heating profile without more knowledge of the building schedule due to the coarse data resolution. Figure 69 shows the predicted hourly heating load while considering scheduling, which is only applicable when hourly measured electricity data is available. High spikes are predicted better than the model without scheduling. However, using the hourly electricity data to separate day types and day or nighttime has resulted in the weekends being predicted poorly which results in a worse NRMSE of 0.3. The issue of not being able to capture the daily variation of the hot water heating load is also present. The daily and hourly heating errors are summarised in

Table 12 12. On a daily scale, the space heating and hot water loads are predicted reasonably well with NRMSE of 0.20 and 0.28 respectively.
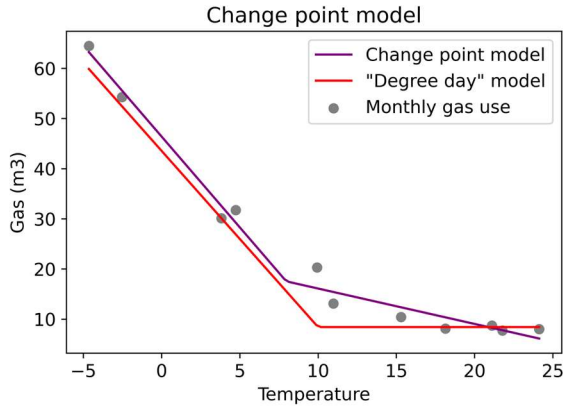
Figure 66: Synthetic apartment monthly heating change point model
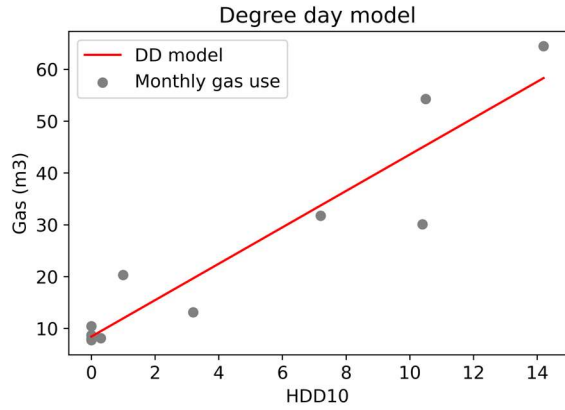
Figure 67: Synthetic apartment monthly heating degree-day model
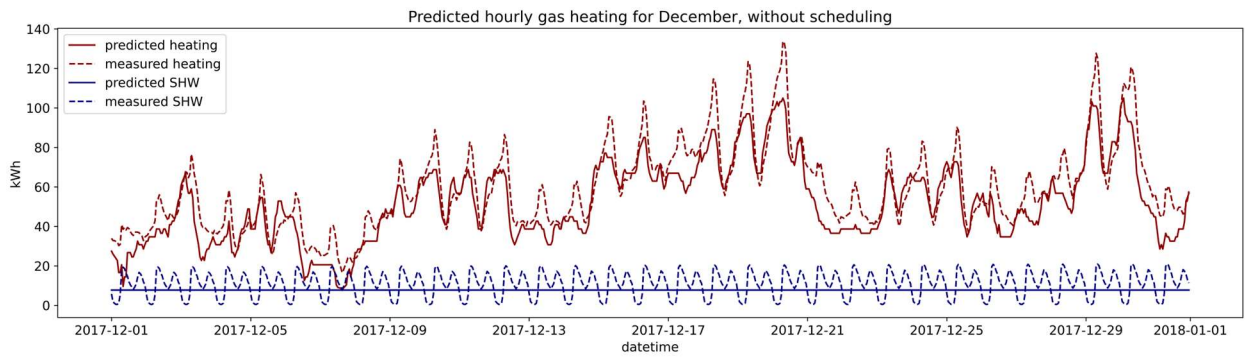
Figure 68: Synthetic apartment hourly heating prediction without scheduling for the month December
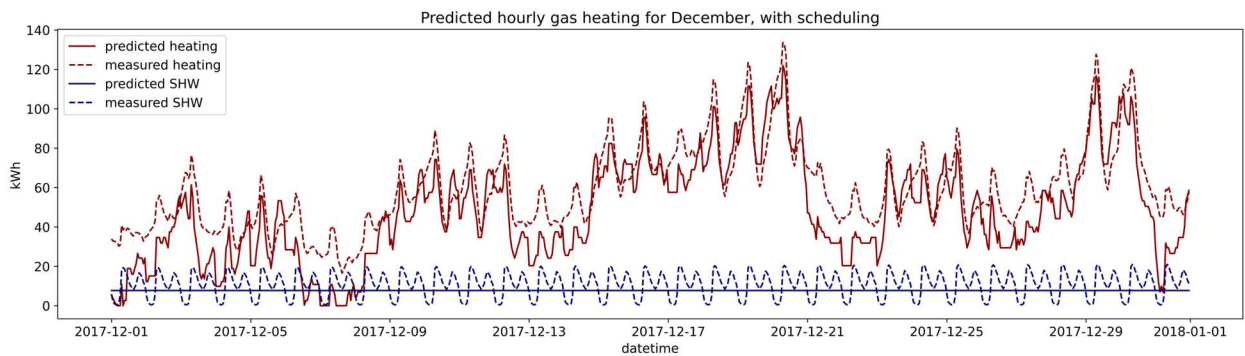
Figure 69: Synthetic apartment hourly heating prediction with scheduling for the month of December

Table 12: Normalized root mean square error for synthetic apartment heating

	Normalized root mean square error					
	Total gas [hr]	Total gas [day]	Space heating [hr]	Space heating [day]	Hot water [hr]	Hot water [day]
Unscheduled	0.15	0.07	0.20	0.11	0.65	0.28
Scheduled	0.21	0.14	0.30	0.15	0.65	0.28

3.7.5.2   Medium Office

The office linear monthly models are shown in Figure 70 and Figure 71. Similar to the synthetic apartment, the change-point model has a higher R^2 value than the degree-day model. However, while the monthly models appear similar, the office hourly prediction is poor with an NRMSE greater than 1 as shown in Figure 72. This is due to the heavy scheduling influence of both the heating system and heat from appliances and occupants, making it difficult to temporally disaggregate the data without the schedule, which results in a smoother prediction. The measured data shows the heating system turned off at night, however, the predicted hourly heating is highest at night when temperatures are cooler. The modification with scheduled degree days, seen in Figure 73, shows some improvement. However, the night heating is still overpredicted while the day heating is underpredicted. The model could be improved by increasing the temperature difference used to calculate the scheduled degree days, however without knowledge of the building setpoints and hourly heating profile, it is difficult to justify what values should be selected. Additionally, the model does not explicitly account for appliance and occupant heat gains that would reduce the heating load. When fitting a model at the monthly scale using both HDDs and summed electricity use, both tend to have positive regression coefficients. The monthly electricity use is positively correlated with heating demand because the heating load required by occupants using the appliances is greater than the heat given off by the appliances. The tested model with HDDs and electricity use as regressors captured more of the scheduling impact, specifically in the coldest months.

However, the addition of the electricity term produced unphysical predictions, especially during the shoulder and summer seasons. Therefore the scheduled model was created using only scheduled HDDs.
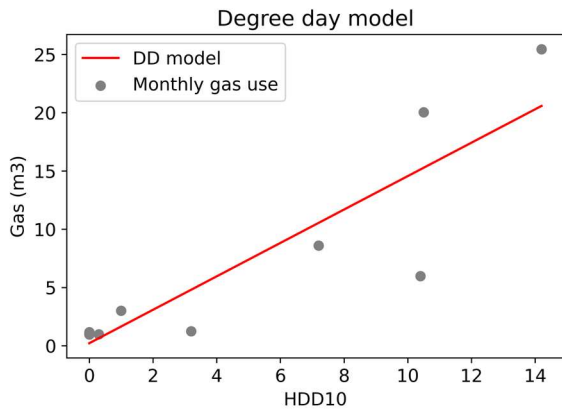
Figure 70: Synthetic office monthly heating change point model
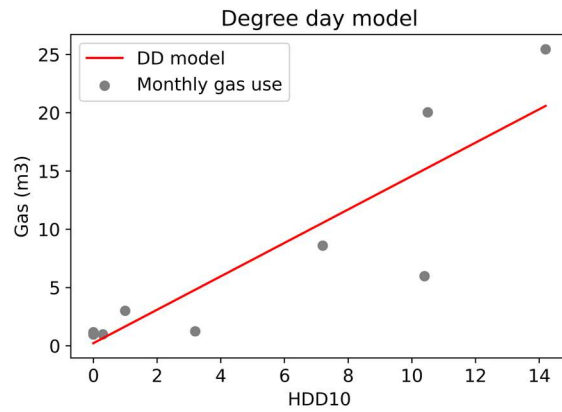
Figure 71: Synthetic office monthly heating degree day model
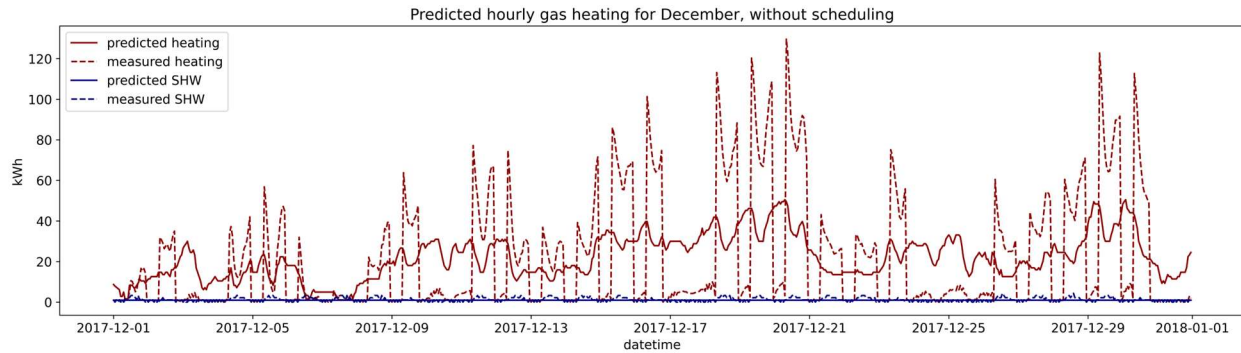
Figure 72: Synthetic office hourly heating prediction without scheduling for the month of December
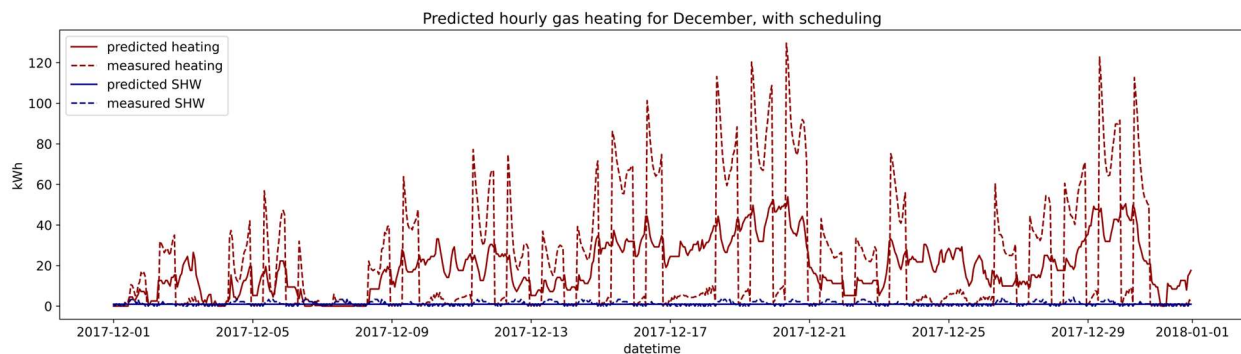
Figure 73: Synthetic office hourly heating prediction with scheduling for the month of December

Table 13: Normalized root mean square error for synthetic office heating

	Normalized root mean square error					
	Total gas [hr]	Total gas [day]	Heating [hr]	Heating [day]	Hot water [hr]	Hot water [day]
Unscheduled	1.21	0.52	1.25	0.53	0.84	0.39
Scheduled	1.13	0.49	1.17	0.50	0.84	0.39

The NRMSEs for the office heating predictions are summarized in Table 13. Overall, the heating model has difficulty going from a monthly to hourly resolution. For weather-dominated buildings, the hourly prediction is acceptable, as seen with the apartment. However, the model does not perform well for scheduling-dominated buildings without any knowledge of the schedule.

3.8 Summary

Electricity and gas models were created for several buildings and seasons, as summarized in Table 14 and Table 15. Separate electricity models were proposed for conventional buildings, supermarkets and arenas for the heating and cooling seasons. The supermarket and arena models were built upon the conventional building models (EL-CT and EL-HT) to forecast the refrigeration load as well. Additionally, a 5-minute compressor load model was created to predict compressor loads for one arena. Lastly, degree-day and change-point methods were used to predict hourly heating demand from monthly natural gas measurements for all building types.

Table 14: Summary of electricity models

Section	Model	Building type	Verification data	Description
3.6.3	Electricity-cooling (EL-CT)	Conventional	Synthetic	Conventional buildings with electrical baseload and space cooling
3.6.3	Electricity-heating (EL-HT)	Conventional	Synthetic	Conventional buildings with electrical baseload (and space heating if applicable)
3.6.4	Supermarket, winter	Supermarket	Synthetic	Supermarkets with electrical baseload and refrigeration

3.6.4	Supermarket, summer	Supermarket	Synthetic	Supermarkets with electrical baseload, refrigeration and space cooling
3.6.5	Arena, winter	Arena	Real	Ice rinks with electrical baseload and refrigeration
3.6.5	Arena, summer	Arena	Real	Ice rinks with electrical baseload, refrigeration and space cooling
3.6.6	Arena, 5-minute compressor	Arena	Real	Ice rinks with detailed information to predict 5-minute compressor loads

Table 15: Summary of gas models

Section	Model	Building type	Verification data	Description
3.7	Heating, degree day (HT-DD)	Any	Synthetic	Use monthly gas data to predict hourly heating demand with a degree day approach
3.7	Heating, change point 1 (HT-CP1)	Any	Synthetic	Use monthly gas data to predict hourly heating demand with a change point approach. The change point separates the space heating demand in the winter and hot water heating energy in the summer
3.7	Heating, change point 2 (HT-CP2)	Any	Synthetic	Use monthly gas data to predict hourly heating demand with a change point approach. The change point separates two heating regimes: one at medium temperatures and one at very low temperatures

Chapter 4

4 Results and analysis

The following chapter analyzes the capability of the models proposed in Chapter 3 to predict real building data. Chapter 3 described the models and the verification with synthetic or submetered data, to evaluate the disaggregation approach. Chapter 4 analyzes the predictions using real data. Error is provided for the total energy prediction because most buildings do not have submetering systems. The models are applied to data from real buildings from the database described in Section 3.2. For in-sample predictions, the model is trained on historical data from a single building. The trained model is then used to predict energy use during a period that is excluded from the training set as depicted in Figure 11 from Chapter 3. For out-of-sample predictions, the model is trained on several buildings of the same type and used to predict energy use for a building that was not included in the training dataset (Figure 11).

A brief description of each section in this chapter is provided in Table 16. First, real sample results of the hourly electricity models for the conventional buildings, supermarkets and arenas are shown for each case outlined in Section 3.3. Note that conventional buildings, defined as all of the building types other than ice rinks and supermarkets, are expected to have relatively low or no refrigeration loads. Each building-type model is then fit to all of the corresponding buildings within the database and evaluated based on NRMSE of total electricity use. Second, the natural gas model was evaluated on a monthly scale for all the buildings with monthly gas data available, using only Case 1 (a building predicting itself). A brief summary of each model use case is provided in Table 17, with detailed descriptions of each case found in Table 3.

Table 16: Summary of assessments performed in Chapter 4

Section	Building type	Energy	Description
4.1.1.1	Apartment	Electricity	Sample predictions for real apartments, using buildings with median error. Day-ahead (both summer and winter) and year-ahead predictions at an hourly scale for the in-sample case. Year-ahead predictions at an hourly scale for the out-of-sample cases
4.1.1.2	Supermarket	Electricity	Sample predictions for real supermarkets, using buildings with median error. Day-ahead (both summer and winter) and year-ahead predictions at an hourly scale for the in-sample case. Year-ahead predictions at an hourly scale for the out-of-sample cases
4.1.1.3	Arena	Electricity	Sample predictions for real arenas, using buildings with median error. Day-ahead (both summer and winter) and year-ahead predictions at an hourly scale for the in-sample case. Year-ahead predictions at an hourly scale for the out-of-sample cases
4.1.1.4	All	Electricity	NRMSE values for all building models, by building type. Evaluating in-sample day-ahead (both summer and winter) and year-ahead as well as out-of-sample year-ahead predictions
4.1.2	All conventional	Electricity	Comparing the fraction of annual electricity used for space cooling of conventional buildings with NRCAN reference values for year-ahead predictions
4.2.1	All	Natural gas	Non-scheduled hourly gas model sample prediction and monthly error values for all buildings with monthly gas data available. Evaluated for in-sample, year-ahead predictions

4.2.2	All	Natural gas	Schedule hourly gas model sample prediction and monthly error values for buildings with monthly gas data and hourly electricity data. Evaluated for in-sample, year-ahead predictions

Table 17: Brief summary of model use cases

Case	Description	Application
1) In-building sample	Training and test sets are data from the same building	Designing and controlling community energy systems when hourly data is available
2) Out-of-building sample	Using data from other buildings of the same type to predict a new building.	Forecasting when buildings have no measured data available
3) Calibrated out-of-building sample	Case 2 model, calibrated with monthly aggregate energy use values	Forecasting for buildings with only monthly bills available

4.1 Electricity

4.1.1 Total electricity prediction

The results in this section are for the electricity model applied to real data from conventional buildings, supermarkets and arenas. For the conventional building electricity model, only the apartment building type time series plots are shown. Each example time series plot is for the building with the median NRMSE for the sub-case specified within its building type. For example, the day-ahead summer and winter plots for the apartment model may be for two different apartment buildings. The median was used because it is more representative and less sensitive to outliers. The best training length was determined for each building model by training a model with different training set lengths and using the length with the lowest error. The learned model parameters for conventional buildings were also analyzed in Appendix F. Additionally, the stackplots of year-ahead predictions will contain holiday dates where the model prediction is omitted. In those cases, the predicted stacked loads and total load simply

skip the holiday date, which is seen by days where the last and next data point are joined by a line (e.g. May 21st, 2018 in Figure 76 is Victoria Day).

4.1.1.1   *Apartment*

Figure 74 shows the summer in-sample day-ahead prediction using Equation 21 for a sample apartment while Figure 75 shows the winter in-sample day-ahead prediction using Equation 22. As seen in Figure 74 and Figure 75, the sample apartment day-ahead demand profiles are predicted well. The summer day-ahead predictions were trained with the best training length of 60 days and tested on a test set of 1 day, resulting in an average NRMSE of 0.085. The winter day-ahead prediction was trained on the best length of 30 days, with an average NRMSE of 0.083. In the heating season, a significant amount of electricity use is attributed to thermal loads, however, the heating load depends on the building's heating system type. The daily baseload profile for both seasons is seen to increase slightly during the day when occupants are awake.
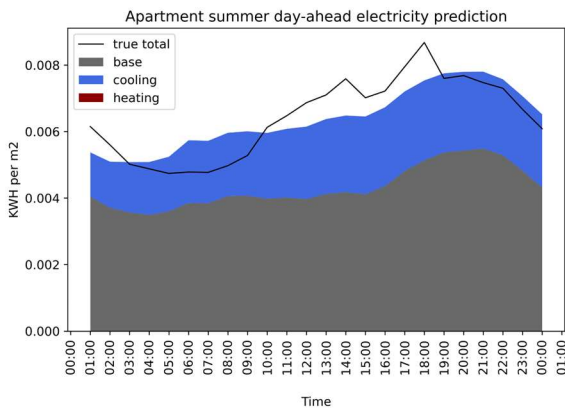
Figure 74: Real apartment summer day-ahead electricity prediction for August 6th (Case 1)
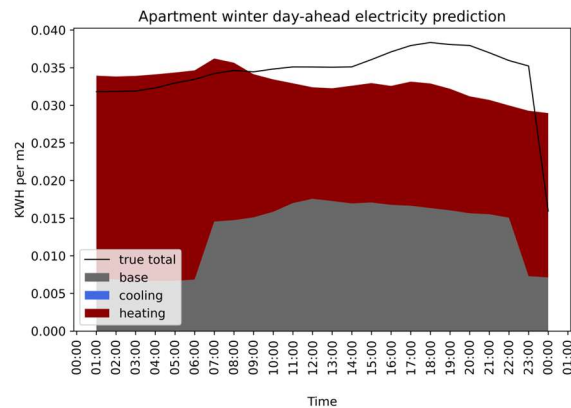
Figure 75: Real apartment winter day-ahead electricity prediction for January 28th (Case 1)

Figure 76 displays a sample apartment for the year-ahead in-sample prediction. The baseload, cooling and heating loads appear to be well-captured, with the cooling load constituting 10% of the annual electricity load. The total load was predicted with an NRMSE of 0.13 after training on one year of data. Figure 77 displays the out-of-building-sample year-ahead prediction for an apartment building. As shown in Figure 77, the total electricity prediction is underestimated with an NRMSE of 0.27 for the out-

of-sample case. This indicates that the test building has higher electricity consumption than most apartment buildings in the database. Figure 78 displays the year-ahead prediction for an out-of-sample prediction that is calibrated with monthly data. As shown in Figure 78, calibrating the out-of-sample annual prediction improves the prediction greatly with an NRMSE of 0.11. This indicates that the out-of-sample model may predict the profile shape well, however various magnitudes of energy use between buildings are what result in poor predictions. The median NRMSE for each test case for the apartment building is summarized in Table 18.

(a) January to March 2018

(b) April to June 2018

(c) July to September 2018

(d) October to December 2018
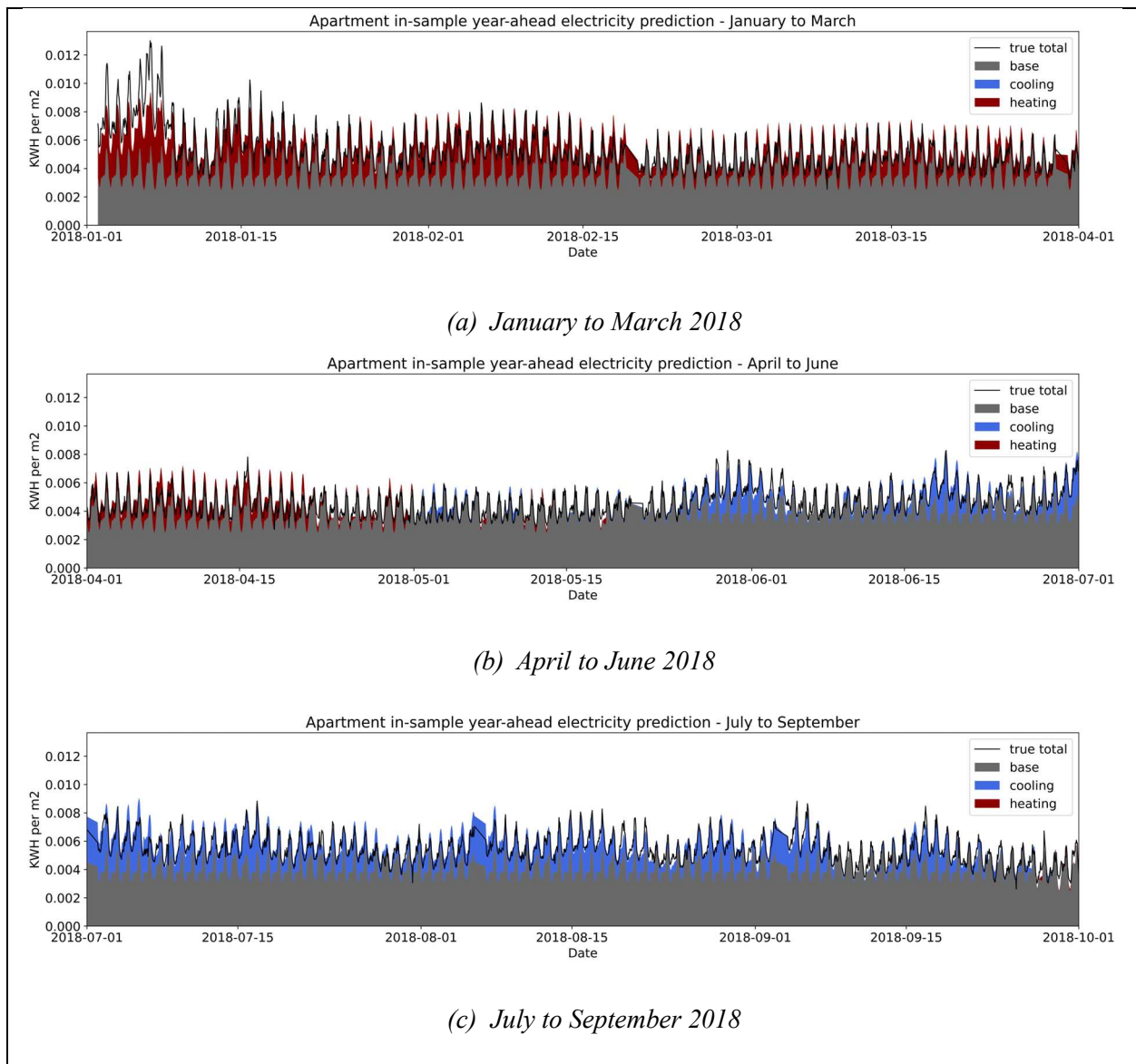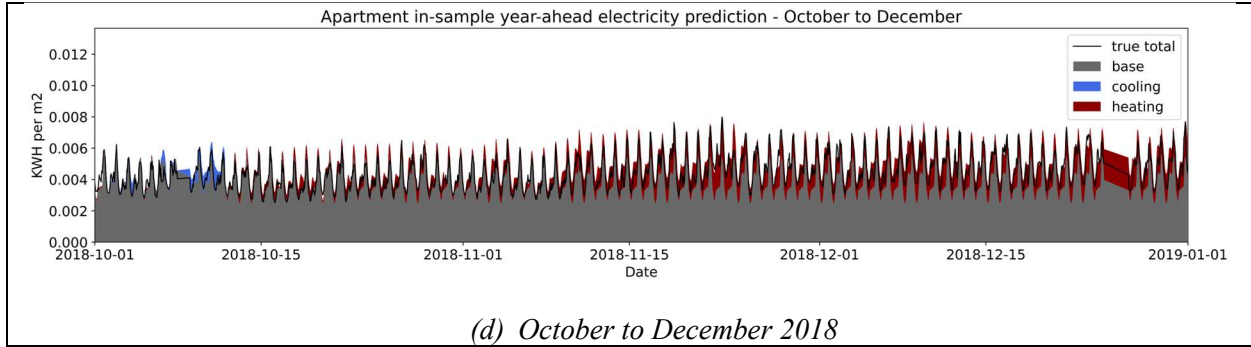
Figure 76: Real apartment in-sample year-ahead electricity prediction (Case 1) from January 2018 to January 2019, divided by quarter of the year

(a) April to June 2017

(b) July to September 2017

(c) October to December 2017

(d) January to March 2018
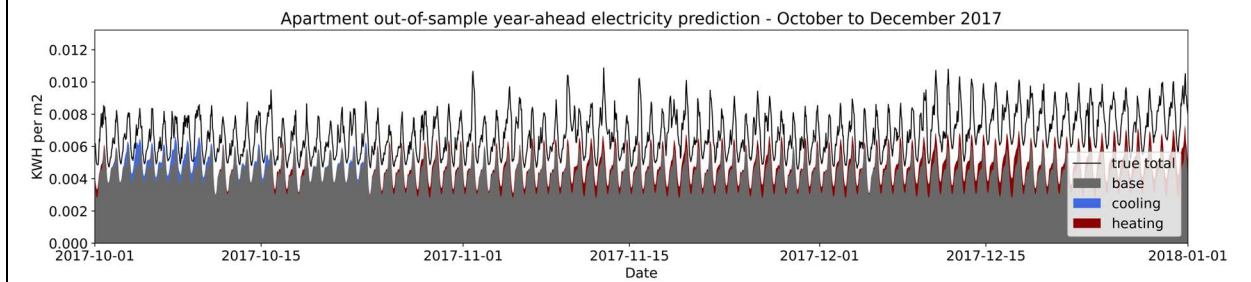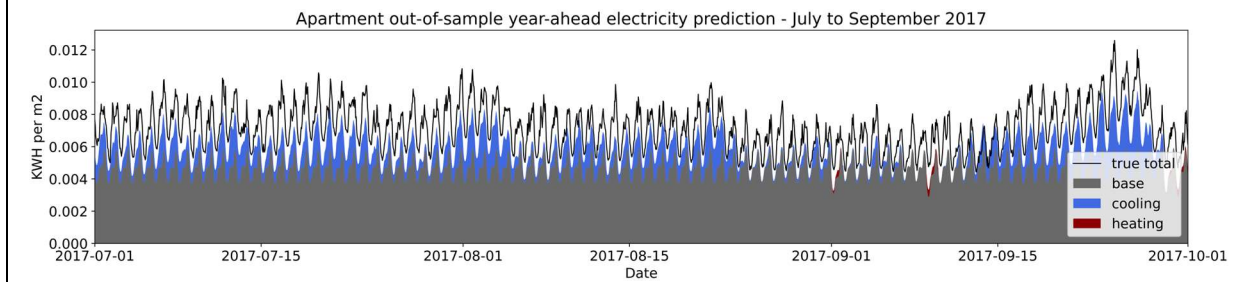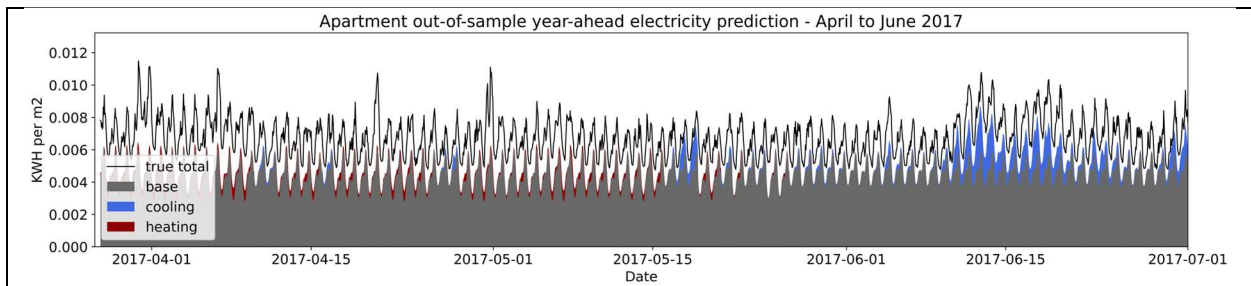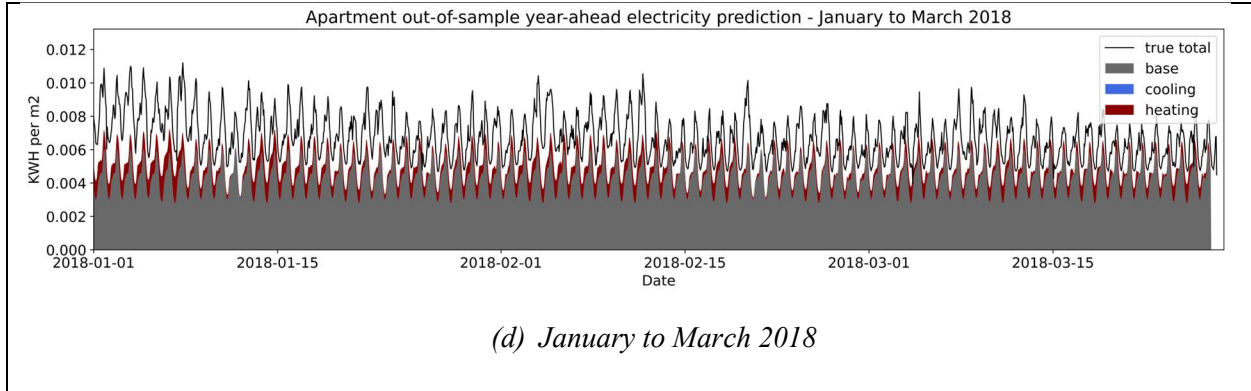
Figure 77: Real apartment out-of-sample year-ahead electricity prediction (Case 2) from April 2017 to April 2018, divided into quarters of the year

(a) April to June 2017

(b) July to September 2017

(c) October to December 2017

(d) *January to March 2018*
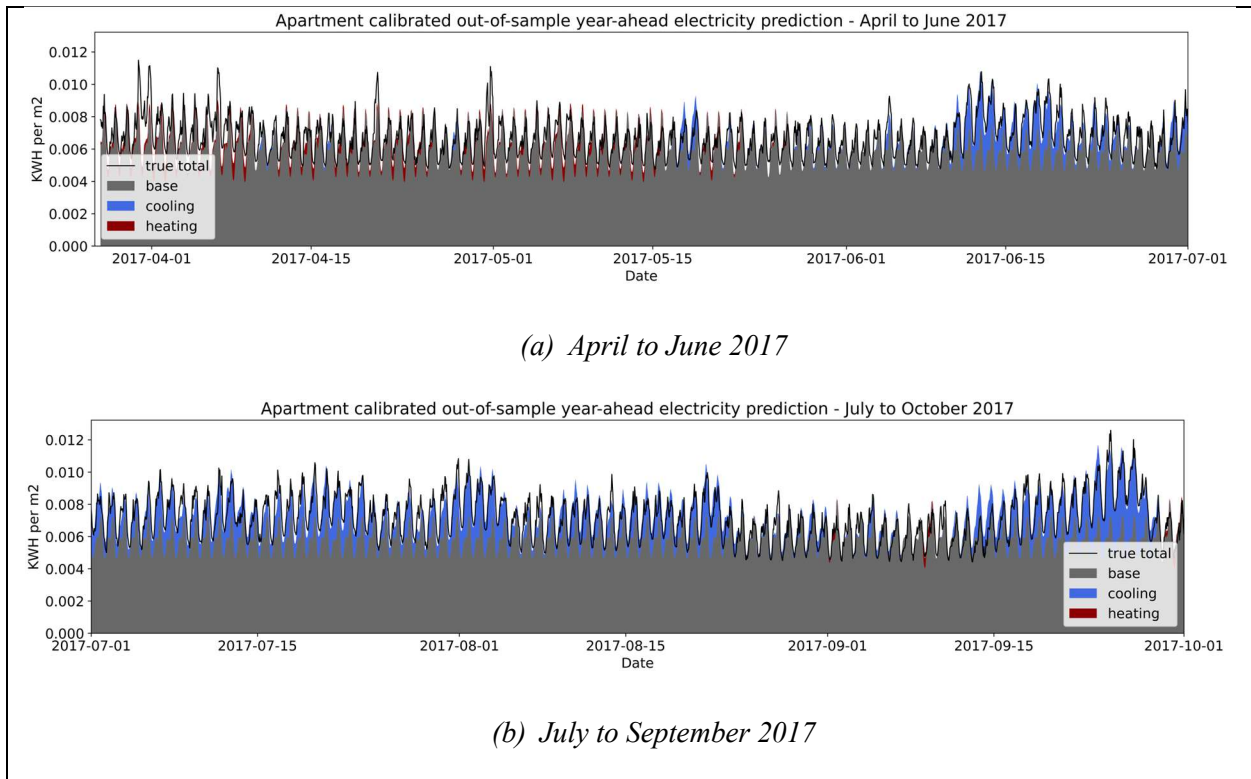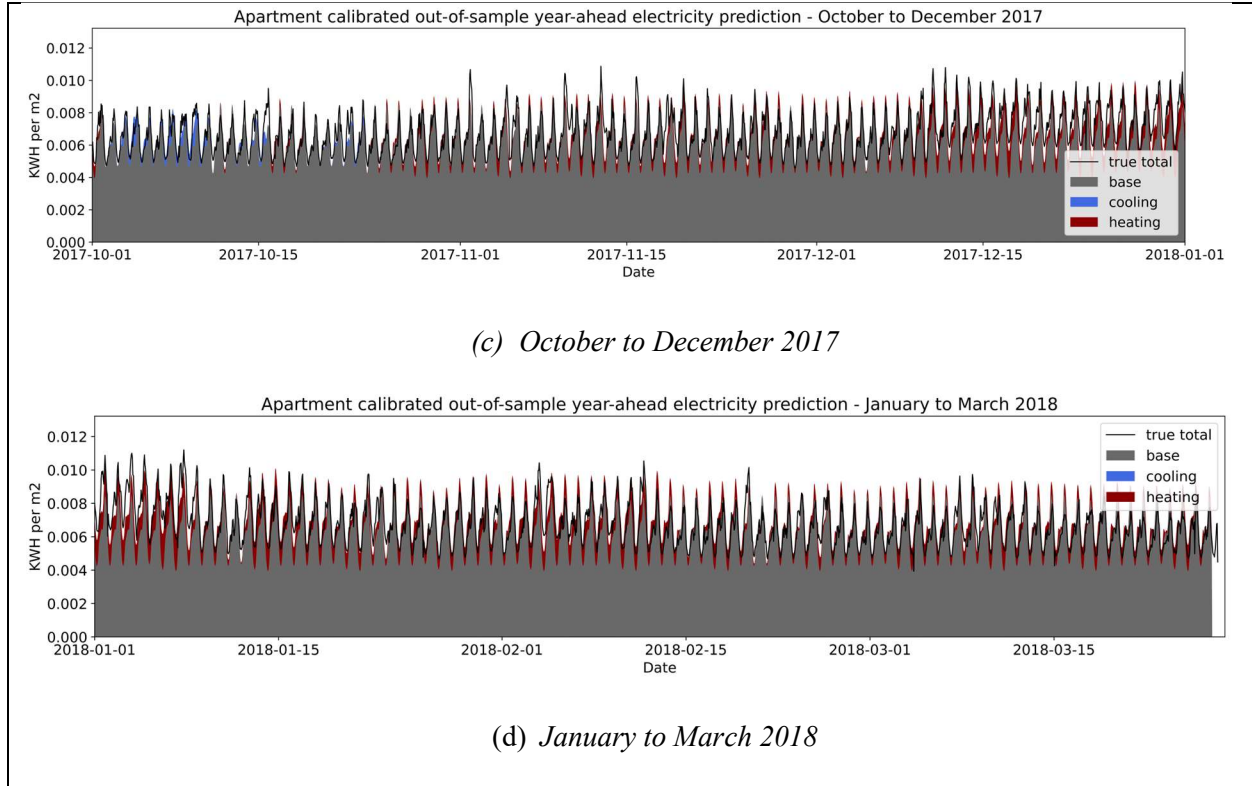
Figure 78: Real apartment calibrated out-of-sample year-ahead electricity prediction (Case 3) from April 2017 to April 2018, divided into quarters of the year

Table 18: Median NRMSE of different test cases for real apartment buildings

Season	Case	Train set length	Test set length	Total electricity NRMSE [hr] (for median error building plotted)
Winter	1 (in-sample)	30 days	1 day	0.083
Summer	1 (in-sample)	60 days	1 day	0.085
Full-year	1 (in-sample	1 year	1 year	0.13
Full-year	2 (out-of-sample)	4 years	1 year	0.27
Full-year	3 (calibrated out-of-sample)	4 years	1 year	0.11

4.1.1.2 Supermarket

Figure 79 and Figure 80 display the sample day-ahead predictions for the supermarket for the summer and winter respectively. The summer model uses Equation 34 while the winter model uses Equation 31. As seen in Figure 79, the supermarket sample summer day-ahead forecast is overpredicted throughout the day, especially in

the morning and evening with an average NRMSE of 0.069. As seen in Figure 80, the sample winter day-ahead prediction is mainly underpredicted with an average NRMSE of 0.065. The sample winter day-ahead prediction has a small spike in electricity use in the morning, however, it does not capture the magnitude of the spike. The year-ahead in-sample prediction for a sample grocery store is displayed in Figure 81. For year-ahead in-sample predictions, the median NRMSE is 0.11. The error may be due to the difficulty in predicting the refrigeration system compressor cycling which will depend on defrost cycles, food restocking schedules, occupant behaviour and the refrigeration control systems. As mentioned previously, this results in the model smoothing out the spikes in electricity use because they do not occur at the same time or with the same magnitude each day. Figure 82 displays the out-of-sample year-ahead prediction for a supermarket. As seen in Figure 82, the prediction is poor with an NRMSE of 0.95. The use of other grocery stores to predict a new grocery store does not perform well, perhaps due to the range of operation in this building type. For the median case shown, the out-of-sample model did not capture the daily variation in load well. The calibrated, year-ahead model is shown in Figure 83 and has an NRMSE of 1.01. The summer and winter averages between the sample building and others were similar, however, the peak and valley values were not accurately modelled and therefore scaling did not improve model predictions. A summary of the NRMSE for the sample supermarkets is provided in Table 19.
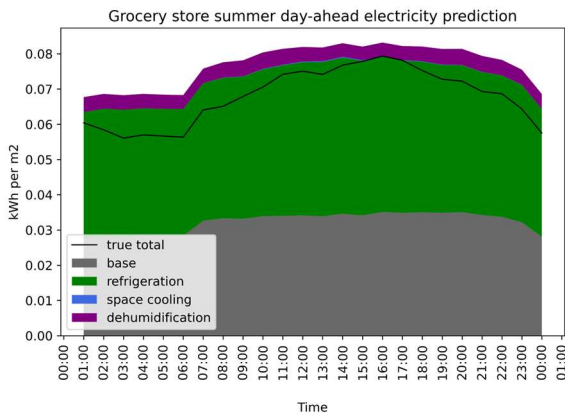
Figure 79: Real supermarket summer day-ahead electricity prediction for August 17th (Case 1)
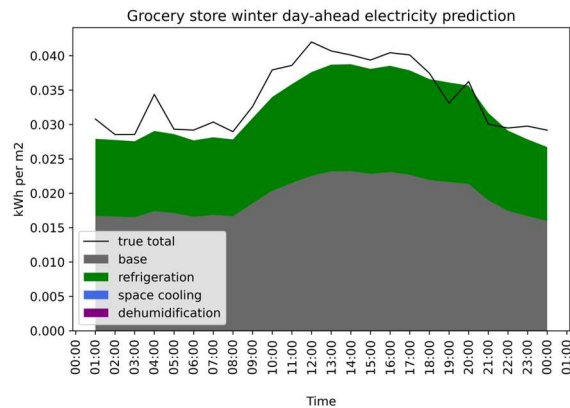
Figure 80: Real supermarket winter day-ahead electricity prediction for December 31st (Case 1)

(a) January to March 2018

(b) April to June 2018

(c) July to September 2018

(d) October to December 2018
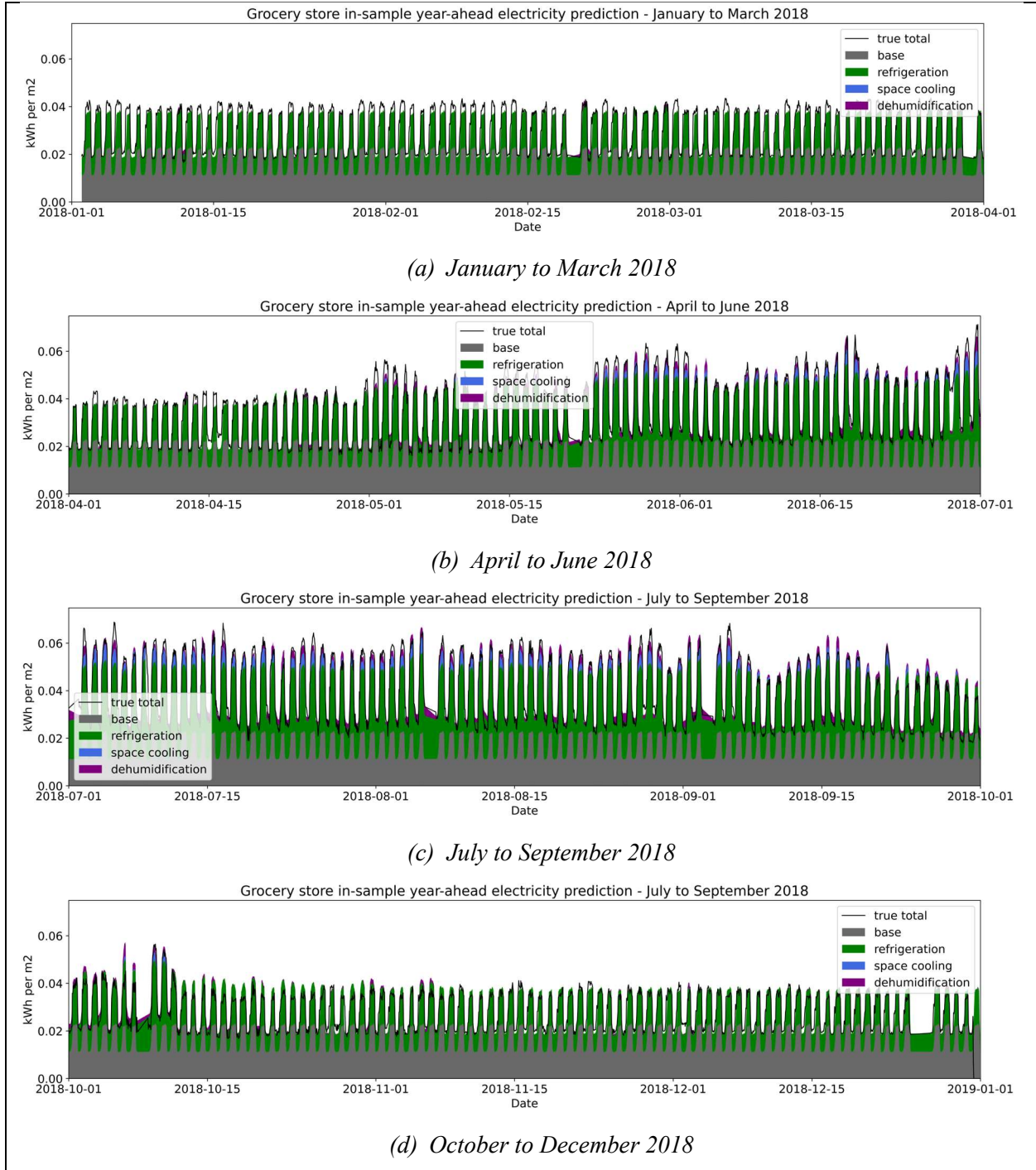
Figure 81: Real supermarket in-sample year-ahead electricity prediction (Case 1) from January 2018 to January 2019, divided into quarters of the year

(a) April to June 2018

(b) July to September 2018

(c) October to December 2018

(d) *January to March 2019*
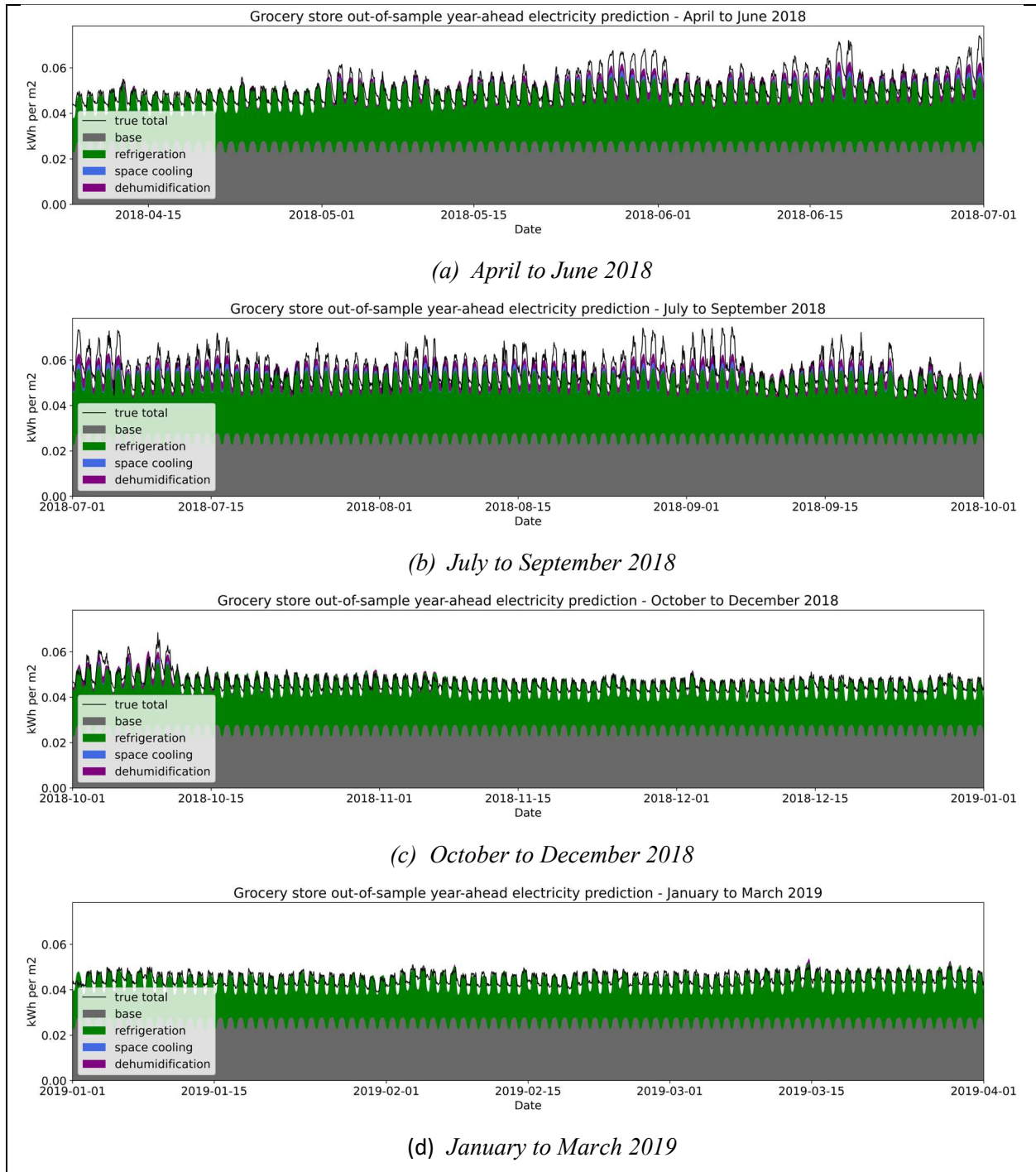
Figure 82: Real supermarket out-of-sample year-ahead electricity prediction (Case 2) from April 2018 to April 2019, divided into quarters of the year

(a) April to June 2018

(b) July to September 2018

(c) October to December 2018

(d) *January to March 2019*
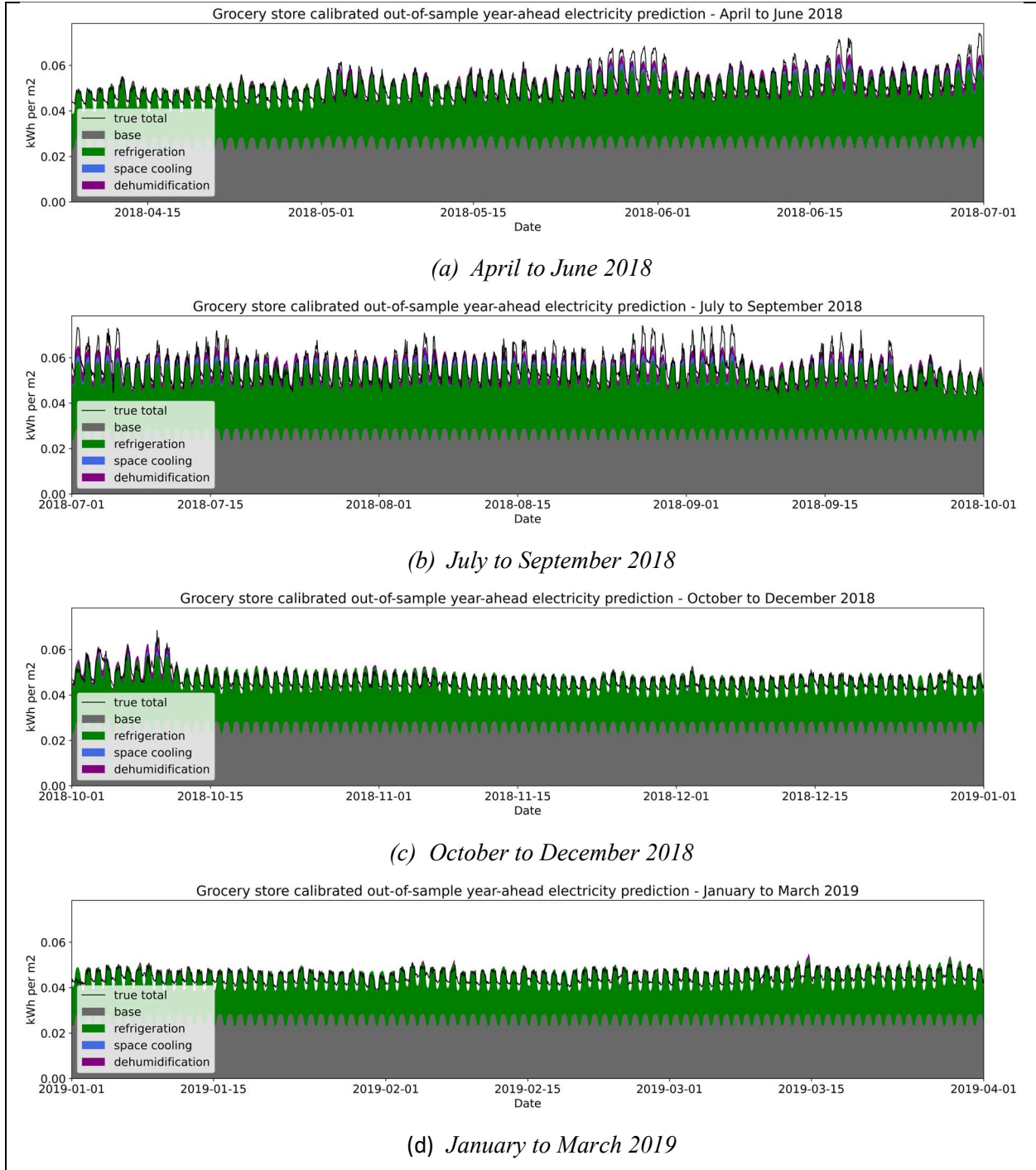
Figure 83: Real supermarket calibrated out-of-sample year-ahead electricity prediction (Case 3) from April 2018 to April 2019, divided into quarters of the year

Table 19: Median NRMSE of different test cases for real supermarkets

Season	Case	Train set length	Test set length	Total electricity NRMSE [hr] (for median error building plotted)
Winter	1 (in-sample)	120 days	1 day	0.069
Summer	1 (in-sample)	30 days	1 day	0.065
Full-year	1 (in-sample	3 years	1 year	0.11
Full-year	2 (out-of-sample)	2 years	1 year	0.95
Full-year	3 (calibrated out-of-sample)	2 years	1 year	1.01

4.1.1.3   Arena

Figure 84 and Figure 85 show sample day-ahead predictions for arenas in the summer and winter, respectively. The summer model uses Equation 45 while the winter model uses Equation 44. As seen in Figure 84, the summer estimated electricity is not able to capture the fluctuations in electricity use. The large spike in electricity use around 4 am is not captured by the model. A sample winter day-ahead prediction is shown in Figure 85. As seen in Figure 85, the time and magnitude of the rises and falls in electricity use are not predicted exactly; however, the general trend is captured. This is likely due to the compressor and pumps cycling at different times each day, so the model predicts a smoother profile, similar to the supermarket. Overall, the sample day-ahead predictions are predicted with an average hourly NRMSE of 0.26 and 0.18 during the summer and winter respectively.
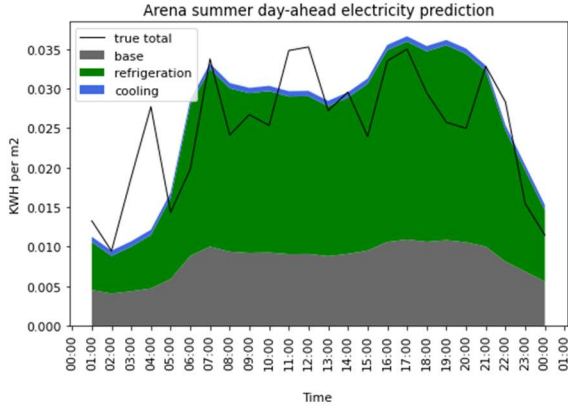
Figure 84: Real arena summer day-ahead electricity prediction for July 31ˢᵗ (Case 1)
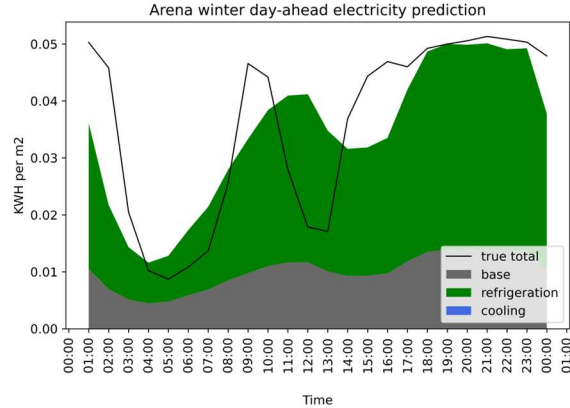
Figure 85: Real arena winter day-ahead electricity prediction (Case 1)

Figure 86 shows the year-ahead in-sample prediction for a full-year operational ice rink with an NRMSE of 0.29. Figure 87 displays an out-of-sample year-ahead prediction, which has a similar error to the in-sample building with an NRMSE of 0.31. Figure 88 shows the calibrated out-of-sample prediction, where the out-of-sample prediction was calibrated with monthly data, which increases the NRMSE to 0.33. As seen in Figure 88, the prediction appears nearly identical to Figure 87, meaning the average loads over each season are predicted well but the source of error is the difference in the hourly profile. This is likely due to not capturing the refrigeration plant equipment cycles properly, as mentioned previously and some buildings may have lower or higher refrigeration loads during the day or night. Table 20 displays the median NRMSE for each model use case for the arena.

(a) January to March 2018

(b) April to June 2018

(c) July to September 2018

(d) *October to December 2018*
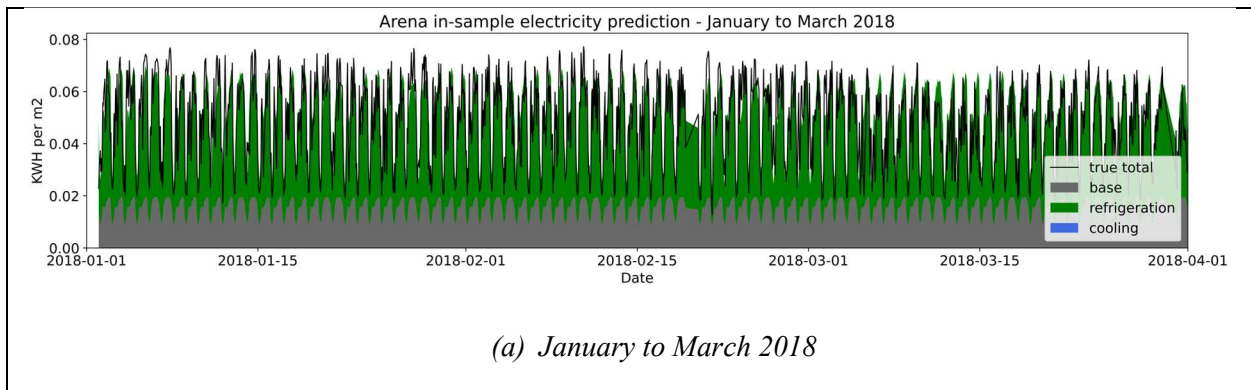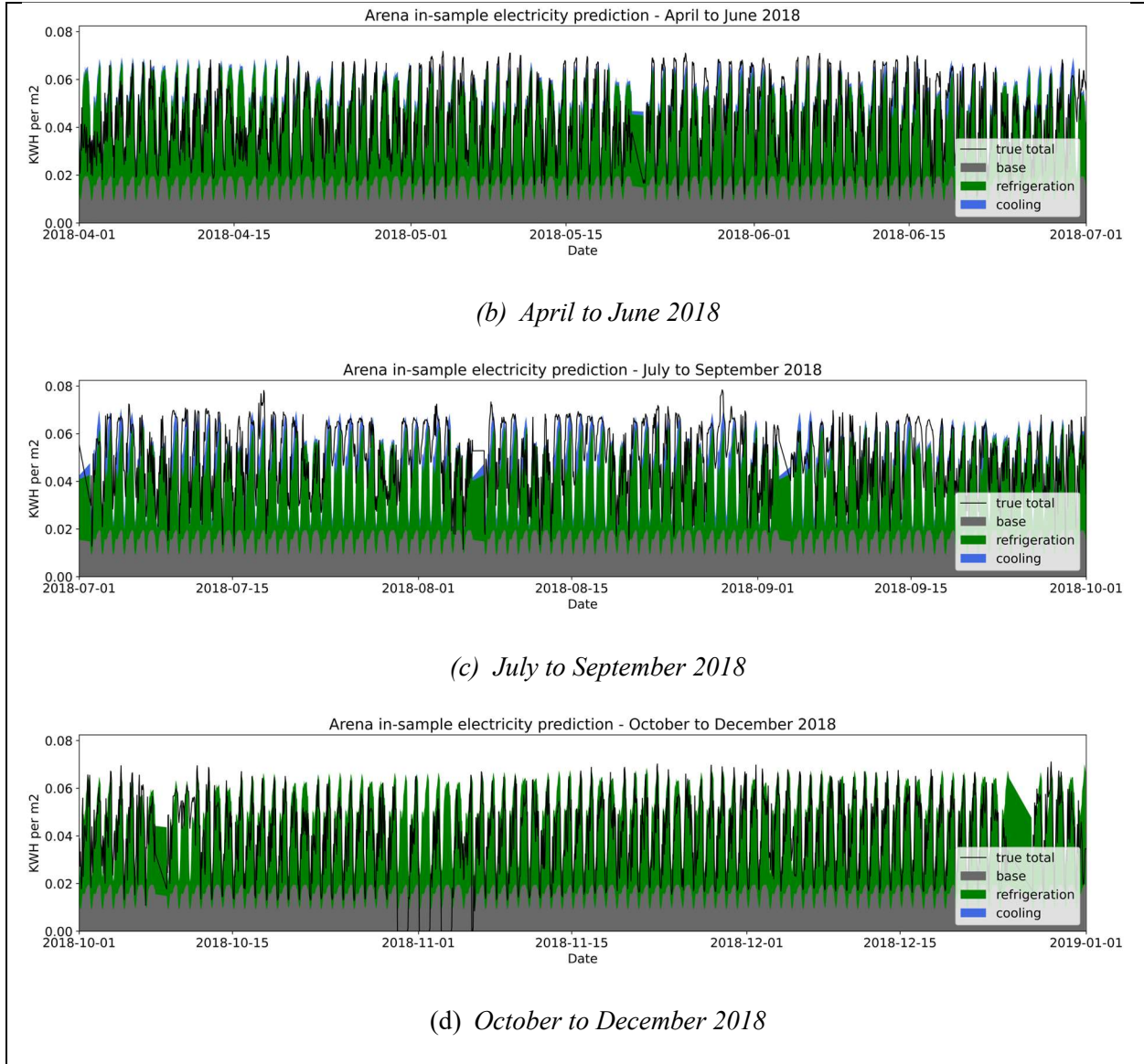
Figure 86: Real arena in-sample year-ahead electricity prediction (Case 1) from January 2018 to January 2019, divided into quarters of the year

(a) November 2017 to January 2018

(b) February to April 2018

(c) May to July 2018

(d) August to November 2018
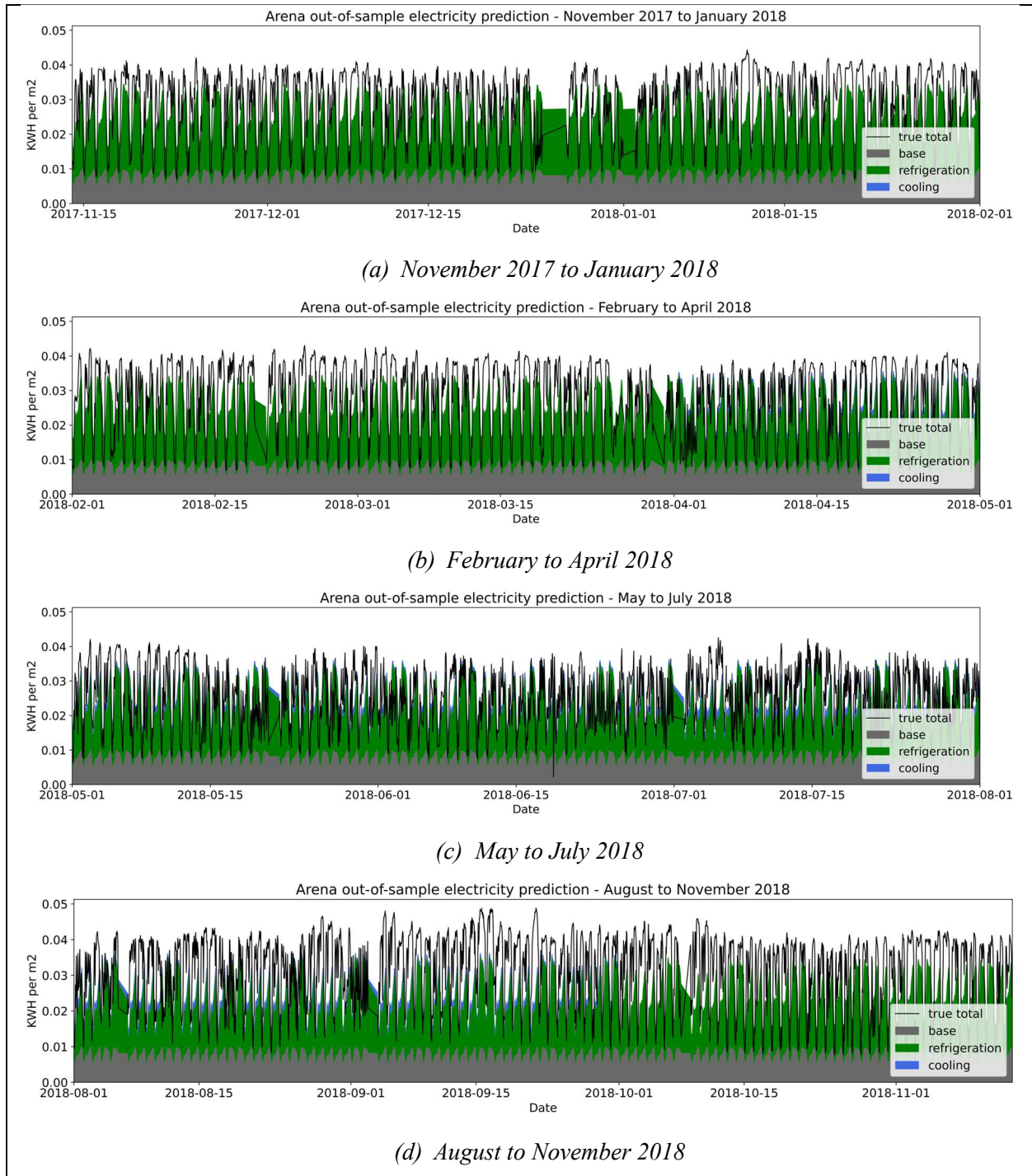
Figure 87: Real arena out-of-sample year-ahead electricity prediction (Case 2) from November 2017 to November 2018, divided into quarters of a year

(a) November 2017 to January 2018

(b) February to April 2018

(c) May to July 2018

(d) August to November 2018
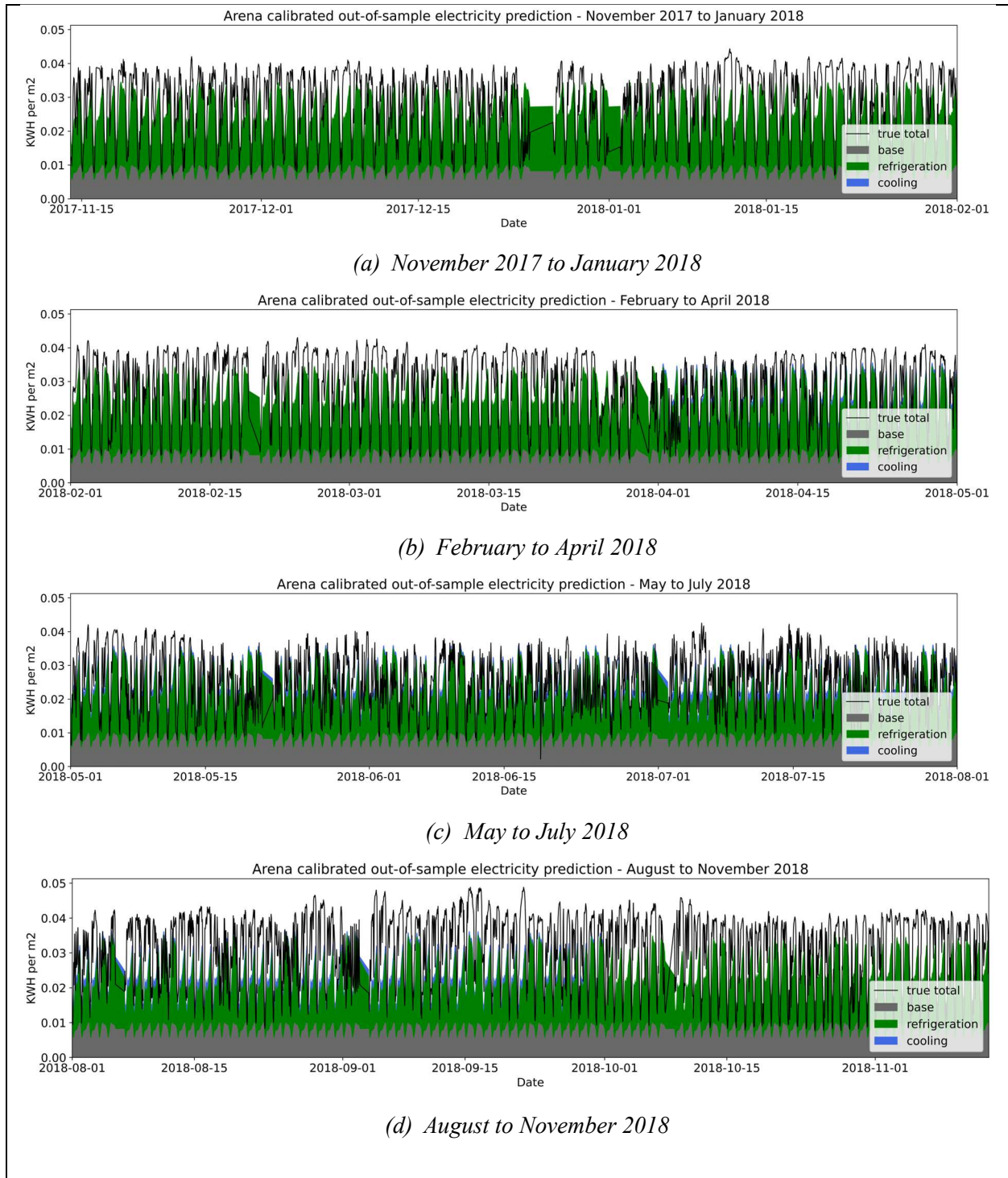
Figure 88: Real arena calibrated out-of-sample year-ahead electricity prediction (Case 3) from November 2017 to November 2018, divided into quarters of a year

Table 20: Median NRMSE of different test cases for real arenas

Season	Case	Train set length	Test set length	Total electricity NRMSE [hr] (for median error building plotted)
Winter, on-season	1 (in-sample)	60 days	1 day	0.18
Summer, on-season	1 (in-sample)	120 days	1 day	0.26
Full-year	1 (in-sample	2 years	1 year	0.29
Full-year	2 (out-of-sample)	3 years	1 year	0.31
Full-year	3 (calibrated out-of-sample)	3 years	1 year	0.33

4.1.1.4   Summary of all building models

The electricity model results for all building types are summarized in this section. Figure 89 displays a boxplot of the NRMSE for each building (grouped by building type) for the summer and winter day-ahead predictions. The number of buildings that were modelled for each building type is displayed in Figure 6. Electricity models were created for all of the buildings with hourly or sub-hourly electricity data which are shown in green in Figure 6. In the boxplot, the median for each building type is shown as the horizontal line located within the building type's respective box. As shown in Figure 89, the median day ahead predictions during the summer and winter are below 0.4 for all the building types. Most building types have outliers with some having an NRMSE greater than 1. This could be due to an operation change between the training and test set. Alternatively, it may be due to weather conditions that were not seen during training, so the model is unable to accurately capture the building's response. The arena model does not perform as well as the conventional and grocery store models with a median NRMSE of 0.34 and 0.25 in the summer and winter respectively. The higher summer NRMSE may be due to the randomness of occupants during that season as some arenas may be operating sporadically during the summer, making it difficult to predict. The community centre model performance is also poor with a median value of 0.34 and 0.21 in the summer and winter respectively.
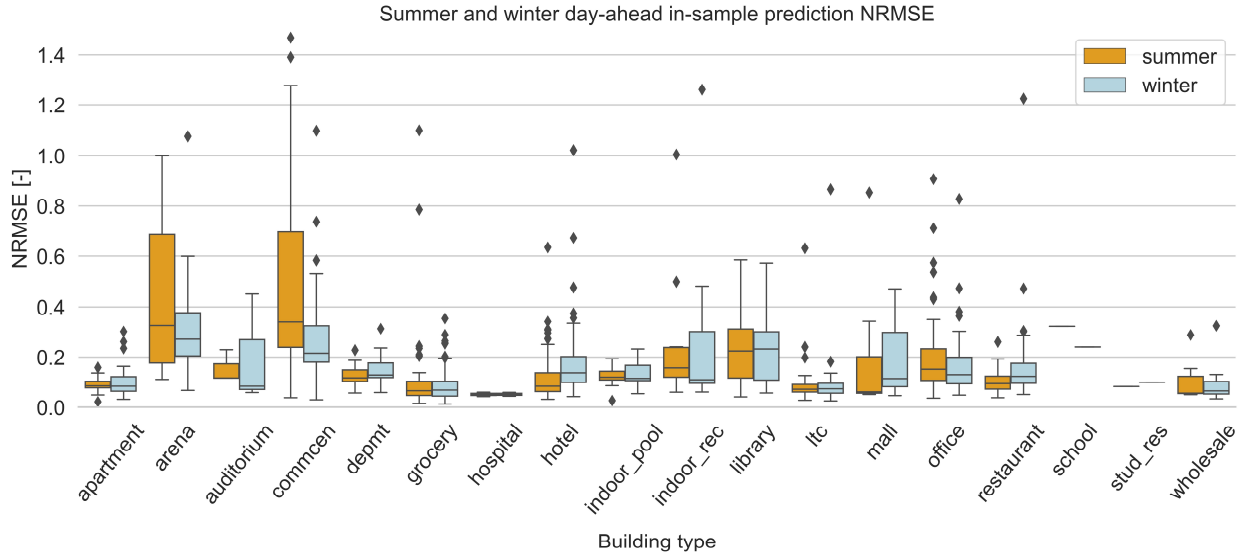
Figure 89: Summer and winter day-ahead electricity prediction NRMSE by building type

The yearly in-sample prediction NRMSE values are displayed in Figure 90. Some building-type models are seen to perform significantly better than others. The arena model generally performs worst in terms of predicting total electricity use. As mentioned in Section 3.6.5.4, one contributor to this error is misassigning the ice-operational and non-ice-operational seasons because electricity use levels will vary greatly depending on if the refrigeration system is operating. When implementing the model in real scenarios, the rink manager can provide the exact dates of arena opening and closing to improve model accuracy. The apartment and long-term care home models perform well with the upper quartile of NRMSE below 0.2 for both building types. The models appear to work better for buildings that are more responsive to weather rather than scheduling, such as apartment buildings. Because the base load is assumed to be the same each day, it loses the ability to account for different scheduling between days and occupant behaviour. Therefore buildings with energy use dominated by the baseload and occupants such as offices, are not predicted as well.
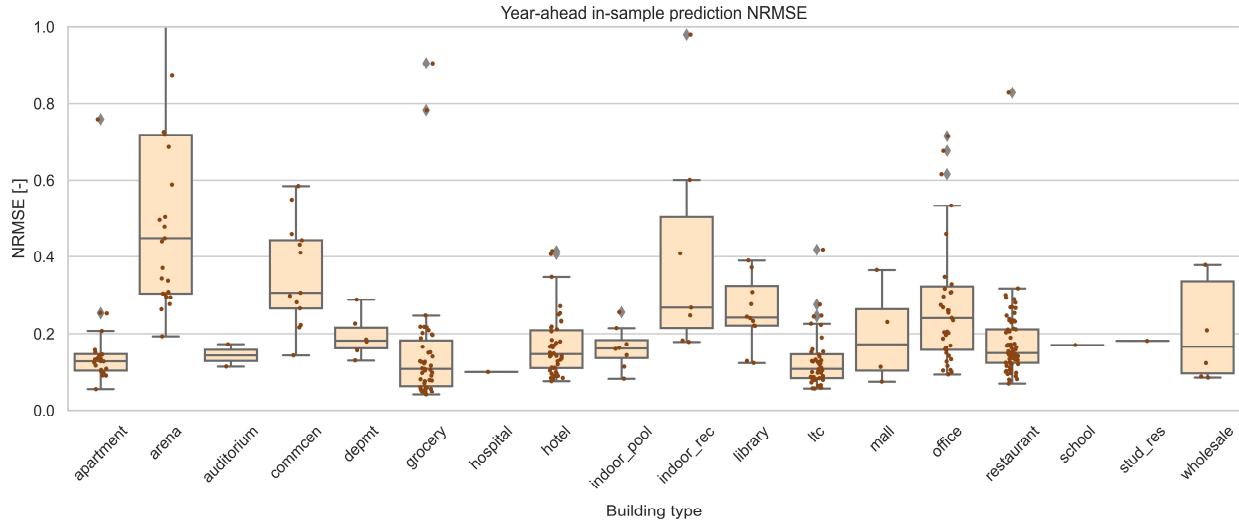
Figure 90: In sample, year-ahead electricity prediction normalized root mean squared error by building type. Each red dot represents a single data point for one building

The out-of-sample year-ahead NRMSEs by building type are displayed in Figure 91. To maintain visibility, the scale was adjusted, however, the upper quartile for each box is displayed on the plot. Additionally, the out-of-sample error will vary based on the number of buildings within each building type in the database. The out-of-sample predictions were performed without training on the test building, except in the case where there is only one building. In general, the out-of-sample model is expected to generalize better for building types with more building data available. However, it is also possible with smaller building datasets, that each building has similar energy-use patterns and the model appears to generalize well. As seen in Figure 91, the auditorium, community centre, grocery store and shopping mall have poor out-of-sample predictions. However, as seen in Figure 90, several of these building types also do not perform well for in-sample testing. The poor out-of-sample performance may be because each building within its type has different schedules or equipment needs. For example, grocery stores' energy use will depend on the amount of refrigerated space or if there is a kitchen at the store. Auditoriums and community centres may operate on different schedules or have irregular energy use depending on when events are run. The use of monthly data for calibration is shown to greatly improve model accuracy, as illustrated by the green boxes in Figure 91. This indicates that generally the range and shape of electricity

use profiles are similar for the same building type, however the magnitude changes. This may be due to different densities of appliances to floor area, insulation levels and system or appliance efficiencies.
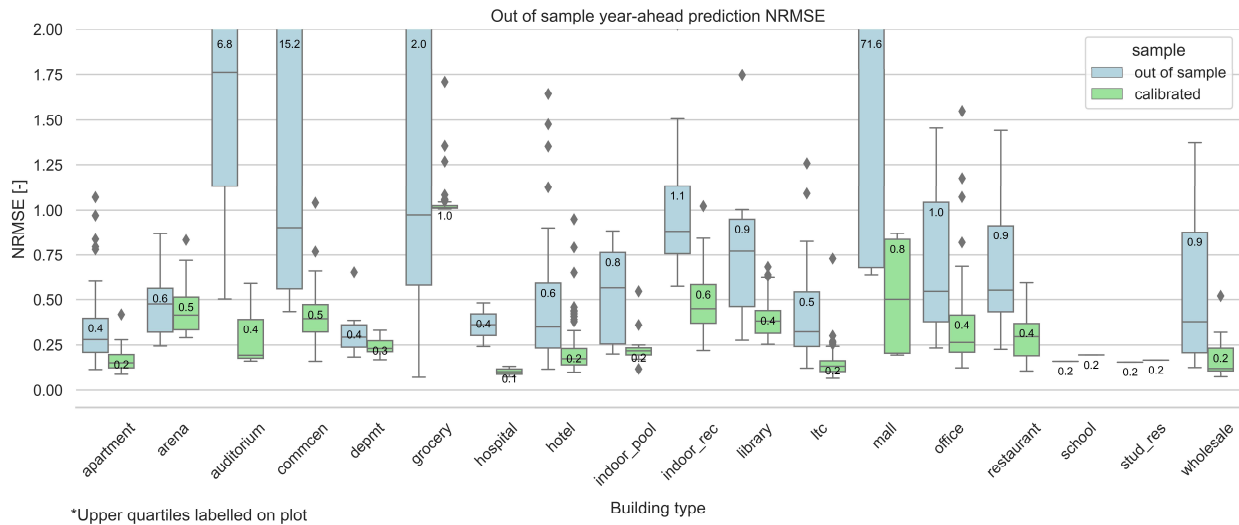
Figure 91: Out of sample, year-ahead electricity prediction normalized root mean squared error by building type

4.1.2 Annual cooling load comparison

In this work, hourly predicted space cooling loads cannot be evaluated for most real buildings because the cooling systems are not submetered.   Therefore the cooling load disaggregation was checked on an annual scale by comparing the predicted annual electrical cooling load ratio to ratios calculated from NRCAN's National Energy Use Database - Comprehensive Energy Use Database [105]. NRCAN used aggregate energy use data from Statistics Canada along with a Commercial/Institutional End-Use Model developed by the Office of Energy Efficiency to estimate the energy breakdown [106]. The annual electricity cooling load ratio is calculated as:

$$\text{Annual electricity cooling load ratio} = \frac{\text{Annual electricity used for space cooling}}{\text{Total annual electricity use}}$$
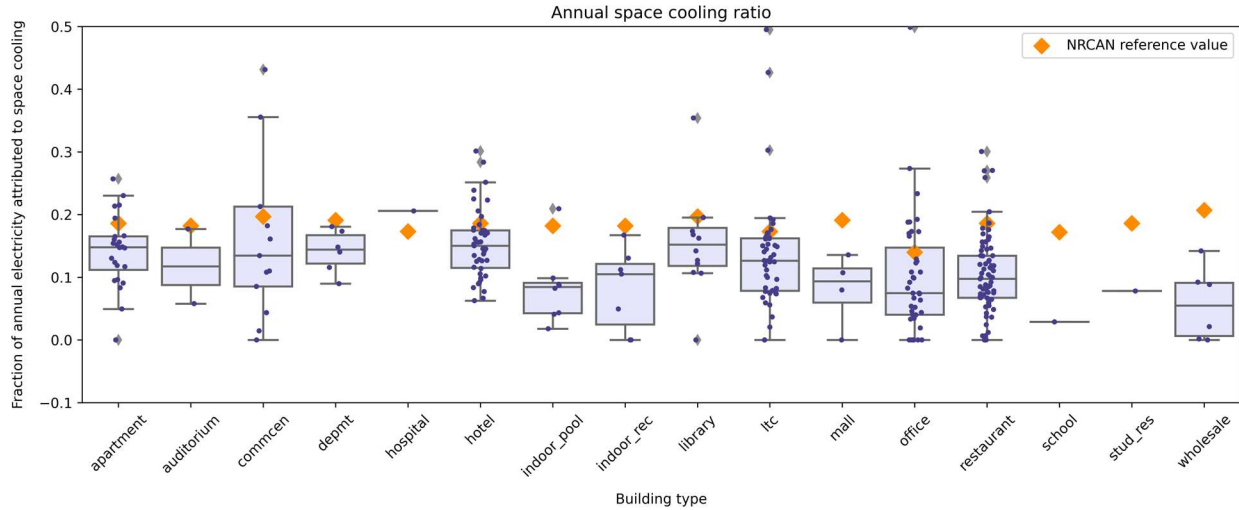
Figure 92: Annual predicted space cooling loads compared to NRCAN averages by building type (each dark blue dot represents the annual space cooling ratio for one building)

Figure 92 displays the predicted cooling load ratio for real buildings compared to the NRCAN values, plotted with an orange diamond. As seen in Figure 92, the annual building cooling loads are underpredicted for most buildings when compared with NRCAN average values. This is likely due to the attribution of only weather-dependent energy use to space cooling. There is often a scheduling component to air-conditioning use, especially in scheduling-dominant buildings like offices. The model may misclassify part of the cooling load may as part of the baseload. The scheduled portion of cooling may be due to HVAC scheduling as well as the heat coming from electrical appliances and occupants. To improve the model, a percentage of the baseload can be reassigned to the cooling load, however, analysis from literature and real submetered data should be performed to determine what percentage should be reassigned. It should also be noted that the NRCAN values are calculated for 2018, but the annual cooling load will depend on the temperature during the predicted year which was selected as the last available year of data for each building. Additionally, some NRCAN values are provided for general archetypes that do not exactly match the building types in this work. For example, the indoor pool and indoor recreation types both use the NRCAN reference value for the "Arts, Entertainment and Recreation" building type.

4.2   Gas prediction

4.2.1 Non-scheduled model

The non-scheduled heating model was applied to approximately 200 buildings in the database with gas data available. Figure 93 displays the hourly space heating and service hot water (SHW) gas-use forecasts of a sample community centre for one year using the non-scheduled model. The true and predicted monthly values are also displayed. On the monthly scale, the model performs fairly well, however, February 2020 was overpredicted by around 2 m^3 per hour. The predicted SHW gas use varies slightly in the summer months compared to the winter from the use of the change-point model. The monthly heating prediction NRMSE for all buildings with gas data is shown in Figure 94. The majority of buildings are well predicted for one year, with an NRMSE below 0.25. Some buildings have high NRMSE values that are greater than 1 which may be due to changes in the building heating system operation for the test set compared to the training set.
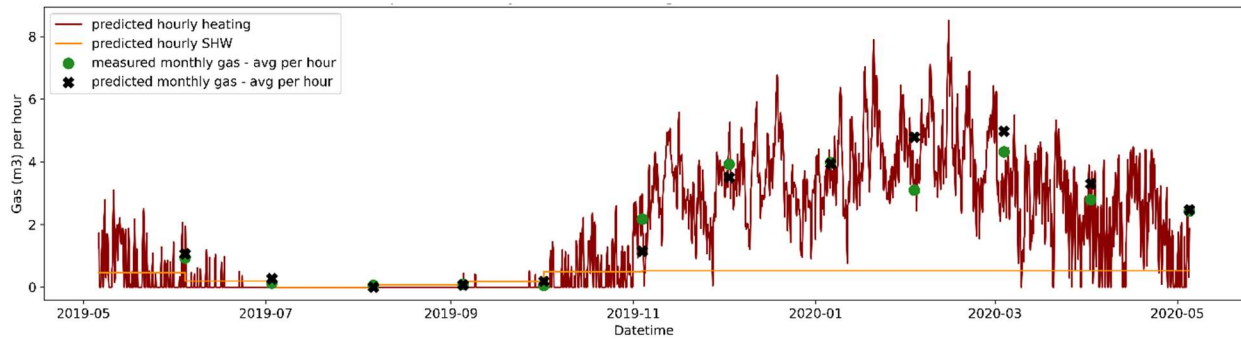
Figure 93: Sample real building non-scheduled heating prediction
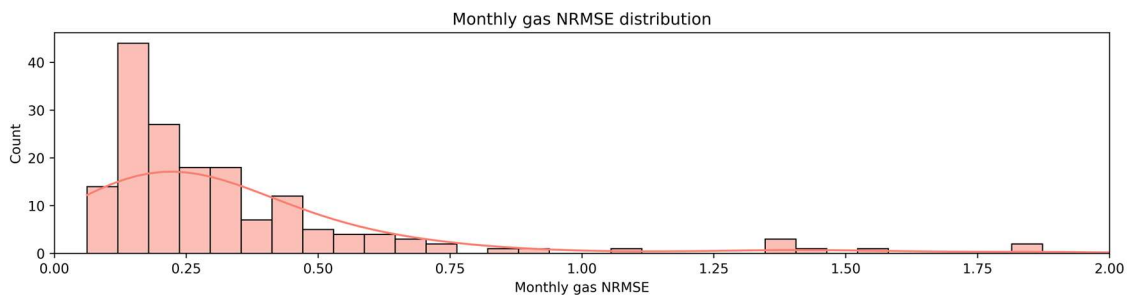
Figure 94: Non-scheduled monthly heating prediction normalized root mean squared error distribution

4.2.2 Scheduled model

The scheduled model was applied to approximately 60 buildings with both hourly electricity and monthly gas data. The hourly space heating and SHW gas-use forecasts of the community centre for one year using the scheduled model are shown in Figure 95. Similar to the non-scheduled model, most months are well predicted except for February 2020. However, June 2019 is also not predicted well. The monthly heating prediction NRMSE for the buildings is shown in Figure 96. In general, the non-scheduled model (pink) has a lower NRMSE than the scheduled model (blue). Based on these results the non-scheduled gas heating model is preferred over the scheduled model. As mentioned in Section 3.7.5, it is difficult to justify the addition of scheduling in the model without knowledge of the building control system and schedule.
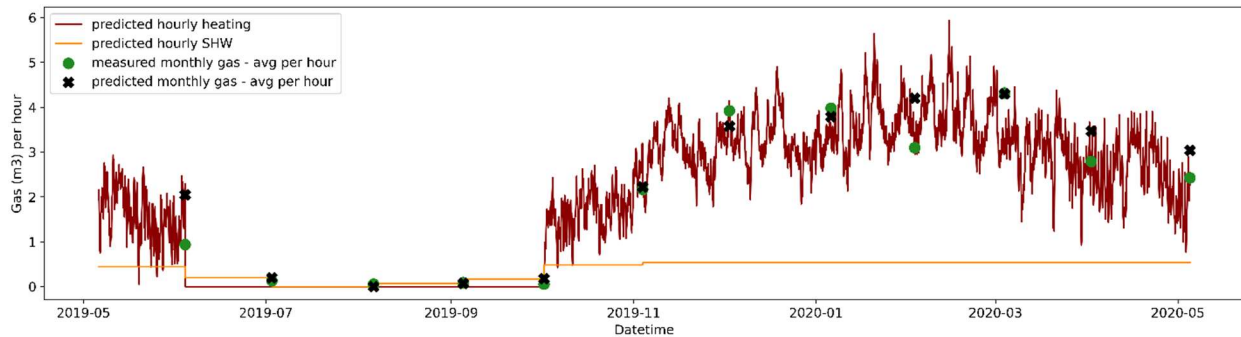
Figure 95: Sample real building scheduled heating prediction
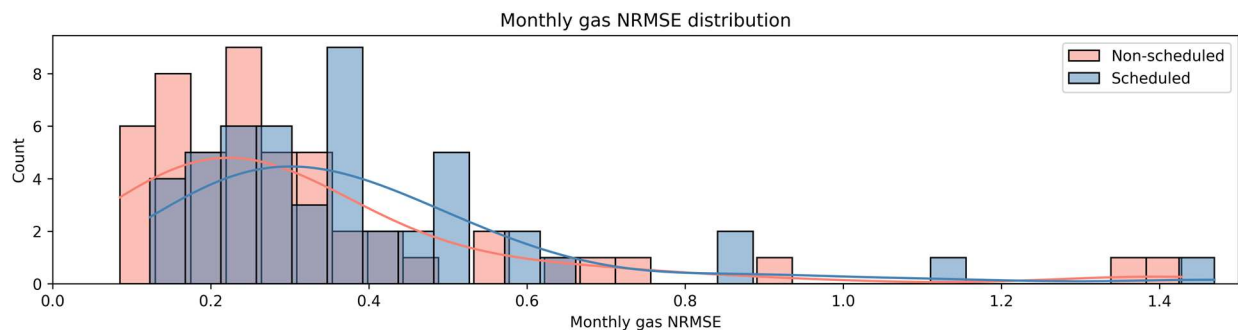
Figure 96: Scheduled monthly heating prediction normalized root mean squared error distribution

Chapter 5

5 Conclusions and future work

To reduce Canada's greenhouse gas emissions in the building sector, building energy forecasting tools are necessary to manage grid supply and control building energy systems efficiently. Measured electricity data has increased in recent years with smart meter installations, leading to the use of statistical forecasting models in addition to the traditional physics-based approaches. Integrated community building energy systems can reduce emissions by meeting community thermal and electrical demands simultaneously while responding to the electricity grid. These systems can be designed and controlled based on forecasts from data-based energy models that also disaggregate total energy by end-use. In this work, several data-driven building energy models were proposed to predict individual building end-use disaggregated electricity and natural gas consumption. First, a literature review was performed to determine the state of the art for building energy models. Next, the building energy database used in this work and model cases were described to provide background for the methodology. Hourly electricity models were then created for conventional, supermarket and arena-type buildings and validated on

submetered data. A 5-minute resolution model was proposed for an arena for short-term predictions. A natural gas model was also created using monthly gas measurements to predict heating at an hourly rate. The models were trained and tested on a database of approximately 900 high energy density buildings around Ontario for which hourly electricity and/or monthly gas data were provided by utility partners. The performance of the models and results were then discussed.

5.1 Model performance

Electricity and natural gas models were trained and tested on real buildings for short- and long-term scales as well as in- and out-of-building-sample predictions. The median NRMSE for most building types was below 0.2 for short-term, in-sample predictions although some building models had worse performance. For year-ahead predictions, NRMSE for the majority of buildings was below 0.3. Therefore, a linear regression approach was able to forecast total electricity use while providing physical insight into the factors of building energy use. This also allowed for the disaggregation of total electricity into its thermal and base load components.

While real building space cooling load predictions could not be validated at an hourly scale, preliminary results from a synthetic apartment had hourly NRMSE ranging from 0.23 to 0.34 for the summer depending on the training and testing lengths. The NRMSE on a daily scale was lower, ranging from 0.02 to 0.29. However, space cooling loads predicted during the winter had a high NRMSE due to incorrect assumptions of when the cooling system is on or off. The annual portion of the electricity used for space cooling in real buildings was checked against reference values from NRCAN [105]. The forecasted annual space cooling loads were underpredicted compared to the NRCAN values, likely due to neglecting scheduled contributors to the cooling load such as heat coming from electrical appliances and occupants.

Additionally, a generalized model was tested to determine how well existing buildings can be used to predict a new building. Model performance was found to differ depending on the building type.

For example, apartments have similar usage patterns resulting in a relatively low median NRMSE of 0.4 compared to the office building type having a median NRMSE greater than 0.5. The results of the out-of-sample predictions indicate which types of buildings behave similarly or have different patterns. The out-of-sample predictions were then scaled based on monthly sums to represent scenarios where monthly electricity bills are available but not hourly measurements. The model accuracy improved greatly for all building types. This indicates that a large source of error in the initial out-of-sample predictions is the large difference in the magnitude of the loads, not only scheduling differences. The error may also be due to the inaccuracy of the estimated areas which can be investigated with improved area data, as mentioned in Section 5.2.2.

Lastly, an hourly gas model trained on monthly measurements was shown to predict monthly aggregates with NRMSE below 0.25 for most buildings. However, the hourly predictions were only verified with synthetic data and buildings with high degrees of scheduling were not predicted well on an hourly scale. Therefore, the use of this model can be helpful for initial heating estimates based on monthly bills however it may not accurately capture the peaks and valleys of heating use.

5.2 Recommendations for future work

5.2.1 Automated data pipeline

This thesis focused on using historical data to train predictive models. However, during deployment, energy consumption data should be continuously measured to retrain the model and provide more accurate forecasts. The cleaning process for large sets of historical data is outlined in Appendix B, which should be modified for continuous data intake. Furthermore, if more energy data becomes available for new buildings or additional data for buildings already in the database, a pipeline to automatically track, anonymize, clean, join with weather data and save files can be developed to save time.

5.2.2 Improved input feature data

Higher quality and additional input feature data or metadata related to buildings could improve model performance. In this work, the floor area was predicted by manually measuring footprints with Google Earth and counting the number of levels. However, the Municipal Property Assessment Corporation (MPAC) contains data on most Ontario buildings including assessed value, site area, year of construction, number of levels and gross leasable area classified by occupancy level. This metadata could help with adjusting the generalized models based on building parameters. It can also help modellers perform more in-depth analyses of each attribute's impact on energy use. Furthermore, the MPAC area data is expected to be significantly more accurate than the calculated values in this work. Accessing MPAC data for a large number of buildings is expensive (approximately $6000). However, most of their data is acquired from municipalities so accessing property data through them could be more cost-effective.

One limitation of the hourly model in this work is that the only information related to the building considered by the model is the building type, floor area and location (to acquire weather data). In the case where further data is available, the model can be adapted to consider more information. For example, while Google Maps was used to estimate floor areas in this work, there is additional data available on the platform that can be accessed through the Google Maps API. Scheduling data can also be acquired from building owners and managers. Hours of operation, events and activity levels are available for many buildings which can be used as input features to improve predictive capabilities.

5.2.3 Impact of the COVID-19 pandemic

On March 11, 2020, the World Health Organization "declared the novel coronavirus (COVID-19) outbreak a global pandemic" [107]. In Canada, the behaviour of building occupants changed during the pandemic as office-workers worked from home, non-essential businesses and services closed, schools shifted online and in-person socializing was reduced. Some building types may not have experienced a

drastic change in energy use such as grocery stores which remained open. However, many of the building types observed are expected to have different energy-use patterns during and following the pandemic.

During the pandemic, multi-unit residential buildings likely saw an increase in energy use as occupants remained at home during the day, operating more electronic devices and running their HVAC systems more frequently. Recreational buildings such as ice rinks or indoor gyms were not open during times of high caseloads and saw energy use decline. Therefore, if more energy data becomes available, analysis of how the COVID-19 pandemic affected energy use for different building types could provide further insight into the drivers of building energy consumption. Furthermore, the aggregate impact could also be analyzed such as how centralized servers or HVAC systems in offices compared to individual computers at home affect total electricity consumption.

There will also be a difference in energy-use patterns following the pandemic. Many companies have developed remote or hybrid approaches where employees still work from home. This would decrease office energy consumption and increase residential energy consumption. Additionally, working from home offers more flexibility to occupants which could redistribute demand times and reduce peak demand. Recreational buildings may see a return to pre-pandemic energy patterns as most of their operation involves in-person activity. The majority of the data used in this work was measured before 2020, meaning the trained models may not be accurate for patterns after the pandemic. Therefore, the models should be retrained with sufficient data following the pandemic to account for behaviour changes. The new model parameters could also be compared with the pre-COVID-19 parameters to observe how energy use has changed.

5.2.4 Reactive and apparent powers

In this work, simple electricity models were proposed using only true power (kW) and energy (kWh) measurements. However, some buildings also provide reactive (kVAr) and apparent (kVA) power or power factor (PF) measurements. Reactive power will change depending on the inductive and

capacitive loads in the building. Inductive loads can come from induction motors and transformers while capacitive loads may come from variable speed motors and inverters. Integrating these measurements into a model could improve the accuracy of the end-use load disaggregation because most HVAC systems use large motors.

5.2.5 Accounting for COP and efficiency

Thermal energy systems such as the ICE-Harvest system require a building's cooling and heating load in terms of the amount of heat provided to or removed from the space. The proposed model aims to disaggregate total electricity into the cooling, heating and baseload components in kWh. To calculate the thermal cooling load, the electrical cooling load must be multiplied by the cooling system COP or efficiency. Often, a constant COP is assumed based on common values found in the literature. However, COP will change depending on the building's cooling system, and outdoor and indoor temperature. Therefore, to obtain an accurate estimate of thermal cooling load, more research and data collection can be conducted concerning different cooling system COP curves. Similarly, to convert natural gas predictions to thermal heating load prediction, the heating value and furnace efficiency must be factored in. The conversion of heating and cooling loads from their sources to the thermal load will allow for thermal energy to be accounted for in the same units within the thermal energy network system.

5.2.6 Model error and controls

In this work, only forecasting model performance was evaluated, assuming the input data is accurate. Measured weather values were used as input features, however, in real implementation, weather forecasts will be used with greater error. Furthermore, when the models are used for the control of community systems, the effects of model accuracy on system optimization should be investigated. The control framework for ICE-Harvest systems is complex, and therefore the impact of model error may not be straightforward. The control framework can be tested, similar to work conducted by Hilliard and Swan [108], by inputting models of varying accuracy to compare the optimization results. This allows for the

evaluation of the control framework and forecasting model together, in addition to evaluating the forecasting model on its own.

5.2.7 Heat from electrical appliances

If data is available related to the building electrical appliances, occupancy schedules and HVAC system efficiency, the positive or negative contribution to the cooling or heating loads can be factored into the load disaggregation. The majority of the electricity used to power electrical appliances will be converted into heat, however, the proposed model considers all scheduled components to contribute to the baseload for end-use disaggregation. Therefore a portion of the scheduled load should be considered as part of the thermal load to improve the predictions, especially for buildings with high internal electrical loads.

References

[1]   Natural Resources Canada, "National Energy Use Database," 2019. [Online]. Available: https://oee.nrcan.gc.ca/corporate/statistics/neud/dpa/showTable.cfm?type=HB&sector=aaa&juris=ca&rn=3&page=0. [Accessed: 29-Jun-2022].

[2]   R. Royal, "Heat Recovery in Retail Refrigeration," *ASHRAE J.*, no. February, pp. 14–22, 2010.

[3]   A. Abdalla, S. Mohamed, S. Bucking, and J. S. Cotton, "Modeling of thermal energy sharing in integrated energy communities with micro-thermal networks," *Energy Build.*, vol. 248, p. 111170, 2021, doi: 10.1016/j.enbuild.2021.111170.

[4]   IIHF, "IIHF Ice rink guide," p. 108, 2016.

[5]   D. George and L. G. Swan, "A method for distinguishing appliance, lighting and plug load profiles from electricity 'smart meter' datasets," *Energy Build.*, vol. 134, pp. 212–222, 2017, doi: 10.1016/j.enbuild.2016.10.048.

[6]   Independent Electricity System Operator, "Ontario's Power System A Smarter Grid." [Online]. Available: https://www.ieso.ca/en/Learn/Ontario-Power-System/A-Smarter-Grid. [Accessed: 06-Jul-2022].

[7]   Ontario Energy Board, "Smart Meter Implementation Plan," 2005.

[8]   Independent Electricity System Operator, "Building Privacy into Ontario ' s Smart Meter Data Management System : A Control Framework," no. May, 2012.

[9]   G. W. Hart, "Nonintrusive Appliance Load Monitoring," *Proc. IEEE*, vol. 80, no. 12, pp. 1870–1891, 1992, doi: 10.1109/5.192069.

[10]   Natural Resources Canada, "Survey of Commercial and Institutional Energy Use (SCIEU) - Buildings 2014," 2014.

[11]   Natural Resources Canada, "Survey of Energy Consumption of Multi-Unit Residential Buildings (SECMURBs) 2018," 2018.

[12]   X. Lü, T. Lu, C. J. Kibert, and M. Viljanen, "Modeling and forecasting energy consumption for heterogeneous buildings using a physical-statistical approach," *Appl. Energy*, vol. 144, pp. 261–275, 2015, doi: 10.1016/j.apenergy.2014.12.019.

[13]   A. Foucquier, S. Robert, F. Suard, L. Stéphan, and A. Jay, "State of the art in building modelling and energy performances prediction: A review," *Renew. Sustain. Energy Rev.*, vol. 23, pp. 272–288, 2013, doi: 10.1016/j.rser.2013.03.004.

[14]   O. Bellache, R. Sunyé, N. Galnis, D. Giguère, and M. Ouzzane, "Two-dimensional transient model of airflow transfer in ice rinks," in *ASHRAE Transactions*, 2006, vol. 112 PART 2, pp. 706–716.

[15]   M. Ouzzane, R. Sunyé, R. Zmeureanu, D. Giguère, J. Scott, and O. Bellache, "Cooling load and environmental measurements in a Canadian indoor ice rink," in *ASHRAE Transactions*, 2006, vol. 112 PART 2, pp. 538–545.

[16]   J. Schiefelbein, J. Rudnick, A. Scholl, P. Remmen, M. Fuchs, and D. Müller, "Automated urban energy system modeling and thermal building simulation based on OpenStreetMap data sets," *Build. Environ.*, vol. 149, no. December 2018, pp. 630–639, 2019, doi: 10.1016/j.buildenv.2018.12.025.

[17]   OpenStreetMap contributors, "Planet dump retrieved from https://planet.osm.org," 2021. [Online]. Available: https://www.openstreetmap.org.

[18]   J. K. Kissock, J. S. Haberl, and D. E. Claridge, "Development of a toolkit for calculating linear change point linear multiple linear inverse building energy analysis models," 2002.

[19]   S. R. Iyer, M. Sankar, P. V. Ramakrishna, V. Sarangan, A. Vasan, and A. Sivasubramaniam,

"Energy disaggregation analysis of a supermarket chain using a facility-model," *Energy Build.*, vol. 97, pp. 65–76, 2015, doi: 10.1016/j.enbuild.2015.03.053.

[20] A. A. A. Gassar and S. H. Cha, "Energy prediction techniques for large-scale buildings towards a sustainable built environment: A review," *Energy and Buildings*, vol. 224. Elsevier Ltd, p. 110238, 2020, doi: 10.1016/j.enbuild.2020.110238.

[21] S. Fiorelli and A. H. Neto, "Comparison between detailed model simulation and artificial neural network for forecasting building energy consumption," vol. 40, pp. 2169–2176, 2008, doi: 10.1016/j.enbuild.2008.06.013.

[22] K. Amasyali and N. M. El-Gohary, "A review of data-driven building energy consumption prediction studies," *Renew. Sustain. Energy Rev.*, vol. 81, no. January 2016, pp. 1192–1205, 2018, doi: 10.1016/j.rser.2017.04.095.

[23] L. G. Swan, V. I. Ugursal, and I. Beausoleil-Morrison, "Occupant related household energy consumption in Canada: Estimation using a bottom-up neural-network technique," *Energy Build.*, vol. 43, no. 2–3, pp. 326–337, 2011, doi: 10.1016/j.enbuild.2010.09.021.

[24] M. Heidarinejad, J. G. Cedeño-Laurent, J. R. Wentz, N. M. Rekstad, J. D. Spengler, and J. Srebric, "Actual building energy use patterns and their implications for predictive modeling," *Energy Convers. Manag.*, vol. 144, pp. 164–180, 2017, doi: 10.1016/j.enconman.2017.04.003.

[25] L. Pedersen, J. Stang, and R. Ulseth, "Load prediction method for heat and electricity demand in buildings for the purpose of planning for mixed energy distribution systems," *Energy Build.*, vol. 40, no. 7, pp. 1124–1134, 2008, doi: 10.1016/j.enbuild.2007.10.014.

[26] G. Pagliarini and S. Rainieri, "Restoration of the building hourly space heating and cooling loads from the monthly energy consumption," *Energy Build.*, vol. 49, pp. 348–355, 2012, doi: 10.1016/j.enbuild.2012.02.030.

[27]   M. De Rosa, V. Bianco, F. Scarpa, and L. A. Tagliafico, "Heating and cooling building energy demand evaluation; A simplified model and a modified degree days approach," *Appl. Energy*, vol. 128, pp. 217–229, 2014, doi: 10.1016/j.apenergy.2014.04.067.

[28]   K. S. Cetin, M. Siemann, and C. Sloop, "Disaggregation and Future Prediction of Monthly Residential Building Energy Use Data Using Localized Weather Data Network," *ACEEE Rep.*, no. Figure 1, pp. 1–12, 2016.

[29]   S. A. Brideau, "Estimating Hourly Heating and Cooling Loads from Monthly Results," *ASHRAE J.*, vol. 126, pp. 166–173, 2020.

[30]   C. John, C. Vallianos, J. Candanedo, and A. Athienitis, "Estimating time constants for over 10,000 residential buildings in North America: towards a statistical characterization of thermal dynamics," in *7th International Building Physics Conference*, 2018.

[31]   A. Afshari and N. Liu, "Inverse modeling of the urban energy system using hourly electricity demand and weather measurements, Part 2: Gray-box model," *Energy Build.*, vol. 157, pp. 139–156, 2017, doi: 10.1016/j.enbuild.2017.01.052.

[32]   O. Pasichnyi, J. Wallin, and O. Kordas, "Data-driven building archetypes for urban building energy modelling," *Energy*, vol. 181, pp. 360–377, 2019, doi: 10.1016/j.energy.2019.04.197.

[33]   J. Sokol, "Deriving Archetype Templates for Urban Building Energy Models Based on Measured Monthly Energy Use." Massachusetts Institute of Technology, 2010.

[34]   G. Kazas, E. Fabrizio, and M. Perino, "Energy demand profile generation with detailed time resolution at an urban district scale: A reference building approach and case study," *Appl. Energy*, vol. 193, pp. 243–262, 2017, doi: 10.1016/j.apenergy.2017.01.095.

[35]   U. Ali, M. H. Shamsi, J. O. Donnell, and F. Alshehri, "Comparative Analysis of Machine Learning Algorithms for Building Archetypes Development in Urban Energy Modeling," in *Building*

Performance Modeling Conference and SimBuild, 2018, no. December.

[36]   M. Kuhn and K. Johnson, *Applied predictive modeling*. 2013.

[37]   G. Smpokos, M. A. Elshatshat, A. Lioumpas, and I. Iliopoulos, "On the energy consumption forecasting of data centers based on weather conditions: Remote sensing and machine learning approach," *arXiv*, 2018.

[38]   A. Dhar, T. A. Reddy, and D. E. Claridge, "Using Fourier Series to Model Hourly Energy Use in Commercial Buildings," 1993.

[39]   R. Granell, C. J. Axon, M. Kolokotroni, and D. C. H. Wallom, "Predicting electricity demand profiles of new supermarkets using machine learning," *Energy Build.*, vol. 234, p. 110635, 2021, doi: 10.1016/j.enbuild.2020.110635.

[40]   T. A. Reddy and D. E. Claridge, "Using synthetic data to evaluate multiple regression and principal component analyses for statistical modeling of daily building energy consumption," *Energy Build.*, vol. 21, no. 1, pp. 35–44, 1994, doi: 10.1016/0378-7788(94)90014-0.

[41]   M. F. Fels, "The Princeton Scorekeeping Method: An Introduction," 1984.

[42]   G. Pagliarini and S. Rainieri, "Modeling of a thermal energy storage system coupled with combined heat and power generation for the heating requirements of a University Campus," *Appl. Therm. Eng.*, vol. 30, pp. 1255–1261, 2010, doi: 10.1016/j.applthermaleng.2010.02.008.

[43]   Natural Resources Canada, *Energy Use Data Handbook 1990 and 1984 to 2004*, no. August. Ottawa, 2006.

[44]   J. A. Masiello and D. S. Parker, "Factors Influencing Water Heating Energy Use and Peak Demand in a Large Scale Residential Monitoring Study," *Resid. Build.*, pp. 157–70, 1992.

[45]   M. Hart and R. De Dear, "Weather sensitivity in household appliance energy end-use," *Energy*

Build., vol. 36, no. 2, pp. 161–174, 2004, doi: 10.1016/j.enbuild.2003.10.009.

[46] A. Chmielewska, "Fluctuating temperature of the mains water throughout the year and its influence on the consumption of energy for the purposes of DHW preparation," *E3S Web Conf.*, vol. 44, 2018, doi: 10.1051/e3sconf/20184400017.

[47] C. Aguilar, D. J. White, and D. L. Ryan, "Domestic Water Heating and Water Heater Energy Consumption in Canada," *CBEEDAC*, 2005.

[48] C. Irambona, B. Music, D. Huard, and A. Frigon, "Lake Ontario water temperature in a changing climate," p. 35, 2017.

[49] ASHRAE, *2017 ASHRAE Handbook: Fundamentals*. Atlanta, GA: ASHRAE, 2017.

[50] C. Ghiaus, "Experimental estimation of building energy performance by robust regression." 2005.

[51] D. W. Schrock and D. E. Claridge, "Predicting Energy Usage in a Supermarket," *Proc. Sixth Symp. Improv. Build. Syst. Hot Humid Clim.*, p. F-19-F-27, 1989.

[52] D. Ruch, L. Chen, J. S. Haberl, and D. E. Claridge, "A Change-Point Principal Component Analysis (CP/PCA) Method for Predicting Energy Usage in Commercial Buildings: The PCA Model," 1993.

[53] V. Singh, T. A. Reddy, and B. Abushakra, "Predicting annual energy use in buildings using short-term monitoring and utility bills: The hybrid inverse model using daily data (HIM-D)," *ASHRAE Trans.*, vol. 119, no. PART 2, pp. 169–180, 2013.

[54] T. Hastie, R. Tibshirani, and J. Friedman, *The Elements of Statistical Learning*, 2nd ed. 2017.

[55] P. Nageler *et al.*, "Comparison of dynamic urban building energy models (UBEM): Sigmoid energy signature and physical modelling approach," *Energy Build.*, vol. 179, pp. 333–343, 2018, doi: 10.1016/j.enbuild.2018.09.034.

[56]   M. Sajjad *et al.*, "Towards Efficient Building Designing: Heating and Cooling Load Prediction via Multi-Output Model," 2020.

[57]   C. Cortes and V. Vapnik, "Support-Vector Networks," *Mach. Learn.*, vol. 20, pp. 273–297, 1995.

[58]   K. Yun, R. Luck, P. J. Mago, and H. Cho, "Building hourly thermal load prediction using an indexed ARX model," *Energy Build.*, vol. 54, pp. 225–233, 2012, doi: 10.1016/j.enbuild.2012.08.007.

[59]   X. Luo, T. Hong, Y. Chen, and M. A. Piette, "Electric load shape benchmarking for small- and medium-sized commercial buildings," *Appl. Energy*, vol. 204, no. June, pp. 715–725, 2017, doi: 10.1016/j.apenergy.2017.07.108.

[60]   R. J. Hyndman and G. Athanasopoulos, *Forecasting: Principles and Practice*, 2nd ed. Melbourne, 2018.

[61]   E. M. Pickering, M. A. Hossain, R. H. French, and A. R. Abramson, "Building electricity consumption: Data analytics of building operations with classical time series decomposition and case based subsetting," *Energy Build.*, vol. 177, pp. 184–196, 2018, doi: 10.1016/j.enbuild.2018.07.056.

[62]   F. Niu, Z. O'Neill, and C. O'Neill, "Data-driven based estimation of HVAC energy consumption using an improved Fourier series decomposition in buildings," *Build. Simul.*, vol. 11, no. 4, pp. 633–645, 2018, doi: 10.1007/s12273-018-0431-2.

[63]   M. A. Hossain, A. Khalilnejad, R. Haddadian, E. M. Pickering, R. H. French, and A. R. Abramson, "Data analytics applied to the electricity consumption of office buildings to reveal building operational characteristics," *Adv. Build. Energy Res.*, vol. 0, no. 0, pp. 1–19, 2020, doi: 10.1080/17512549.2020.1730239.

[64]   A. Khalilnejad, R. H. French, and A. R. Abramson, "Data-driven evaluation of HVAC operation

and savings in commercial buildings," *Appl. Energy*, vol. 278, no. July, p. 115505, 2020, doi: 10.1016/j.apenergy.2020.115505.

[65]   M. M. Armstrong, M. C. Swinton, H. Ribberink, I. Beausoleil-Morrison, and J. Millette, "Synthetically derived profiles for representing occupant-driven electric loads in Canadian housing," *J. Build. Perform. Simul.*, vol. 2, no. 1, pp. 15–30, 2009, doi: 10.1080/19401490802706653.

[66]   U. Jordan and K. Vajen, "Realistic domestic hot-water profiles in different time scales," *Rep. Sol. Heat. Cool. Progr. Int. Energy Agency (IEA-SHC)T*, vol. 26, pp. 1–18, May 2001.

[67]   National Research Council of Canada, *National Energy Code of Canada for Buildings*. 2017.

[68]   National Research Council of Canada, *National Building Code of Canada*, 14th ed. Ottawa: NRC Publications, 2015.

[69]   M. Lamagna, B. Nastasi, D. Groppi, M. M. Nezhad, and D. A. Garcia, "Hourly energy profile determination technique from monthly energy bills," *Build. Simul.*, vol. 13, no. 6, pp. 1235–1248, 2020, doi: 10.1007/s12273-020-0698-y.

[70]   B. Zhao, M. Ye, L. Stankovic, and V. Stankovic, "Non-intrusive load disaggregation solutions for very low-rate smart meter data," *Appl. Energy*, vol. 268, no. May, p. 114949, 2020, doi: 10.1016/j.apenergy.2020.114949.

[71]   A. Rodriguez-Silva and S. Makonin, "Universal Non-Intrusive Load Monitoring (UNILM) Using Filter Pipelines, Probabilistic Knapsack, and Labelled Partition Maps," *Asia-Pacific Power Energy Eng. Conf. APPEEC*, vol. 2019-Decem, no. Appeec, 2019, doi: 10.1109/APPEEC45492.2019.8994618.

[72]   J. Kelly and W. Knottenbelt, "Neural NILM: Deep neural networks applied to energy disaggregation," *BuildSys 2015 - Proc. 2nd ACM Int. Conf. Embed. Syst. Energy-Efficient Built*,

pp. 55–64, 2015, doi: 10.1145/2821650.2821672.

[73] A. Srivastava, P. Tehria, and B. K. Pandey, "Energy Disaggregation for Small and Medium Businesses and their Operational Characteristics," *NILM 2020 - Proc. 5th Int. Work. Non-Intrusive Load Monit.*, pp. 59–63, 2020, doi: 10.1145/3427771.3427854.

[74] B. Zhao, L. Stankovic, and V. Stankovic, "On a Training-Less Solution for Non-Intrusive Appliance Load Monitoring Using Graph Signal Processing," *IEEE Access*, vol. 4, pp. 1784–1799, 2016, doi: 10.1109/ACCESS.2016.2557460.

[75] N. Batra *et al.*, "NILMTK: An open source toolkit for non-intrusive load monitoring," *e-Energy 2014 - Proc. 5th ACM Int. Conf. Futur. Energy Syst.*, pp. 265–276, 2014, doi: 10.1145/2602044.2602051.

[76] T. Bernard Dr.-Ing., "Non-Intrusive Load Monitoring (NILM): combining multiple distinct electrical features and unsupervised machine learning techniques," 2018.

[77] J. Holweger, M. Dorokhova, L. Bloch, C. Ballif, and N. Wyrsch, "Unsupervised algorithm for disaggregating low-sampling-rate electricity consumption of households," *Sustain. Energy, Grids Networks*, vol. 19, 2019, doi: 10.1016/j.segan.2019.100244.

[78] H. Kim, M. Marwah, M. Arlitt, G. Lyon, and J. Han, "Unsupervised Disaggregation of Low Frequency Power Measurements."

[79] M. Liang, Y. Meng, N. Lu, D. Lubkeman, and A. Kling, "HVAC load Disaggregation using Low-resolution Smart Meter Data," *2019 IEEE Power Energy Soc. Innov. Smart Grid Technol. Conf. ISGT 2019*, 2019, doi: 10.1109/ISGT.2019.8791578.

[80] A. Afshari and L. Friedrich, "Inverse modeling of the urban energy system using hourly electricity demand and weather measurements, Part 1: Black-box model," *Energy Build.*, vol. 157, pp. 139–156, 2017, doi: 10.1016/j.enbuild.2017.01.052.

[81]   A. Khalilnejad, A. M. Karimi, S. Kamath, R. Haddadian, R. H. French, and A. R. Abramson, "Automated pipeline framework for processing of large-scale building energy time series data," *PLoS One*, vol. 15, no. 12, p. e0240461, 2020, doi: 10.1371/journal.pone.0240461.

[82]   R. El Kontar and T. Rakha, "Profiling Occupancy Patterns to Calibrate Urban Building Energy Models (UBEMs) Using Measured Data Clustering," *Technol. Archit. Des.*, vol. 2, no. 2, pp. 206–217, 2018, doi: 10.1080/24751448.2018.1497369.

[83]   M. Swamynathan, "Step 2: Introduction to Machine Learning," in *Mastering Machine Learning with Python in Six Steps*, Berkeley, CA: Apress, 2019, pp. 65–143.

[84]   Government of Ontario, "Public holidays: Your guide to the Employment Standards Act." .

[85]   L. Pedersen, *Load Modelling of Buildings in Mixed Energy Distribution Systems*, no. February. 2007.

[86]   R. Tavenard *et al.*, "Tslearn, A Machine Learning Toolkit for Time Series Data," *J. Mach. Learn. Res.*, vol. 21, pp. 1–6, 2020.

[87]   Statistics Canada, "Type of main heating fuel used, by province, 2011," *Households and the Environment: Energy Use*, 2011. [Online]. Available: https://www150.statcan.gc.ca/n1/pub/11-526-s/2013002/t002-eng.htm.

[88]   R. Stull, *Meteorology for Scientists and Engineers*, 3rd ed. Vancouver, Canada, 2015.

[89]   P. Virtanen *et al.*, "SciPy 1.0: fundamental algorithms for scientific computing in Python," *Nat. Methods*, vol. 17, no. 3, pp. 261–272, 2020, doi: 10.1038/s41592-019-0686-2.

[90]   F. Pedregosa, G. Varoquaux, A. Gramfort, V. Michel, and B. Thiron, "Scikit-learn: Machine Learning in Python," *J. Mach. Learn. Res.*, vol. 12, no. 85, pp. 2825–2830, 2011.

[91]   M. Deru *et al.*, "U.S. Department of Energy commercial reference building models of the national

building stock," *Publ.*, no. February 2011, pp. 1–118, 2011.

[92] Natural Resources Canada, "Saving Energy Dollars in Stores, Supermarkets and Malls."

[93] L. Harriman, "20 Years of Commercial Desiccant Systems." 2003.

[94] B. Dong *et al.*, "Integrated energy performance modeling for a retail store building," *Build. Simul.*, vol. 6, no. 3, pp. 283–295, 2013, doi: 10.1007/s12273-013-0109-8.

[95] United States Environmental Protection Agency, "Energy Use in Supermarkets." Energy Star Portfolio Manager, 2015.

[96] US Energy Information Administration, "2012 Commercial Buildings Energy Consumption Survey." pp. 1–241, 2016.

[97] J. Arias, *Energy Usage in Supermarkets: Modelling and Field Measurements*. 2005.

[98] ASHRAE, *ASHRAE Handbook Refrigeration*, vol. 1, no. 17. 2018.

[99] L. Nichols, "Improving efficiency in ice hockey arenas," *ASHRAE J.*, vol. 51, no. 6, pp. 16–20, 2009.

[100] Efficiency Manitoba and Association of Manitoba Municipalities, "Energy Efficiency Guide," 2020.

[101] R. Kaya, "Energy Usage in Ice Rink Resurfacing," no. March, 2015.

[102] SaskPower, "Municipal Ice Rink Program."

[103] C. Pilgrim, "piecewise-regression (aka segmented regression) in Python," *J. Open Source Softw.*, vol. 6, no. 68, p. 3859, 2021, doi: 10.21105/joss.03859.

[104] V. M. R. Muggeo, "Estimating regression models with unknown break-points," *Stat. Med.*, vol. 22, no. 19, pp. 3055–3071, Oct. 2003, doi: 10.1002/sim.1545.

[105]   Natural Resources Canada, "Comprehensive Energy Use Database." [Online]. Available: https://oee.nrcan.gc.ca/corporate/statistics/neud/dpa/menus/trends/comprehensive/trends_com_on.cfm.

[106]   Natural Resources Canada, "Energy Use Data Handbook (1990 to 2017)," 2017.

[107]   D. Cucinotta and M. Vanelli, "WHO Declares COVID-19 a Pandemic.," *Acta Biomed.*, vol. 91, no. 1, pp. 157–160, 2020, doi: 10.23750/abm.v91i1.9397.

[108]   T. Hilliard and L. Swan, "Methodology to determine the impact of simplified building models on model-predictive-control morning start optimization performance," *Sci. Technol. Built Environ.*, vol. 24, no. 7, pp. 779–792, 2018, doi: 10.1080/23744731.2017.1415088.

[109]   Ontario Ministry of Energy, "Energy use and greenhouse gas emissions for the Broader Public Sector," *Open Government*, 2018. [Online]. Available: https://open.canada.ca/data/en/dataset/5e976319-9769-4f77-aab9-d170e0131efe.

[110]   Google, "Google Earth." [Online]. Available: https://www.google.com/earth/index.html.

[111]   Ministry of Natural Resources and Forestry, "Ontario Digital Terrain Model (Lidar-Derived)." [Online]. Available: https://geohub.lio.gov.on.ca/maps/mnrf::ontario-digital-terrain-model-lidar-derived/about.

[112]   Statistics Canada, "The Open Database of Buildings," 2019. [Online]. Available: https://www.statcan.gc.ca/en/lode/databases/odb.

[113]   Municipal Property Assessment Corporation, "Municipal Property Assessment Corporation." [Online]. Available: https://www.mpac.ca/en.

[114]   E. Pickering, "Scalable Data Analytics for Commercial Building Virtual Energy Audits," 2016.

[115]   O. Vallis, J. Hochenbaum, and A. Kejariwal, "A novel technique for long-term anomaly detection

in the cloud," *6th USENIX Work. Hot Top. Cloud Comput. HotCloud 2014*, 2014.

[116] R. Cleveland, W. Cleveland, J. McRae, and I. Terpenning, "STL: A Seasonal-Trend Decomposition Based on Loess," *Journal of Official Statistics*, vol. 6, no. 1. pp. 3–33, 1990.

[117] U.S. Department of Energy, Research, National Renewable Energy Laboratory, and Alliance for Sustainable Energy, "NSRDB Data Viewer." [Online]. Available: https://maps.nrel.gov/nsrdb-viewer.

[118] University Corporation for Atmospheric Research, "CEOP Derived Parameter Equations." [Online]. Available: https://archive.eol.ucar.edu/projects/ceop/dm/documents/refdata_report/eqns.html.

[119] D. Bolton, "The computation of equivalent potential temperature.," *Monthly Weather Review*, vol. 108, no. 7. pp. 1046–1053, 1980, doi: 10.1175/1520-0493(1980)108<1046:TCOEPT>2.0.CO;2.

Appendices

Appendix A: Obtaining building metadata

As mentioned in the previous section, detailed data for each building was not readily available for analysis and modelling. One feature that is easily accessible and considered important is the building area. The area data for public buildings were taken from the Energy Use and Greenhouse Gas Emissions for the Broader Public Sector dataset provided by the Government of Ontario [109]. The dataset was also used to classify public building types; however, some buildings are misclassified and were reassigned using Google Maps. The area of private buildings was approximated using Google Earth [110] by measuring the footprint area on Google Earth and counting the number of floors.

An automated area calculator was attempted by combining open datasets such as the Ontario Digital Terrain Model (Lidar-Derived) [111], the Open Database of Buildings [112], OpenStreetMap [17] and Google Earth [110]. The calculator was highly inaccurate because connected buildings (eg. plazas) were not measured properly and many buildings were matched to the wrong footprint due to the incompleteness of the Open Database of Buildings. Additionally, OpenStreetMap is open source and maintained by volunteers, but unfortunately, not all buildings have data available; approximately 1/3 had the level information required. More effort to automate the area data collection or obtain accurate data from the Municipal Property Assessment Corporation (MPAC) [113] would be valuable in the long run.

Since cooling dominant buildings are of interest, specific data related to each arena was found manually as it was considered important for building the model. Most arenas are run by their municipalities which provide some data related to rink operation and Google Maps also provides some information. Information collected for the arenas included:

- o Number of rinks and their dimensions
- o Months of operation

o   Seasonal operation

o   The approximate number of spectator seats

Appendix B: Database preparation procedure

Black-box, hybrid and calibrated simulation models all use data to build and test the models. One of the first steps in data analysis is preparing and organizing the data. Before the analysis is performed, all the data must be in a standard format and of sufficient quality.

B.1 Literature review on preprocessing methods

In literature, data cleaning and transformation are discussed (e.g. [114][37][56][82]); however a distinction should be drawn between standardizing the format (e.g. standard file type, units) and changing values (e.g. imputing outliers). When values are changed, there is a risk of introducing bias into the model. For example, some studies briefly mention that outliers were removed or imputed, but do not discuss in detail how they are detected (e.g. [73][38]). The decision to exclude or impute a datapoint should be justifiable but there are often no clear identifying criteria [39]. Usually, the underlying mechanisms of the problem are not fully known and thus why machine learning techniques are being used in the first place. However, many predictive algorithms are sensitive to outliers, so it may be necessary to identify points that are likely due to measurement error.

Khalilnejad et al. [81] automated the intake and processing of energy data from 816 buildings to evaluate potential retrofit savings. The pipeline involved cleaning, anomaly detection, data quality evaluation and assembly with weather and building properties. During the quality evaluation, files were graded based on the percentage of anomalies and missing data as well as the largest gap of missing values, with low-quality files excluded from the analysis. Anomalies were determined based on the residual component from classical time series decomposition. However, classical time series decomposition is not robust to outliers and may lead to false flags during outlier detection [60].

A simpler approach was taken by Sajjad et al. [56] to account for outliers by normalizing the data based on the minimum and maximum values. However, there is a possibility that the minimum or maximum values are outliers which can skew the normalization.

Vallis et al. [115] used a different method to detect outliers by combining extreme student deviate test (ESD), STL decomposition [116] and robust statistics to automatically detect anomalies in tweets per second for Twitter. They were able to account for daily and weekly cycles by using median and median absolute deviation (MAD) which are less sensitive to anomalies compared to the commonly used mean and standard deviation. First, the series was split into non-overlapping windows. STL decomposition was used for the seasonal component while a piecewise median was used as the trend component. When compared to STL and quantile regression, the proposed method had less false positives and detected most intra-day anomalies with a significantly faster run time.

B.2 Cleaning

Cleaning involves reformatting all of the data files so that they are in a standardized format. The desired format requires a table for each building with datetime, kWh and integrity flag columns. Creating the datetime column involves combining different time-based columns from raw data files to produce a standard datetime object. Additionally, some buildings have electricity recorded in kW instead of kWh. If the initial measurements are not at an hourly scale, measurements are converted to kWh by multiplying by the timescale in hours. For hourly models, the data is resampled to an hourly rate by summing the kWh column to get the total kWh used during each hour. Some buildings also have apparent power (kVa), reactive power (kVar) and power factor (PF) measurements which are kept in the table for future use.

B.3 Integrity

An integrity check was used based on previous work with improvements to reduce computational time. The integrity check searches for missing values in the form of missing time stamps or NaN (Not a Number) values in the data. It checks the time delta between consecutive datetime values to ensure each jump is equal. In some cases, meter readings switched from a low resolution to a high-resolution part way through the measurements. In that case, the data was resampled to the lower frequency to keep all

years of recorded data with a consistent timescale. Missing values were filled with zero-values to ensure functions requiring no NaN values could still be run. However, an additional column is added to flag NaN values so that these entries can be excluded if necessary. Another column was added to tally consecutive zero values. In some cases, many zeros at the start of the measurement interval could indicate the meter was not recording properly and those measurements should be excluded.

B.4 Daylight saving time

Daylight savings was accounted for by excluding the second additional hour during the fall-back period and repeating the previous hour's measurement during the spring-forward hour. This was to maintain 24 hours of data for each day and ensure that daily schedules were captured because the Fourier terms are based on hour of day. While this introduces some error into the dataset, two out of the 8760 hours in a year is only 0.02% of the dataset.

B.5 Weather Data

The weather data used for hourly modelling is from the National Renewable Energy Laboratory [117]. Depending on location, weather data is provided in 30 or 60-minute intervals. To resample weather data, the average value is taken since each value is an instantaneous measurement. When downsampling 30-minute data to 60-minute data it is assumed that data from the previous hour's measurements are represented by the current timestamp. This is from the assumption that an electricity measurement is the kWh used over the past hour (e.g. 5 pm value is the energy used from 4 pm to 5 pm) and the weather data should reflect this as well. The following weather features are used for modelling:

- Global Horizontal Irradiance [W/m^2]
- Temperature [°C]
- Pressure [mbar]
- Relative Humidity [%]

Specific humidity is calculated using data provided for temperature, pressure and relative humidity. The specific humidity can then be calculated using equations from [118]:

$$\text{specific humidity} \approx 0.622 * \frac{e}{p - 0.378 * e}$$

Where:

e = vapour pressure (mbar)
p = pressure (mbar)

The saturation vapour pressure is calculated from Bolton's correlation [119] which approximates Wexler and Goff and Gratch's experimental results to an accuracy of "0.3% or better for -30°C ≤ T ≤ 35°C" [119].

$$e_s(T) = 6.112 \exp\left(\frac{17.67 * T}{T + 243.5}\right)$$

Where T is the temperature in degrees Celsius.

Vapour pressure can then be calculated using relative humidity:

$$e = e_s * \frac{\text{Relative humidity}}{100}$$

B.6 Outliers

In literature, outliers may be excluded during modelling because they can skew the model depending on the objective function. In this work, outliers were generally not excluded from the dataset because it is difficult to determine and prove which data points are outliers.

Depending on the training set length, if there is a sufficient amount of data used, the impact of the outliers can be minimized. Furthermore, the use of regularized regression models can reduce the outlier influence. However, with small training lengths (e.g. 30 days), outliers may need to be removed. Some techniques were used to flag potential outliers such as time series decomposition which may be of use for:

- small training samples, where the influence of erroneous values is greater
- identifying anomalous usage patterns within buildings
- detecting sensor errors or power outages

B.7 Monthly Data

Cleaning monthly data had challenges because the bill date for gas or electricity may fall on random days, thus the period between consecutive measurements is not consistent. Gas bills also have adjustment factors where consumption is estimated and then adjusted once the technician can read the meter on site. As a result, it is difficult to align bills when buildings have multiple accounts that need to be added together. Additionally, the weather data must be resampled at different timescales to match the bill read date. Monthly electricity was neglected in this work because there is a considerable amount of hourly electricity data, however, future work could include the monthly electricity as well

Appendix C: Moisture terms

The latent load is an important contributor to building space cooling and refrigeration loads. Several weather-related moisture terms can be utilized to capture the impact of air moisture such as relative humidity, dew point temperature, precipitable water, mixing ratio and specific humidity. In reality, these terms may have a combinatorial impact, however each was observed separately for simplicity and to reduce the correlation between features.

$$Q_{cooling,t} = \beta_1 * (GHI_t) + \beta_2 * (T_{out,t} - T_{in})^+ + \beta_3(SH_{out,t} - SH_{in})^+ + \beta_4 * \overline{(T_{out} - T_{in})^+}_{t-N,t-1} \qquad (16)$$

$$Q_{cooling,t} = \beta_1 * (GHI_t) + \beta_2 * (T_{out,t} - T_{in})^+ + \beta_3 X + \beta_4 * \overline{(T_{out} - T_{in})^+}_{t-N,t-1}$$

Equation 16 was reformulated using the listed moisture terms with cut-offs in place of X and used in Equation 21. The models were then tested on a synthetic building to calculate the cooling load error and on a set of real buildings to see the impact on total error.
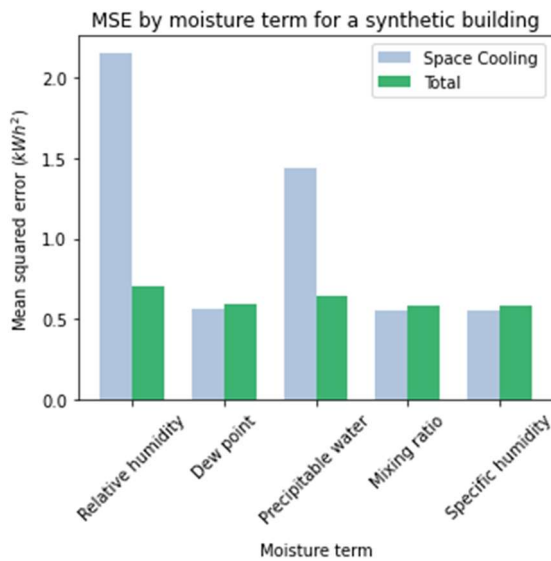
Figure 97: MSE by moisture term for a synthetic building
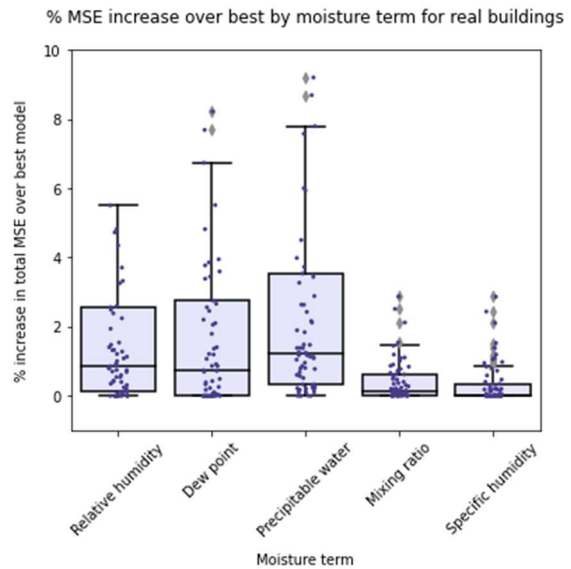
Figure 98: % MSE increase over best model by moisture term for set of real buildings

As seen in Figure 97, specific humidity, mixing ratio and dewpoint performed best for modelling total and space cooling electricity use for the synthetic building. Figure 98 displays the results for total electricity use prediction. Specific humidity displayed the best performance compared to the other parameters with the mixing ratio showing comparable performance. This is expected because the mixing ratio and specific humidity values are similar at low humidity values. Specific humidity is directly related to the amount of moisture in the air, therefore it captures the latent load best because it will represent the amount of moisture removed by the cooling system.

Therefore specific humidity was used as the moisture term to capture the latent load. Direct specific humidity measurements were not available from the measured weather data; however it was calculated from relative humidity, temperature and pressure as explained in Appendix B. As a result, relative humidity and pressure are used indirectly as input features.

Appendix D: Algorithm

Due to the nonlinear terms, the model equations outlined in Section 3.6 can be solved using an iterative method to minimize least squares (nonlinear least squares). The Python scipy library [89] curvefit function is able to apply bounds and solve for the unknown coefficients. It uses the dog box method which is a mix of gradient descent and the Gauss-Newton algorithm. However, the solver has downsides: the solution is dependent on the initial guess, may be a local minimum, the solver may not converge and potential long computational time. Multiple linear regression with a grid search to determine the base temperature and specific humidity values was tested as an alternative.

A comparison of nonlinear least squares, OLS linear regression and ridge regression was performed to observe how algorithms performed in terms of the test set error and computation time. For synthetic day ahead predictions, the ordinary least squares (OLS) algorithm performed best in terms of computation time (Figure 99) and all three algorithms had similar NRMSE values (Figure 101, Figure 103). Ridge regression with parameter tuning had a slightly shorter training time compared to scipy curvefit depending on the data (Figure 99). Ridge regression training time for one fit is similar to OLS, however with parameter tuning it is longer. The algorithms were also tested for year-ahead predictions on a set of real buildings. As seen in Figure 100, OLS is the fastest algorithm, followed by ridge regression and then the curvefit algorithm. While OLS is the fastest, it has the risk of unstable models with large regression coefficients, resulting in extremely large NRMSE values for some cases (Figure 102). Therefore ridge regression provides a good combination of accuracy, stability and computation time as shown in Figure 104.

Day-ahead, synthetic data
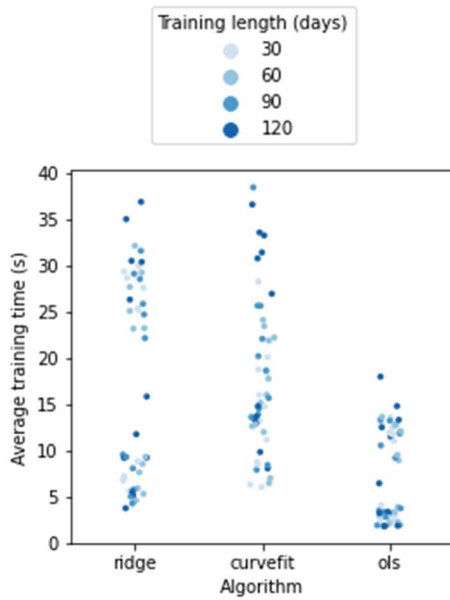
Figure 99: Day-ahead prediction training time by algorithm

Year-ahead, real data
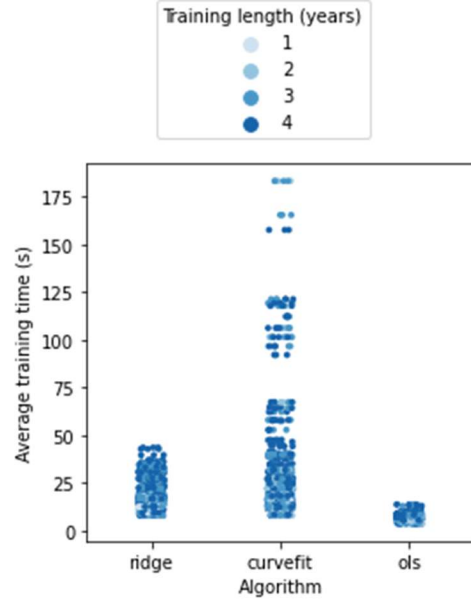
Figure 100: Year-ahead prediction training time by algorithm
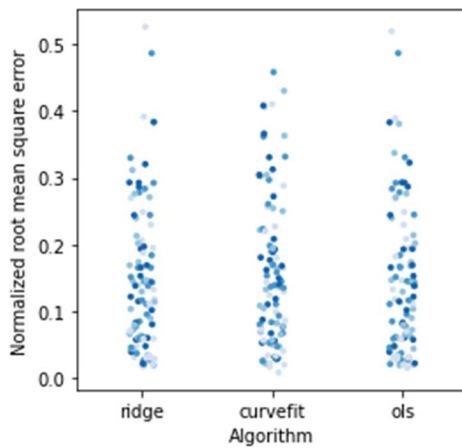
Figure 101: Day-ahead prediction NRMSE by algorithm
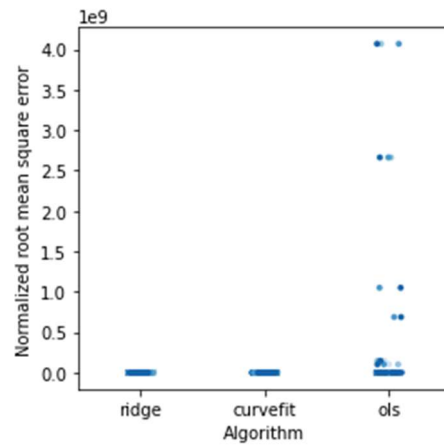
Figure 102: Year-ahead prediction NRMSE by algorithm
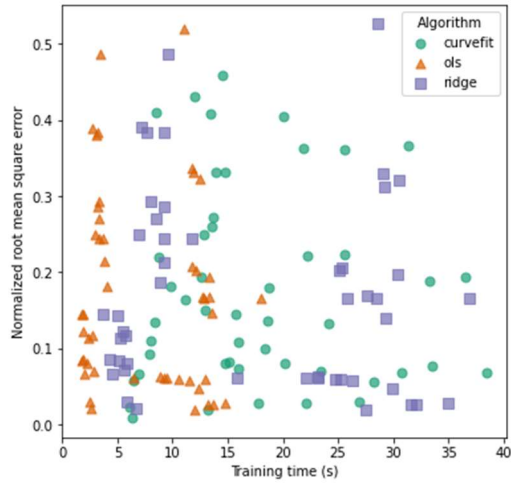
Figure 103: Day-ahead prediction NRMSE vs training time by algorithm
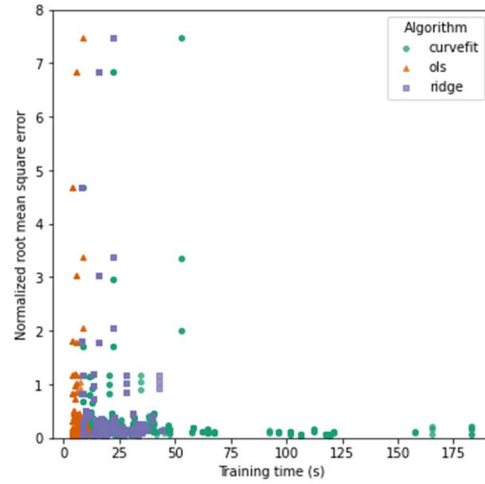
Figure 104: Year-ahead prediction NRMSE vs training time by algorithm

*some NRMSE values extend beyond the y-axis cut off of 8

Appendix E: Ice rink refrigeration system

The refrigeration system is responsible for maintaining the proper ice temperature and creating ice sheets at the beginning of the operation season [98]. Most arena refrigeration systems have two loops, a primary cooling loop and a secondary loop which runs under the ice surface to cool the ice. This helps reduce the risk of refrigerant leaks since it will be contained in the refrigeration equipment room. Examples of primary refrigerants are R22, R-404A, R-507, R-717, with some being phased out due to their environmental impact. Secondary coolants may be glycol, methanol, ethanol or calcium chloride. Sometimes the primary coolant is used directly to cool the slab such as with CO_2 systems which are becoming more common [98]. Ice rinks may use equipment such as evaporative condensers or cooling towers to reject heat to the environment. The refrigerant and number, rating and control systems of compressors used will impact how and when electricity is used for refrigeration purposes. Moreover, some arenas have heat recovery systems which reuse heat removed from the ice surface for the other heating needs such as under floor heating or snow melting. If heat recovery is not present, more heat is rejected to the ambient. All of these refrigeration system specifications will impact the refrigeration load.

Similar to grocery stores, separate dehumidification systems are commonly used to reduce the load on the refrigeration system in ice rinks [93]. They can also reduce condensation on the glass and ceiling. Desiccant dehumidifiers are commonly used, which are explained in Section 3.6.4.1.

Additionally, the slab type and piping geometry will influence the refrigeration load. There are various piping considerations for the secondary cooling loop which cools the ice sheet. The location of supply and return header pipes that feed the subfloor tubes will impact the efficiency and effectiveness of the refrigeration system. Longer piping lengths can result in greater heat gains to the pipes. Further, there are several floor types for recreational ice rinks [98]. Multi-purpose floors use poured concrete, with pipes fixed in the concrete. This allows for use of the pad without ice, for example, floor hockey games in the summer months. On the other hand, some rinks use sand floors, where sand is filled in around the

subfloor pipes. Underfloor heating is also necessary depending on the floor type. If permafrost forms beneath the ice surface, the ground may heave which can damage and warp the ice surface and slab. Thus underfloor heating systems are used, which will add to the refrigeration load. Some ice rinks may use recovered heat for subfloor heating purposes. Ground conduction is also a contributing factor.

One of the main contributors of heat to the ice sheet is resurfacing as it can contribute to around 14-20% of the refrigeration load [14]. To maintain ideal ice conditions, the ice is resurfaced several times a day using a resurfacing machine driven over the ice surface. As it travels across the ice, a blade scrapes up the top layer of ice and collects the snow in a tank. Hot water is then laid out behind the resurfacer which freezes on top of the existing ice. Resurfacing will introduce a significant amount of heat into the ice since the hot water must be cooled to the freezing point, frozen, then further cooled to the ice temperature. The resurfacing schedule will be dependent on the activity and outdoor conditions. For example, high-level hockey games may require resurfacing between every period (approximately 20-30 minutes) while lower-level recreational activities may only require resurfacing between activities. Higher external temperatures and humidity may require the ice to be resurfaced more often, which usually occurs during the summer when some rinks are not operating. Furthermore, for arenas with multiple ice rinks, the schedules may be offset between rinks so that the resurfacer can be used on multiple surfaces. To add more complexity, ice resurfacing machines can be gas or electricity-powered; gas-powered machines will have exhaust fumes which input heat into the building. Therefore, ice resurfacing is an important consideration yet its contribution is difficult to predict without knowledge of each ice pad's schedule.

For buildings whose main operation is the ice surface, approximately 50-65% of the electricity is used to refrigerate the ice pad [4][99][100][101][102]. Some buildings such as community centres or entertainment arenas may have other activities that contribute to building energy demand

Appendix F: Analysis of building model parameters

This section analyzes the output building parameters from the EL-CL (electricity-cooling) model on energy use intensity. Several models and data subsets were used in the modelling process. In this case, the year-ahead, summer weekday building parameters are analyzed. The summer model parameters are investigated because the correlation between electricity use and weather data tends to be higher in the summer due to electrified space cooling. The initially unknown parameters from Equation 21, which are solved for while training, are plotted against the annual electricity use for each building. The investigated parameters are shown in bold in Equation 21 below:

$$
W_{total} = \boldsymbol{\beta_0} + \sum_{n=1}^{11} \left(a_n \cos\left(\frac{2\pi nh}{24}\right) + b_n \sin\left(\frac{2\pi nh}{24}\right) \right) + \boldsymbol{\beta_1} * (GHI) + \boldsymbol{\beta_2} * (T_{out} - \mathbf{T_{in}})^+
$$
$$
+ \boldsymbol{\beta_3}(SH_{out} - \mathbf{SH_{in}})^+ + \boldsymbol{\beta_4} * \overline{(T_{out} - \mathbf{T_{in}})^+}_{t-N,t-1} \tag{21}
$$

F.1 All buildings

Figure 105 displays the learned parameters from the electricity-cooling (EL-CL) model for conventional buildings plotted against electricity use intensity. Electricity use intensity is calculated as the average annual electricity consumption per square meter of floor area, similar to energy use intensity (EUI). When a model parameter has a high correlation with electricity use intensity (the points are more densely clustered around the line of best fit), the parameter can generally be considered more influential on total electricity use. Subfigures (a) and (b) display the impact of the predicted base temperature and specific humidity values. The base temperature has a weak negative correlation with electricity use because a higher setpoint will reduce cooling system energy use, however, many buildings do not appear to follow the trend. Additionally, the most common base temperature value is 18°C which is the value used in the National Energy Code of Canada for Buildings to calculate cooling degree days [67]. The base specific humidity value does not have a large influence on annual electricity use. For the base specific humidity, several buildings may have a high humidity impact because the majority of building

models selected a value of 0. The second most common base value is 0.008 which is found in the literature [31]. The moving average degree day window shows a very weak, negative correlation with annual electricity use. Buildings with larger window sizes may have larger thermal mass or lower ventilation rates, meaning they are less responsive to outdoor condition changes and use less energy. An approximately equal number of buildings selected the largest window size of 60 hours to those that selected a small window below 10 hours. The weather-based regression coefficients are shown in subfigures d, e, f and h, with each showing a positive correlation with annual electricity use. Buildings with higher degree day coefficients may have higher air ventilation rates, lower insulation levels and less efficient cooling systems. Greater specific humidity coefficients could indicate higher ventilation rates or low-efficiency dehumidification systems. Some buildings also have negative humidity coefficients because the algorithm does not constrain them to be positive. The other terms may be greater and offset the negative humidity contribution, however, this could lead to unphysical predictions of the space cooling load. A higher global horizontal irradiance coefficient can signify a greater external surface area to internal surface area ratio, high window areas, high absorptivity and low emissivity of external materials and minimal shading around the building. Negative GHI coefficients can be due to offsetting lighting electricity use. Lastly, the intercept is an important portion of the predicted baseload and has a strong correlation with annual electricity use (g) because it represents the constant amount of electricity used by the building.

(a)   (b)   (c)

(d)   (e)   (f)

(g)   (h)
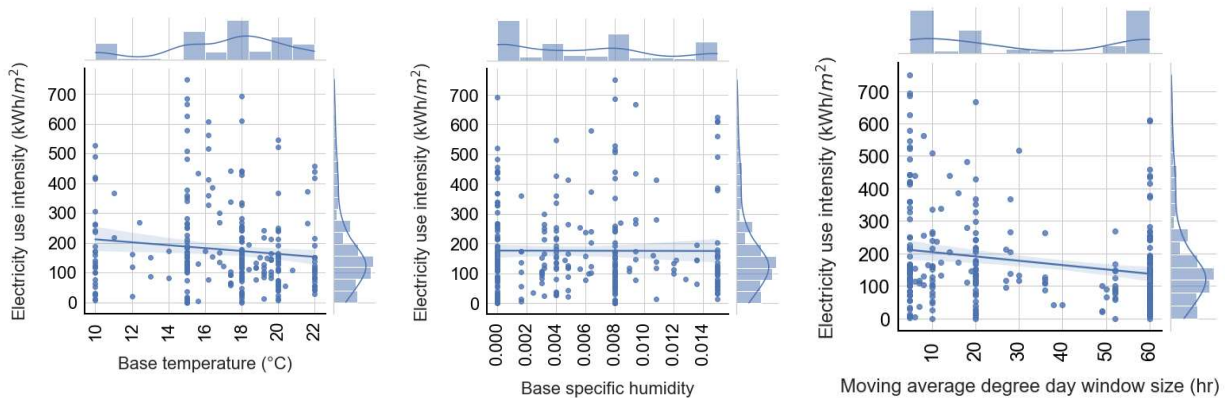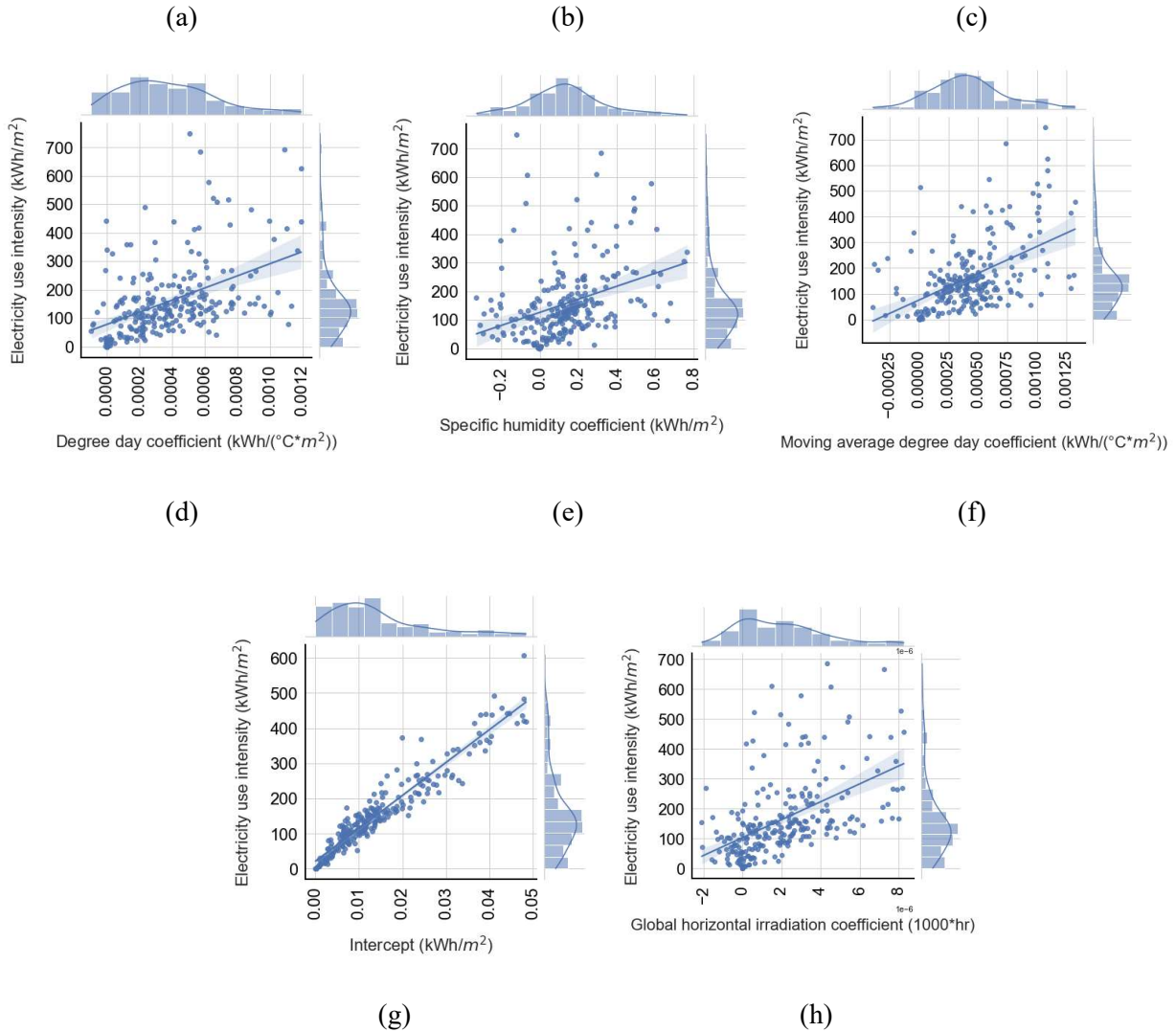
Figure 105: Electricity use intensity vs EL-CL model parameters from Equation 21 for each building

a) *Base temperature (T_{in})*
b) *Base specific humidity (SH_{in})*
c) *Moving average degree day window size (N)*
d) *Degree day term coefficient (β_2)*
e) *Specific humidity term coefficient (β_3)*
f) *Moving average degree day term coefficient (β_4)*
g) *Intercept (β_o)*
h) *Global horizontal irradiance coefficient (β_1)*

F.2 Analysis by building type

Detailed analysis can also be performed based on the building type. In this section, only three building types were investigated: long-term care (LTC) homes, apartments and offices. Each building

type has at least 30 buildings with hourly electricity data, however, there are fewer apartments compared to long-term care and office buildings. Plots similar to Figure 105 but grouped by building type are displayed in Figure 106. The kernel density estimate is also plotted for the three building types. In Figure 106 a), each building type is seen to have a similar range of base temperature values. It is difficult to discern any trends in electricity use with the base temperature, base specific humidity and window size parameters. In general, the apartment building parameters are more densely concentrated, which contributes to the higher quality performance of the apartment out-of-sample model. The moving average degree day window size is 60 hours for every apartment building, while it ranges for the long-term care home and office. The degree day, specific humidity and GHI coefficients are also lower for apartments, corresponding to the lower electricity use intensity of the building type. The moving average degree day coefficient is greater for the apartment, which may indicate a higher thermal mass impact for apartments. Finally, the intercept values are lowest for the apartment as well, indicating that the baseload use is generally lower than the other two building types.

(a)   (b)   (c)
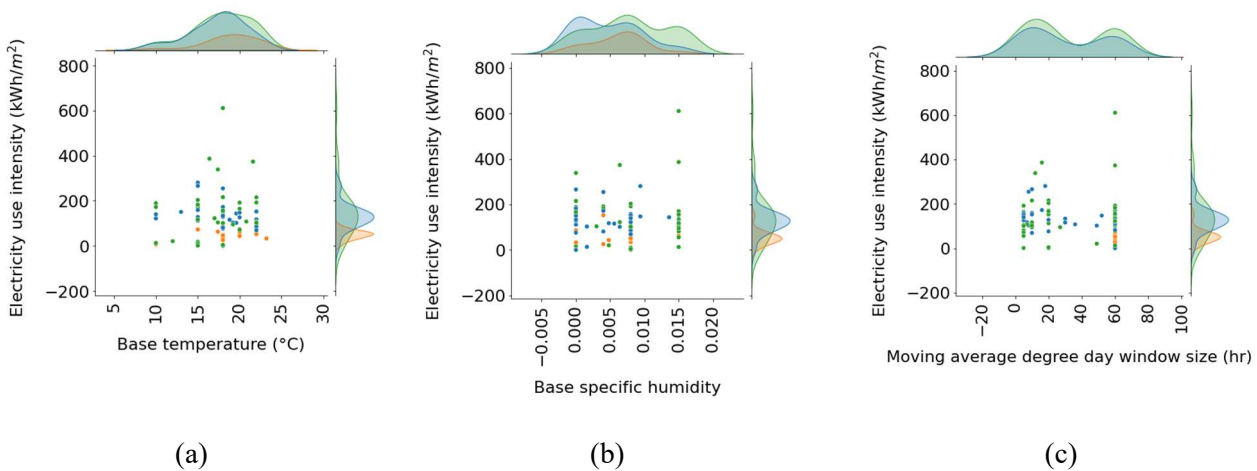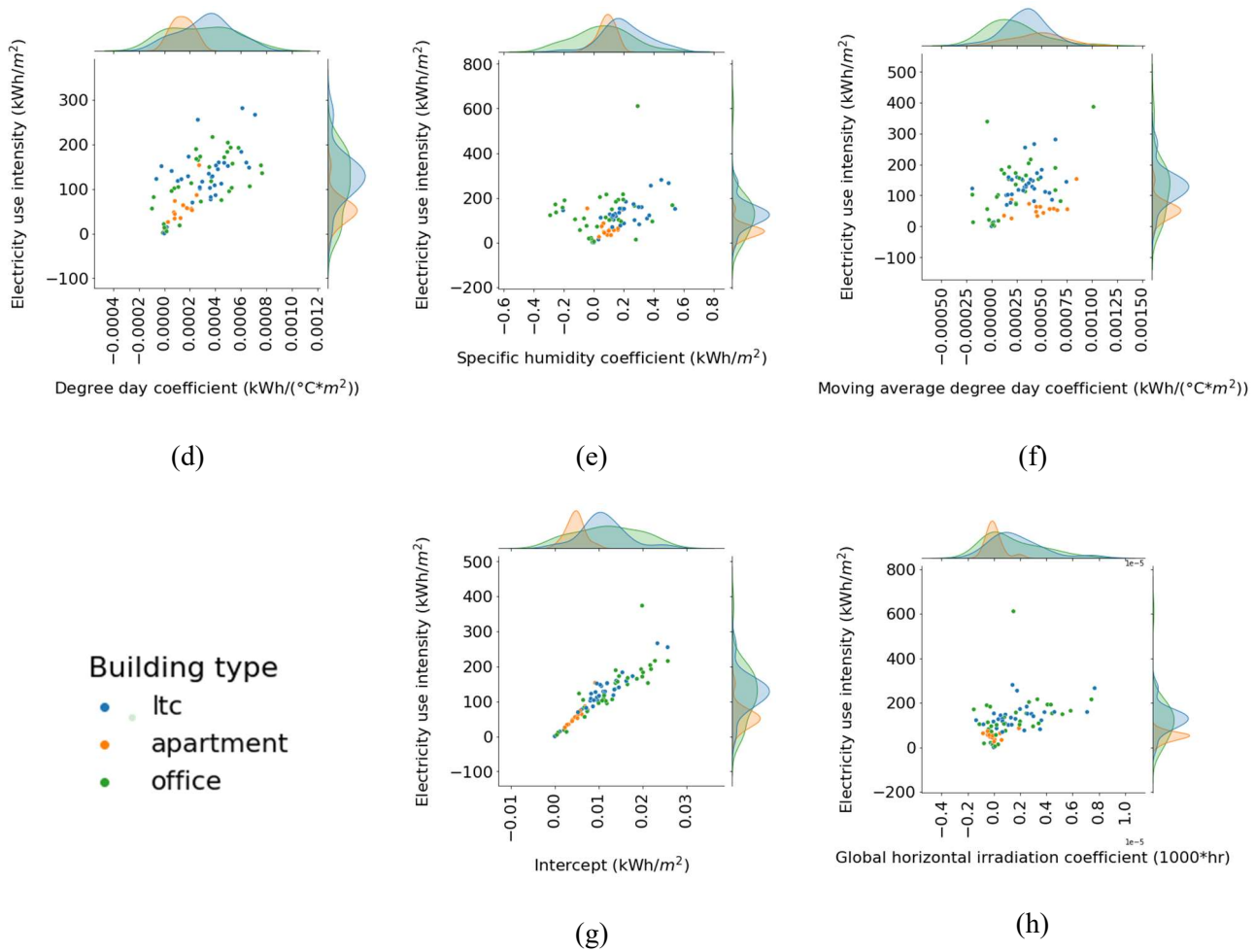
Figure 106: Energy use intensity vs EL-CL model parameters by building type

a) *Base temperature (T$_{in}$)*
b) *Base specific humidity (SH$_{in}$)*
c) *Moving average degree day window size (N)*
d) *Degree day term coefficient (β$_2$)*
e) *Specific humidity term coefficient (β$_3$)*
f) *Moving average degree day term coefficient (β$_4$)*
g) *Intercept (β$_o$)*
h) *Global horizontal irradiance coefficient (β$_1$)*

F.3 Scaled weather regression coefficients

The regression coefficients can also be analyzed by their scaled values. In this work, the input features were scaled by the interquartile range before running the ridge regression algorithm. Sections F.1 and F.2 display the regression coefficients scaled back to their original form so that input features can be used with no preprocessing required. However, analyzing the regression coefficients for the scaled

data can provide insight into which features have a greater influence on electricity use. For this analysis, the cooling season weather parameters for both on- and off-hours are observed. Figure 107 displays the scaled weather regression coefficients for summer weekdays during on-hours for all conventional buildings trained with the electricity-cooling model. In general, the degree day terms (corresponding to temperature) have the largest values. Heat adding to the sensible load will enter the building through envelope conduction as well as ventilation which both relate to the outdoor temperature. The averaged degree day coefficient is slightly larger than that of the instantaneous degree day, indicating that thermal mass plays an important role in electricity demand. Therefore, to reduce electricity consumption in most buildings, it may be more useful to concentrate on temperature-related conservation measures such as improving insulation and air tightness. Specific humidity and global horizontal irradiance (GHI) have similar median values, however, the upper quartile for specific humidity is higher than that of GHI. Figure 108 displays scaled weather regression coefficients for summer weekdays during off-hours for the electricity-cooling model trained on all conventional buildings. The GHI contribution is relatively small which is expected due to the low amount of sunlight during off-hours (nighttime). The averaged degree day coefficient has the highest median value; however, the specific humidity coefficient has a higher upper quartile value. Some buildings also have negative coefficients which may be due to correlation between predictor variables.
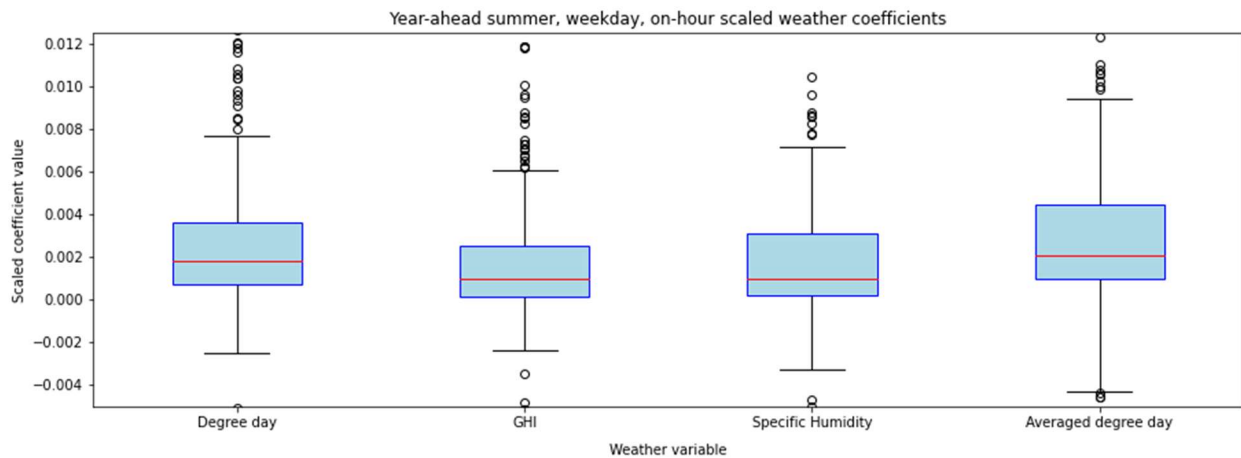
Figure 107: Summer cooling electricity model scaled weather regression coefficients during on-hours
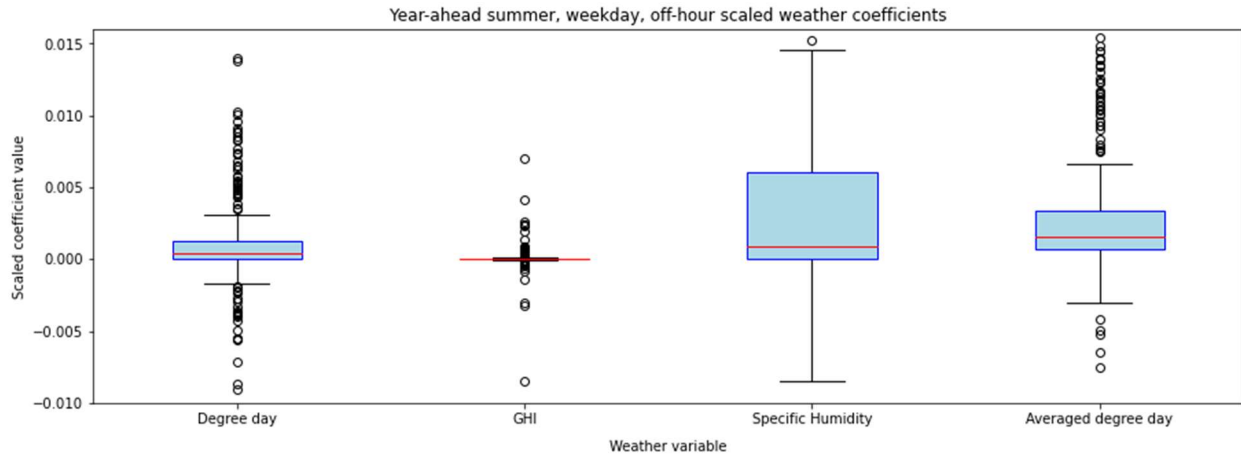
Figure 108: Summer cooling electricity model scaled weather regression coefficients during off-hours